**SANDIA REPORT**
SAND2010-2205
Printed April 2010

# P- and S-body wave tomography of the state of Nevada

Leiph A. Preston

Prepared by
Sandia National Laboratories
Albuquerque, New Mexico 87185 and Livermore, California 94550

Sandia National Laboratories is a multi-program laboratory operated by Sandia Corporation, a wholly owned subsidiary of Lockheed Martin company, for the U.S. Department of Energy's National Nuclear Security Administration under contract DE-AC04-94AL85000.



Issued by Sandia National Laboratories, operated for the United States Department of Energy by Sandia Corporation.



Available to DOE and DOE contractors from
U.S. Department of Energy
Office of Scientific and Technical Information
P.O. Box 62
Oak Ridge, TN 37831

Telephone: (865) 576-8401
Facsimile: (865) 576-5728
E-Mail: reports@adonis.osti.gov
Online ordering: http://www.osti.gov/bridge

Available to the public from
U.S. Department of Commerce
National Technical Information Service
5285 Port Royal Rd.
Springfield, VA 22161

Telephone: (800) 553-6847
Facsimile: (703) 605-6900
E-Mail: orders@ntis.fedworld.gov
Online order: http://www.ntis.gov/help/ordermethods.asp?loc=7-4-0#online

SAND2010-2205
Unlimited Release
Printed April 2010

# P- and S-body wave tomography of the state of Nevada

Leiph Preston
Geophysics
Sandia National Laboratories
P.O. Box 5800
Albuquerque, New Mexico 87185-MS0750

## Abstract

P- and S-body wave travel times collected from stations in and near the state of Nevada were inverted for P-wave velocity and the Vp/Vs ratio. These waves consist of Pn, Pg, Sn and Sg, but only the first arriving P and S waves were used in the inversion. Travel times were picked by University of Nevada Reno colleagues and were culled for inclusion in the tomographic inversion. The resulting tomographic model covers the entire state of Nevada to a depth of ~90 km; however, only the upper 40 km indicate relatively good resolution. Several features of interest are imaged including the Sierra Nevada, basin structures, and low velocities at depth below Yucca Mountain. These velocity structure images provide valuable information to aide in the interpretation of geothermal resource areas throughout the state on Nevada.

## ACKNOWLEDGEMENTS

I would like to thank my colleagues, Glenn Biasi and Ileana Tibuleac, at the University of Nevada Reno for collecting and picking the data for this project. Funding for this project was provided by the office of geothermal research of the Department of Energy through the Great Basin Center for Geothermal Energy.

# CONTENTS



# FIGURES

# 1. Introduction

Understanding the subsurface distribution of P- and S-wave velocities is important for proper construction and interpretation of models that can aide in geothermal resource identification and assessment. As a first step, this report provides the results of P-wave and Vp/Vs tomographic inversion of body wave travel times recorded from earthquakes occurring in and near the state of Nevada. The entire state of Nevada (base map, Section 9) is modeled, however, due to earthquake and receiver distributions, some parts of the state are not well resolved. Besides Vp (Section 10) and Vp/Vs (Section 11) images of the state down to about 45 km depth, this report also provides resolution (Section 12) and error estimates (Section 13) of these parameters. Only a brief interpretation of the resulting images is attempted in this report.

# 2. Travel-time data

Travel times were collected from an Antelope database created by University of Nevada Reno (UNR) colleagues. These travel times were picked from local to regional earthquakes recorded on UNR permanent (Northern Nevada and the Yucca Mountain Network) stations and from the temporary USArray network that marched across Nevada during 2007 and 2008. A total of 249 stations were used. The initial catalog consisted of P, Pg, Pn, Pb, S, and Sn named phases. Some stations had more than one type of P and/or S pick and, thus, the first arriving P and S phases had to be identified. The cross-over distance for Pg (direct crustal phase) to Pn (upper mantle phase) is at about 1° angular distance in Nevada, with Pn arriving before Pg beyond this distance. The ‘Pb’ phase had unknown meaning. The following strategy was used to define first arriving P: 1) if available, use Pn, 2) if available, use ‘P’, 3) use Pg if the angular distance was less than 0.8° unless Pb<Pg then use Pb. For S: 1) if available, use Sn, 2) use S. There were several duplicate named phases on a station for a given event. In this case, the minimum time was used. This somewhat complex approach was used in order to see if the named phases could be relied upon to define actual Pn and Pg phases that could later be used in non-first arrival tomography.

The modeled area was chosen to be slightly bigger than the state of Nevada, ranging from -120.5° to -113.5° longitude and from 34.9° to 42.5° N latitude. Within this range, there were a total of 8999 picks available from over 200 earthquakes. After initial evaluation, it was discovered that many picks were incorrectly identified as first arriving phases, i.e. at farther distances sometimes Pn was picked as a first arrival and at others Pg was mistakenly picked. Fortunately, the large number of stations available for many events allowed visual separation Pn and Pg (and likewise, Sn and Sg). This culled data was then passed through an initial inversion stage with fairly smooth model regularization. This allowed further culling of clearly incorrect time picks. This was done manually by removing picks that clearly fell outside the main travel time residual band for each event. The final travel time data set consisted of 5516 P travel times and 1360 S times from 206 earthquakes.

## 3. Model Inversion

The inversion grid for the tomographic model covered the approximate area from -120.5° to -113.5° longitude, from 34.9° to 42.5° N latitude and from the surface to 91 km depth. All coordinates are first converted to a local cartesian coordinate system based on the Universal Transverse Mercator transformation from latitude and longitude with an origin at -120.5° longitude and 34.9° N latitude. A simple spherical correction was applied to the depth coordinates by adding $R_E(1-\cos(d/R_E))$, where $R_E$ is the radius of the Earth and d is the distance from the center of the grid. The maximum correction on the corners of the model is about 21 km. Grid node spacing was chosen to be 5 km and is the same in all three coordinate directions.

The tomographic inversion proceeds in two basic stages. In the first stage, the forward problem is computed. Travel times are computed throughout the 3-D grid using the Vidale-Hole finite-difference (Hole and Zelt, 1995; Vidale, 1990) algorithm. Rays are then traced from source to receiver by following the travel-time gradient. The second stage is where the matrix inversion occurs. The conjugate-gradient least squares (CGLS) algorithm is utilized to solve the system of equations for model slowness perturbations and earthquake hypocenter perturbations. Since this is a highly non-linear problem, the solution returned is not necessarily the best or even a better solution than the initial model. As such, a search is performed for the best solution assuming that the direction of the CGLS solution vector is correct, but not necessarily the magnitude, i.e., the amplitudes of the model slowness and earthquake hypocentral perturbations are iteratively halved until a minimum is found in model fit. The forward and inverse stages are iteratively repeated until the change in solution is deemed sufficiently small.

Regularization and other controls are imposed on the system of equations both to provide stability and also to ensure that the solution stays within reasonable limits. The P velocity and the Vp/Vs models are constrained to be smooth in a anisotropic Laplacian sense, meaning that the Laplacian operator is used to compute smoothness, but different weighting is allowed for the vertical direction compared to the horizontal directions. This allows a model to be rougher in the z-direction than in the x and y directions. Additionally, Vp is constrained to lie between minimum and maximum values that are depth dependent. Likewise, Vp/Vs is constrained to lie between 1.6 and 2.5 at all depths. Earthquakes and ray paths are also constrained to lie beneath the topographic surface of the earth.

Several tomographic models are computed with variation in some of the parameters in order to explore the model space more effectively. Initially, a fairly smooth model using joint inversion of Vp, Vp/Vs and hypocentral parameters is computed. If too rough a model is sought initially, the solution can easily get trapped within a local minimum. After a fairly smooth solution is found, the roughness of the models are progressively increased until a satisfactory solution is found. A satisfactory solution is somewhat subjective but is chosen near where increasing roughness further does not improve the fit to the travel times significantly. Once the best smoothness is found, further

improvements in overall fit is achieved by using a non-joint inversion process. In this process, one iteration solves for Vp and Vp/Vs while keeping hypocentral parameters fixed while the next iteration one solves for hypocentral parameters while holding Vp and Vp/Vs fixed. Experimentation has shown that better fits to the travel times with smoother models can be achieved if this is done. The final model had an root mean square residual of 0.32 s for P and 0.43 s for S picks.

## 4. Resolution and Error Analysis

Direct information about the standard errors of the model parameters is not available from this procedure. However, indirect methods can be used to obtain estimates of the the achieved resolution of the model and the standard errors. The former is estimated using checkerboard tests. In these tests, a spatially varying pattern of perturbations that resembles a checkerboard are added to the final 3-D model. Theoretical travel times are calculated through this perturbed model, travel time errors with the same distribution as the real data are added to these travel times and then a tomographic inversion is performed with these calculated times. The resulting perturbation pattern is then compared with the original pattern. In places where the pattern is well replicated, resolution at that block size is deemed good. Checkerboard test results are shown in Section 12.

Several different block sizes were used in the checkerboard tests. The smallest horizontal dimension tested was 25 x 25 km for P-waves. In general, only very limited areas show resolution at this scale: near Yucca Mountain and near Wells, NV down to about 20 km depth. Better resolution over a broader region is observed for 50 x 50 km block sizes for P-waves, with decent resolution extending into central NV and slightly deeper. 100 x 100 km block were broadly well resolved down to around 50 km depth in all except the corners, with less resolution in eastern NV. 200 x 200 km blocks were similar to the 100 x 100 km blocks except perhaps extending slightly deeper to about 60 km depth. Vertical resolution for P-waves was only marginal in some areas, namely near Yucca Mountain, western NV and near Wells, NV, for 50 km horizontal by 10 km vertical block dimensions. 20 km vertical block dimensions returned good resolution within the same regions as the 50 x 50 km horizontal blocks down to a maximum of 60 km depth, but more generally down to ~50 km.

The S-waves showed half or less of the resolution of the P-waves. 50 x 50 km horizontal blocks were extremely poorly resolved in all but near Yucca Mountain and Wells, NV, but even those locations were marginal. 100 x 100 km horizontal blocks indicated some resolution in western NV, near Wells and Yucca Mountain down to about 20 km depth. 200 x 200 km block resolution was good over many areas except the model corners down to about 40 km depth.

Standard errors of the model parameters are estimated using a form of the statistical Jackknife test. In this test, ten new data sets are created by randomly removing 10% of the travel time data in such a way that no two data sets have the same datum removed but that among the 10 data sets all data are removed. Each of these 10 data sets are

then inverted to obtain 10 different tomographic models. Standard jackknife equations are applied to obtain an estimate of the standard errors at the 95% confidence level. Jackknife test results are shown in Section 13.

The P-wave standard errors are typically less that 0.1 km/s over most sampled regions down to about 30 km depth. Deeper than 30 km depth, the typical standard error is less than 0.2 km/s. Spotty locations show larger standard errors, with the maximum standard error generally increasing with depth. Maximum standard errors are about 0.2 km/s at the shallowest depths, but increase to over 0.6 km/s at 45 km depth. Generally, these spots of large standard error are relatively small-scale and are located on the fringes of the model or in the east-central portions of the state where ray coverage is poorer. Vp/Vs standard errors are typically less than 0.01, with maximum standard error between 0.02 and 0.025 at all depths. The largest standard errors appear to be more associated with higher absolute Vp/Vs values in the model. However, the magnitude of the standard errors generally are insufficient to call into question whether a region is above average Vp/Vs if it is imaged as a high Vp/Vs region.

## 5. Results

The Vp images are shown in Section 10. The shallowest 15 km of the P-wave model have the highest resolution and the best correlation with known structures. The core of the Sierra Nevada is imaged very well as a fairly high velocity (~6.5 km/s) NW-SE trending structure along the western fringe of the ray coverage. At 0 (sea level) and 5 km depth, this structure stands out well above the average background velocity of the surrounding areas (upper 5 to ~6 km/s range). Station density and resolution is greatest generally along the western border of Nevada running from Yucca Mountain northward to Reno. Smaller low velocity structures on the order of 25 km in diameter and greater are imaged under Reno, Carson City and northern Owen's Valley that correspond to known basin structures. The Carson Sink and Dixie Valley are indicated by a prominent low velocity structure. Prominent low velocity structures also appear NW of Betty, NV and just south of Yucca Mountain under Amargosa Valley. Generally higher than average velocities are seen between about Goldfield, NV and the Carson Sink low velocity structure. The region of the Wells earthquake shows at or slightly above average velocities. High velocities are imaged between Lovelock, NV and the Black Rock Desert.

By 10 and 15 km depth, the surrounding crustal velocities have nearly matched that of the Sierran core (low to mid 6 km/s range). Many detailed structures that are imaged at shallower depths are no longer clearly visible. The low velocity structure under the Carson Sink is still clearly visible as well as the structure just south of Yucca Mountain. An interesting high velocity structure appears southward from Mammoth mountain with imaged velocities exceeding 7 km/s by 15 km depth. This structure is on the very fringe of the ray coverage zone, but, probably due to the dense station coverage in the region, it shows very low standard error and may be reasonably well resolved.

The structure at 20 to 25 km depth is broadly in the upper 6 km/s range with few structures that stand-out as being well-resolved. The high velocity structure south of Mammoth Mountain has roughly the same velocities as at 15 km, but the surrounding velocities have increased so it is a much more subdued feature. Velocities continue to be lower than average near Yucca Mountain.

The 30 km depth section is the first that shows reliably large regions with velocities consistent with the upper mantle where by 35 km depth, many regions show velocities in excess of 7.6 km/s. Deeper than 30 km depth, the Sierra appear as a lower than average velocity, with P velocities in the lower 7 km/s range compared to most areas in the mid to upper 7 km/s range by this depth. This is most likely due to the crustal root of the Sierra invading upper mantle velocities at this depth. The low velocity structure near Yucca Mountain is still present at these depths. The northern third of Nevada broadly shows velocities greater than 7.8 km/s.

Although resolution is beginning to degrade rapidly by 40 km depth, there are some interesting features. The signature of the Sierran root is muted but still discernible at 40 and 45 km depths. The persistent low velocity zone near Yucca Mountain is also muted at these depths. Velocities greater than 8 km/s dominate much of the state, but an ~50 km wide band of lower than average velocities cut through the state at about 39° N latitude. The muted velocities and somewhat banded appearance of the velocities structures at these depths can also be due to decreased ray coverage here, thus masking their true character.

The Vp/Vs images (Section 11) are of a much lower resolution compared to the P-wave images as demonstrated in the checkerboard tests. There is little vertical change in the Vp/Vs as one moves from the surface to 30 km depth, although there is a tendency for higher Vp/Vs at deeper depths. Deeper than 30 km, resolution and ray coverage have degraded significantly. Lower Vp/Vs dominates under the Sierra Nevada and under the NE corner of the state near Wells. Higher than average Vp/Vs are imaged broadly under the Carson Sink and Dixie Valley regions as well as along the NV-CA border between near Mammoth and Yucca Mountain. This particular features appears to spread eastward with depth. Yucca Mountain is at or slightly below average Vp/Vs at shallow depths and tends toward higher than average Vp/Vs at 30 km depth.

## 6. Discussion

Only a brief interpretation of the results will be given in this report. Overall, the results are in accord with those of other investigators of the region. Average crustal velocities obtained by 2-D survey lines across central NV agree with those of this study (e.g., Catchings and Mooney, 1991; Holbrook, 1990; Catchings, 1992; Potter et al., 1987). Similarly, a Moho depth of about 30 km obtained in the above studies is consistent with the tomographic results obtained here based upon P velocities reaching the upper 7 km/s range near that depth. A more precise estimate of Moho depth is not feasible from this tomography given the smoothness of the model and the 5 km block size.

On smaller scales, where resolution is best in western NV, shallow basin structures are well imaged under Reno, Carson City, Owen's Valley and the Carson Sink (see Figure 1 for base map). The Carson Sink anomaly extends deeper than these other basins into the mid crust and is correlated with higher than average Vp/Vs. Additionally, near Yucca Mountain, where station coverage is excellent, low velocities of the Amargosa Basin are imaged. Interestingly, this low velocity structure under the Amargosa Basin is not confined to the upper crust, but extends through the crust into the upper mantle. This structure correlates spatially with what several researchers see as a crustal scale rift perhaps associated with the various caldera complexes found in the area (e.g., Carr, 1990; Fridrich, 1999; Brocher et al., 1998; Crowe et al., 1995).

The Sierran block is also well imaged in the tomography to 40-45 km depth. The Sierran block velocities and crustal root are comparable to other investigators as well (e.g., Fliedner et al., 2000; Mavko and Thompson, 1983; Knuepfer et al., 1987). Lower than average Vp/Vs is also imaged under the Sierra. Perhaps the most interesting aspect of the Sierran image is the high velocity structure just south of Mammoth that extends throughout the mid to lower crust. Since this structure is on the fringe of the region of ray coverage, it should be interpreted cautiously since the likelihood of an artifact is higher. However, given its location this structure would be a good subject for more rigorous study.

Unfortunately, the central part of the state was not well imaged due to the sparse station density and paucity of earthquakes. In order to greatly improve resolution throughout the model domain, significantly more earthquakes need to be picked. A special effort to collect more S travel time picks would greatly enhance the resolution of the S velocity images. Furthermore, the ability to use both crustal and mantle phases (e.g., Pn and Pg) from the same event to the same station would significantly improve mid to lower crustal resolution.

## 7. Conclusion

P- and S-wave earthquake travel time data were inverted for P velocity and Vp/Vs ratio of the entire state of Nevada. P velocity resolution is best primarily from Yucca Mountain northwest to Reno where station density is highest to about 40 km depth. Due to dearth of S travel time picks compared to P, S-wave resolution is significantly lower than P throughout the model and only extends to about 30 km depth. Several features of interest are imaged including the Sierra Nevada, basin structures, and low velocities at depth below Yucca Mountain. These velocity structure images provide valuable information to aide in the interpretation of geothermal resource areas throughout the state on Nevada.

## 8. References

Brocher, T.M., W.C. Hunter and V.E. Langenheim (1998), Implications of seismic reflection and potential field geophysical data on the structural framework of the Yucca Mountain-Crater Flat region Nevada, *Geol. Soc. Am. Bull., 110*(8), 947-971.

Carr, W.J. (1990), Styles of extension in the Nevada Test Site region, southern Walker Lane Belt; An integration of volcano-tectonic and detachment faulting models, in *Basin and Range Extensional Tectonics Near the Latitude of Las vegas, Nevada*, edited by B.P. Wernicke, *Mem. Geol. Soc. Am., 176*, 283-303.

Catchings, R.D. (1992), A relation among geology, tectonics, and velocity structure, western to central nevada Basin and Range, *Geol. Soc. Am. Bull., 104*(9), 1178-1192.

Catchings, R.D. and W.D. Mooney (1991), Basin and Range crustal and upper mantle structure, northwest to central Nevada, *J. Geophys. Res., 96*(B4), 6247-6267.

Crowe, B., F. Perry, J. Geissman, L. McFadden, S. Wells, M. Murrell, J. Poths, G.A. Valentine, L. Bowker, and K. Finnegan (1995), Status of volcanism studies for the Yucca Mountain site characterization project, *Los Alamos Rep. LA-12908-MS*, Los Alamos Natl. Lab., Los Alamos, N.M.

Fliedner, M.M., S.L. Klemperer and N.I. Christensen (2000), Three-dimensional seismic model of the Sierra Nevada arc, California, and its implications for crustal and upper mantle composition, *J. Geophys. Res., 105*(B5), 10,899-10,921.

Fridrich, C.J. (1999), Tectonic evolution of Crater Flat basin, Yucca Mountain Nevada, in *Cenozoic Basins of the Death Valley Region*, edited by L.A. Wright and B.. Troxel, *Spec. Pap. Geol. Soc. Am., 333*, 169-195.

Holbrook, W.S. (1990), The crustal structure of the northwestern Basin and Range province, Nevada, from wide-angle seismic data, *J. Geophys. Res., 95*(B13), 21,843-21,869.

Hole, J. and B. Zelt (1995), 3-D finite-difference reflection traveltimes, *Geophys. J. Int., 121*(2), 427-434.

Knuepfer, P.L.K., P.J. Lemiszki, T.A. Hauge, L.D. Brown, S. Kaufman, J.E. Oliver (1987), Crustal structure of the Basin and Range-Sierra Nevada transition from COCORP deep seismic-reflection profiling, *Geol. Soc. Am. Bull., 98*(4), 488-496.

Mavko, B.B. and G.A. Thompson (1983), Crustal and upper mantle structure of the northern and central Sierra Nevada, *J. Geophys. Res., 88*(B7), 5874-5892.

Potter, C.J., C. Liu, J. Huang, L. Zheng, T.A. Hauge, E.C. Hauser, R.W. Allmendinger, J.E. Oliver, S. Kaufman, and L. Brown (1987), Crustal structure of north-central Nevada: Results from COCORP deep seismic profiling, *Geol. Soc. Am. Bull., 98*(3), 330-337.

Vidale, J. (1990), Finite-difference calculation of traveltimes in three-dimensions, *Geophysics, 55*(5), 521-526.

## 9. Base Map

Figure 1: Base map showing the stations and features of interest mentioned in the text.

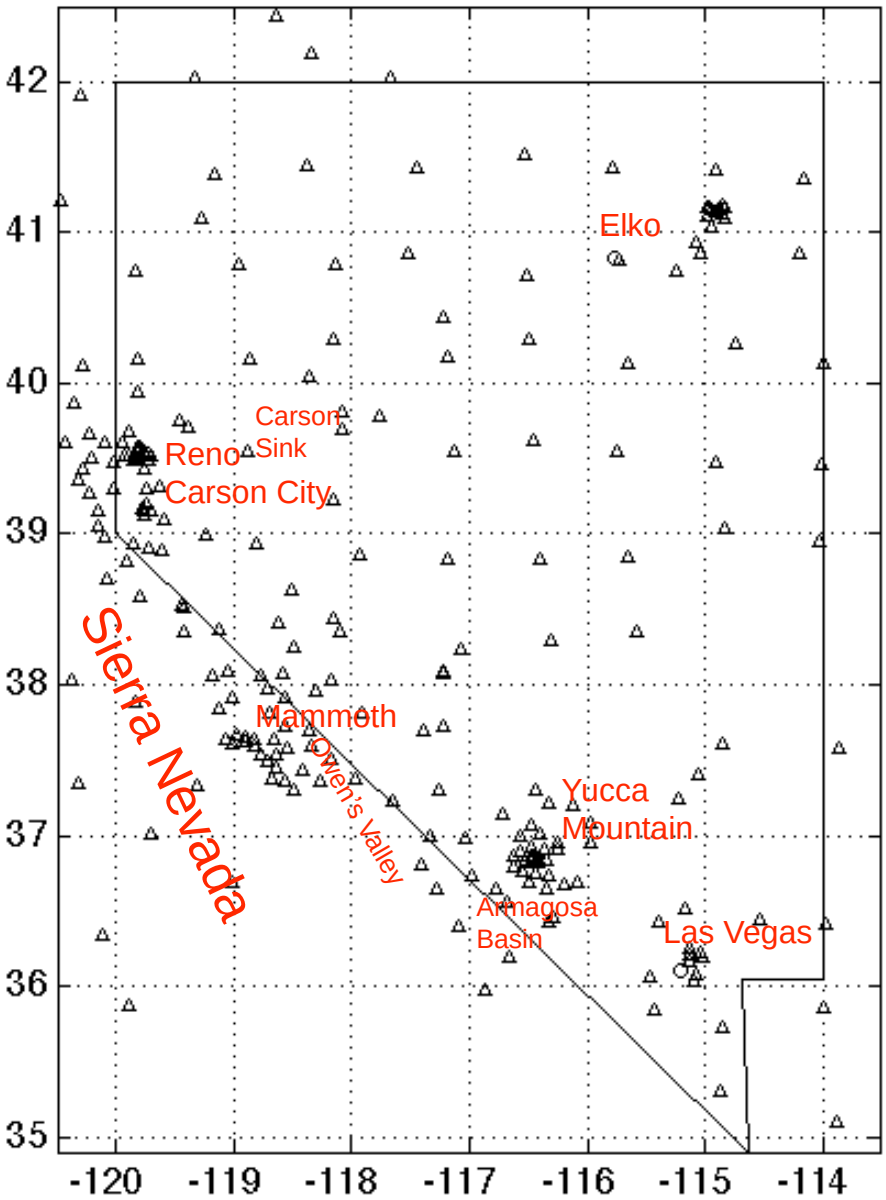

## 10. Vp Depth Sections

Figures 2-11 are the P-wave velocity images in depth sections from 0 km (sea level) to 45 km depth in 5 km increments. Latitude and longitude are the plot coordinates. The color bar at the bottom of each figure gives the color scale. Note that the color scale changes with each depth. Stations are shown as triangles in all sections for reference. Black dots are earthquakes that locate within ±2.5 km of the given depth.

Figure 2

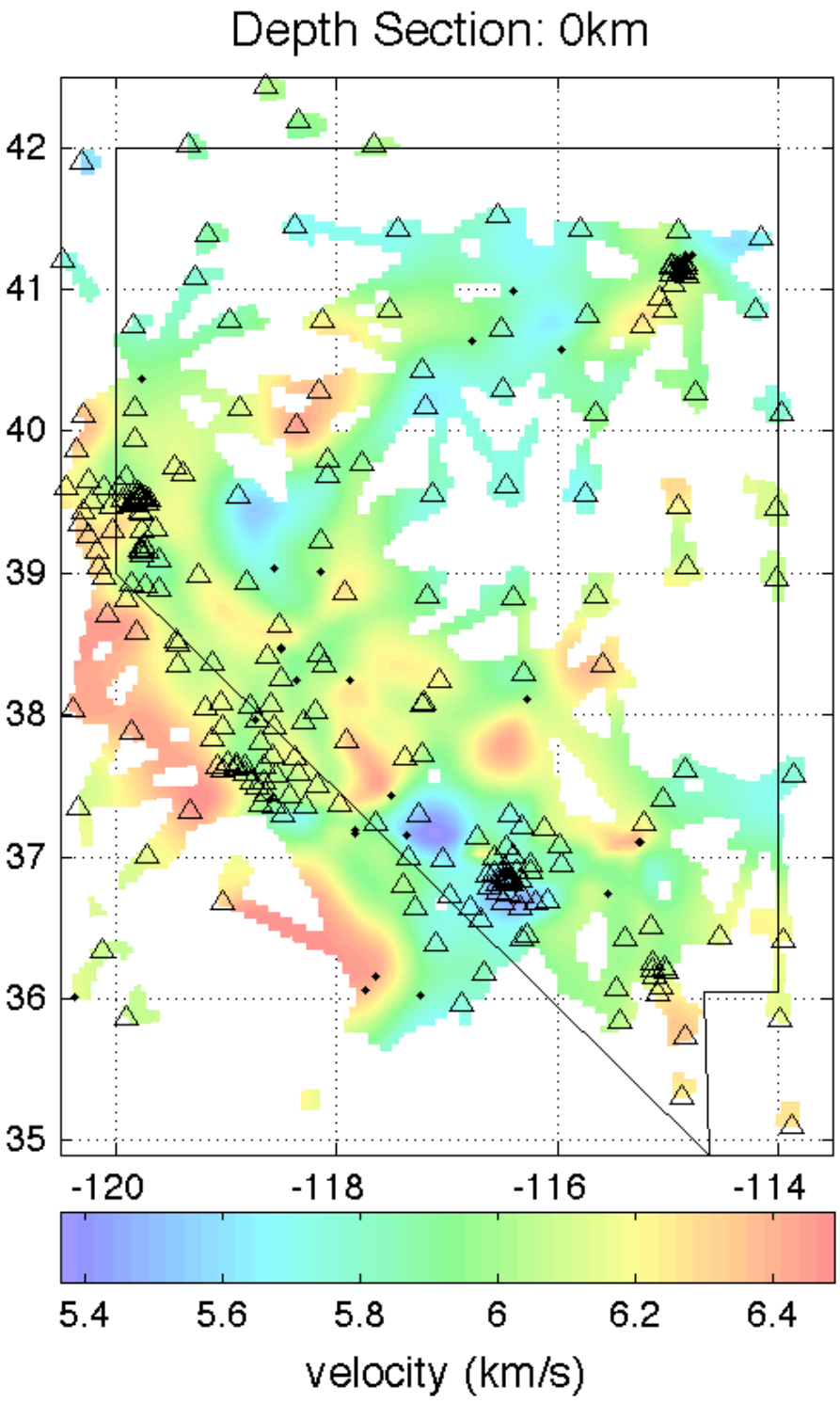
Depth Section: 0km
42
41
40
39
38
37
36
35
-120
-118
-116
-114
5.4
5.6
5.8
6
6.2
6.4
velocity (km/s)

Figure 3

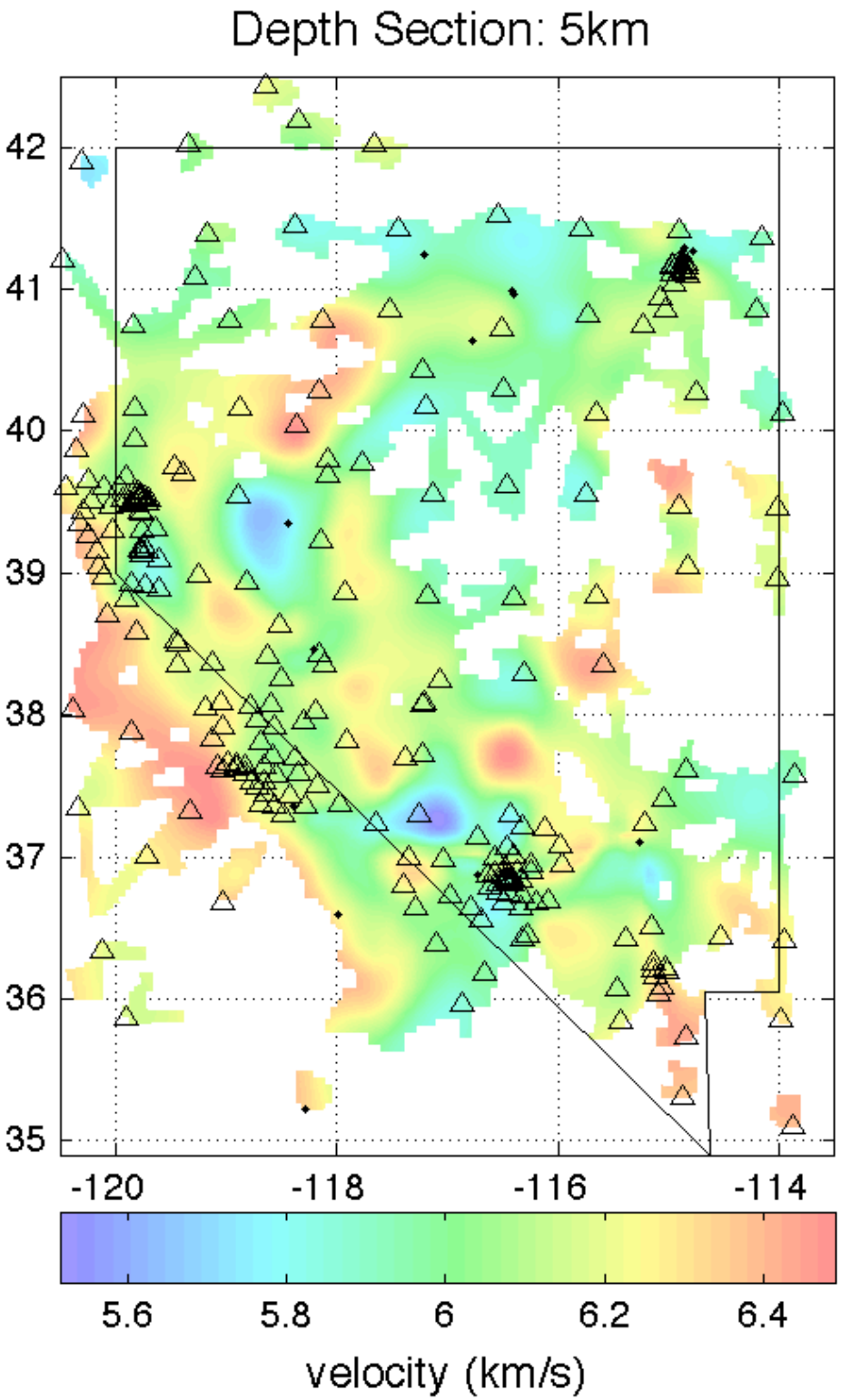
Depth Section: 5km
42
41
40
39
38
37
36
35
-120
-118
-116
-114
5.6
5.8
6
6.2
6.4
velocity (km/s)

Figure 4

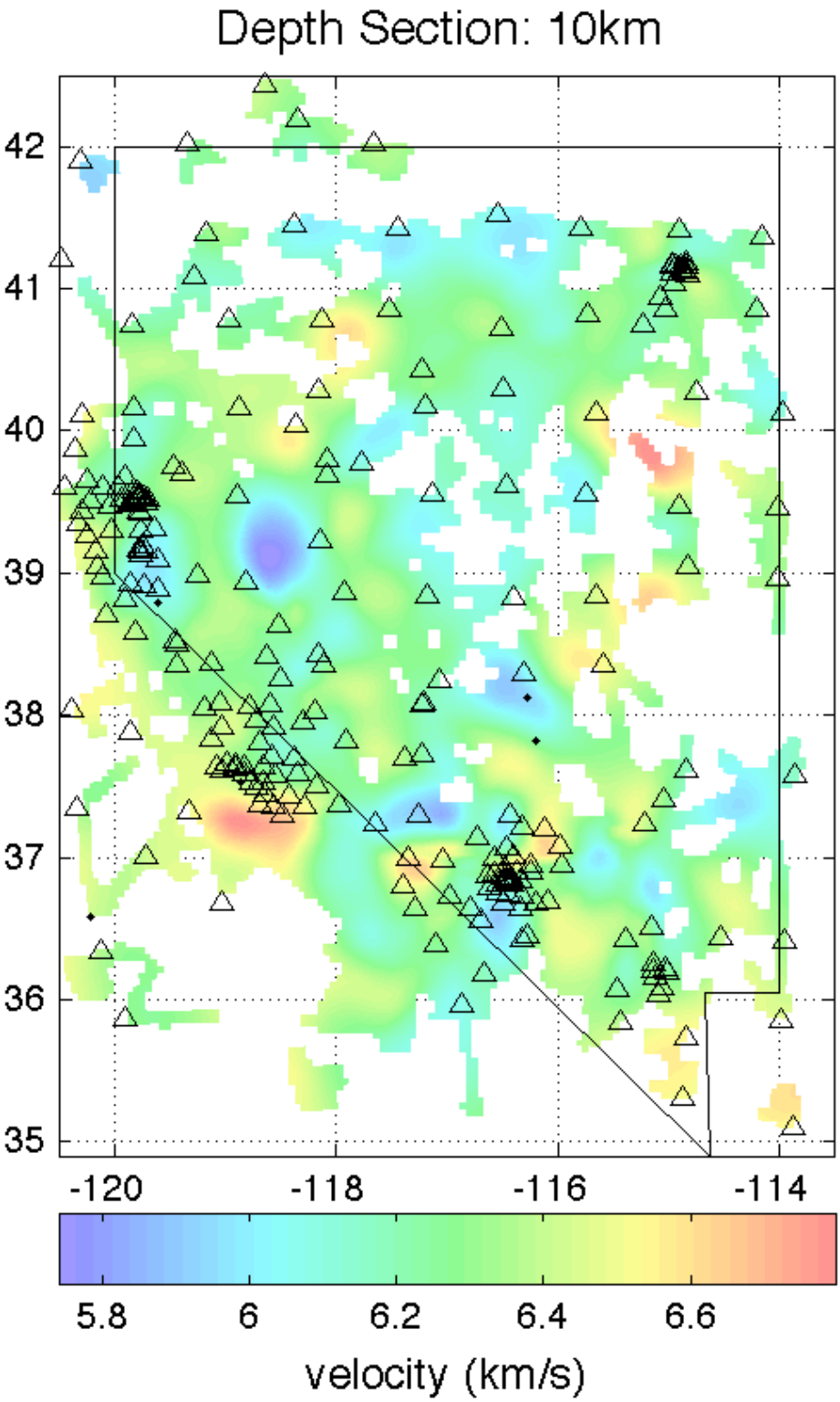
Depth Section: 10km
42
41
40
39
38
37
36
35
-120
-118
-116
-114
5.8
6
6.2
6.4
6.6
velocity (km/s)

Figure 5

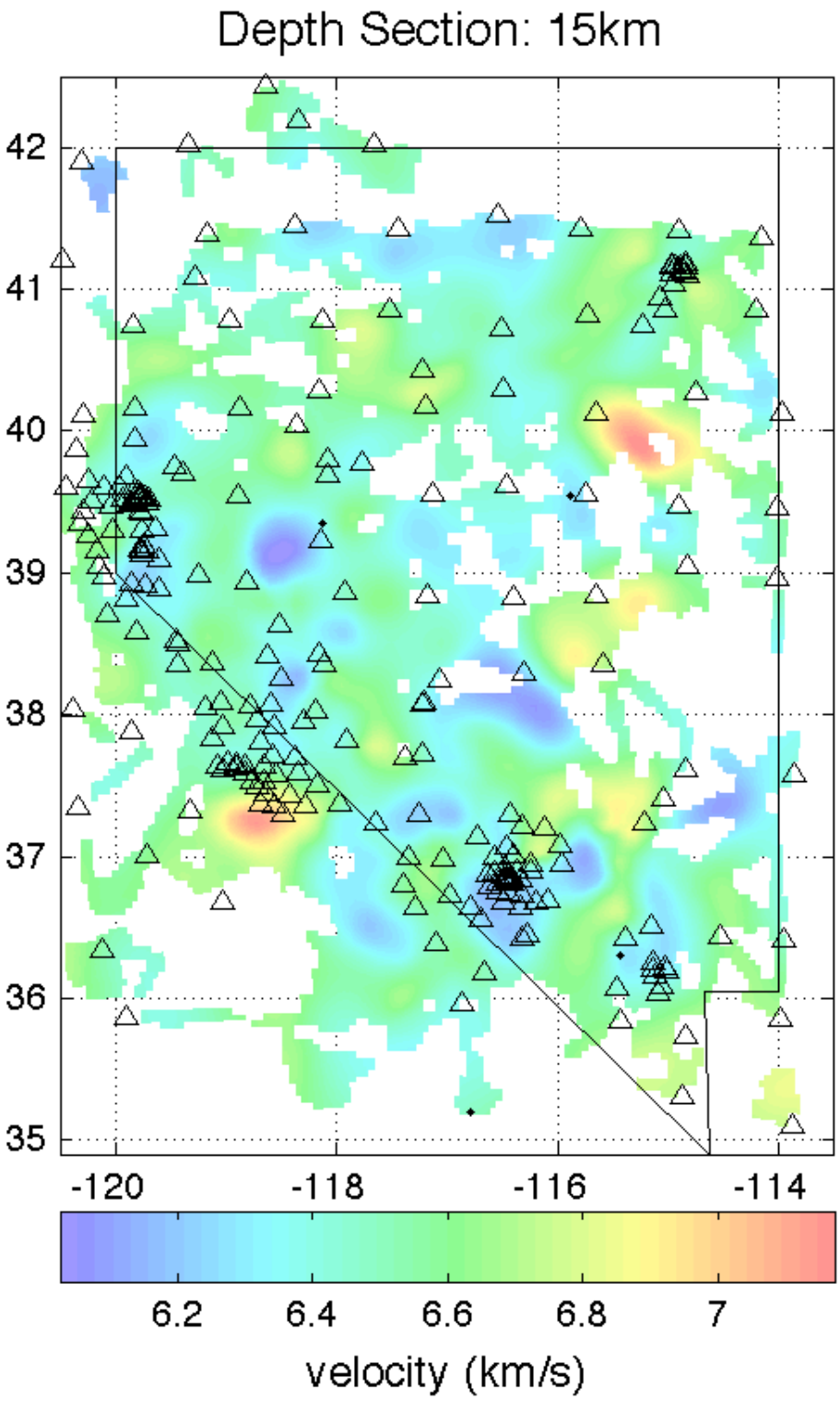
Depth Section: 15km
42
41
40
39
38
37
36
35
-120
-118
-116
-114
6.2
6.4
6.6
6.8
7
velocity (km/s)

Figure 6

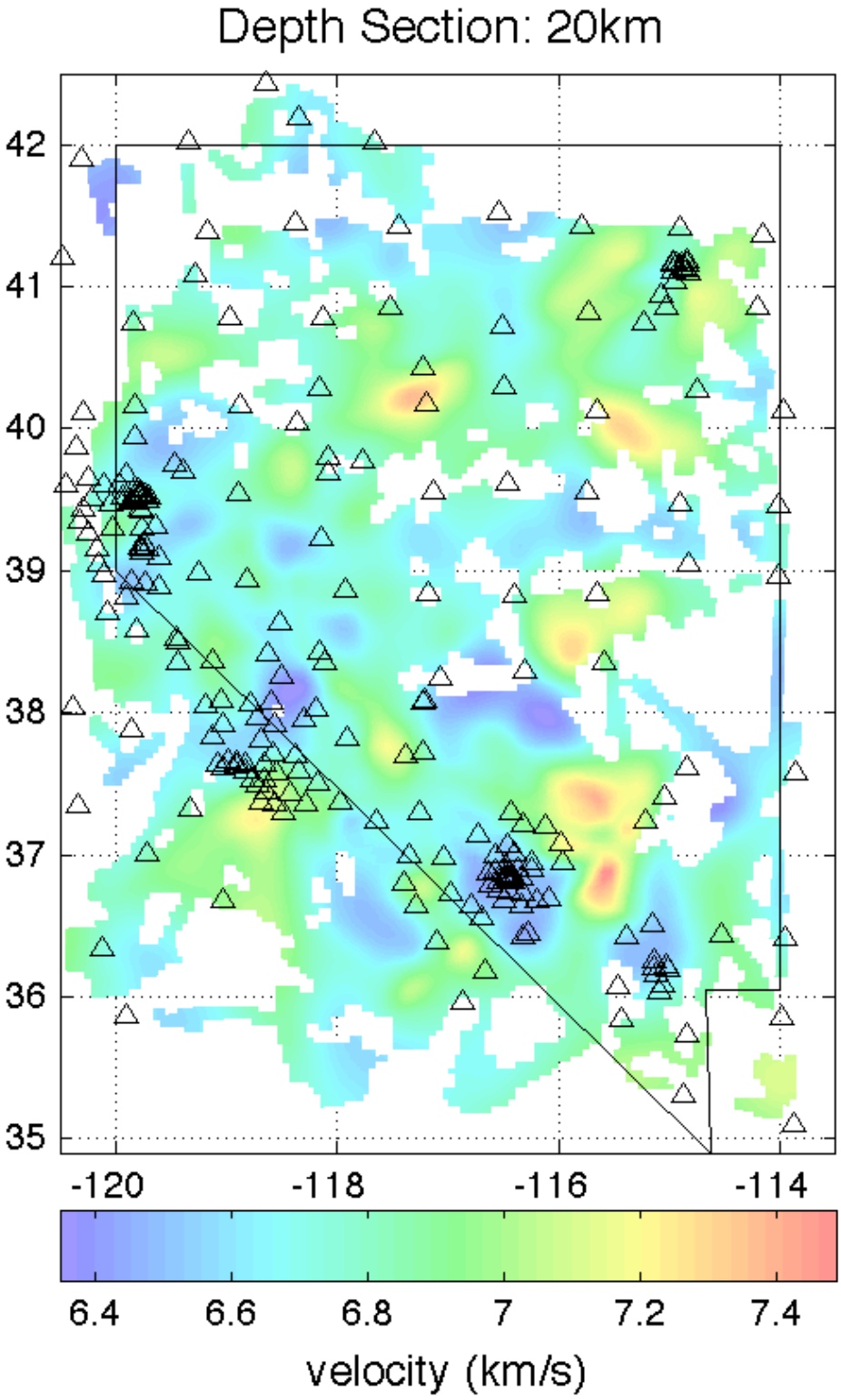
Depth Section: 20km
42
41
40
39
38
37
36
35
-120
-118
-116
-114
6.4
6.6
6.8
7
7.2
7.4
velocity (km/s)

Figure 7

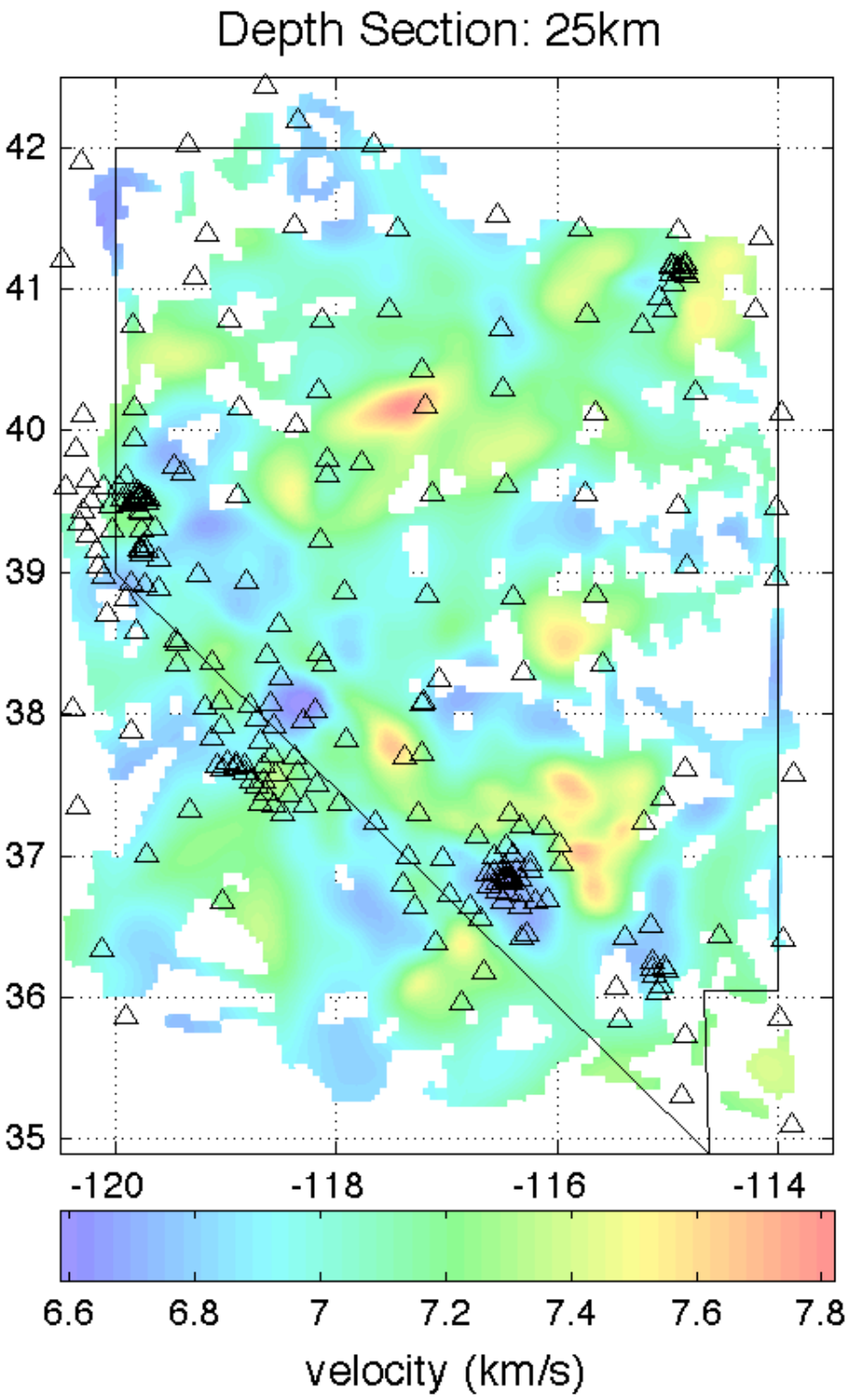
Depth Section: 25km
42
41
40
39
38
37
36
35
-120
-118
-116
-114
6.6
6.8
7
7.2
7.4
7.6
7.8
velocity (km/s)

Figure 8

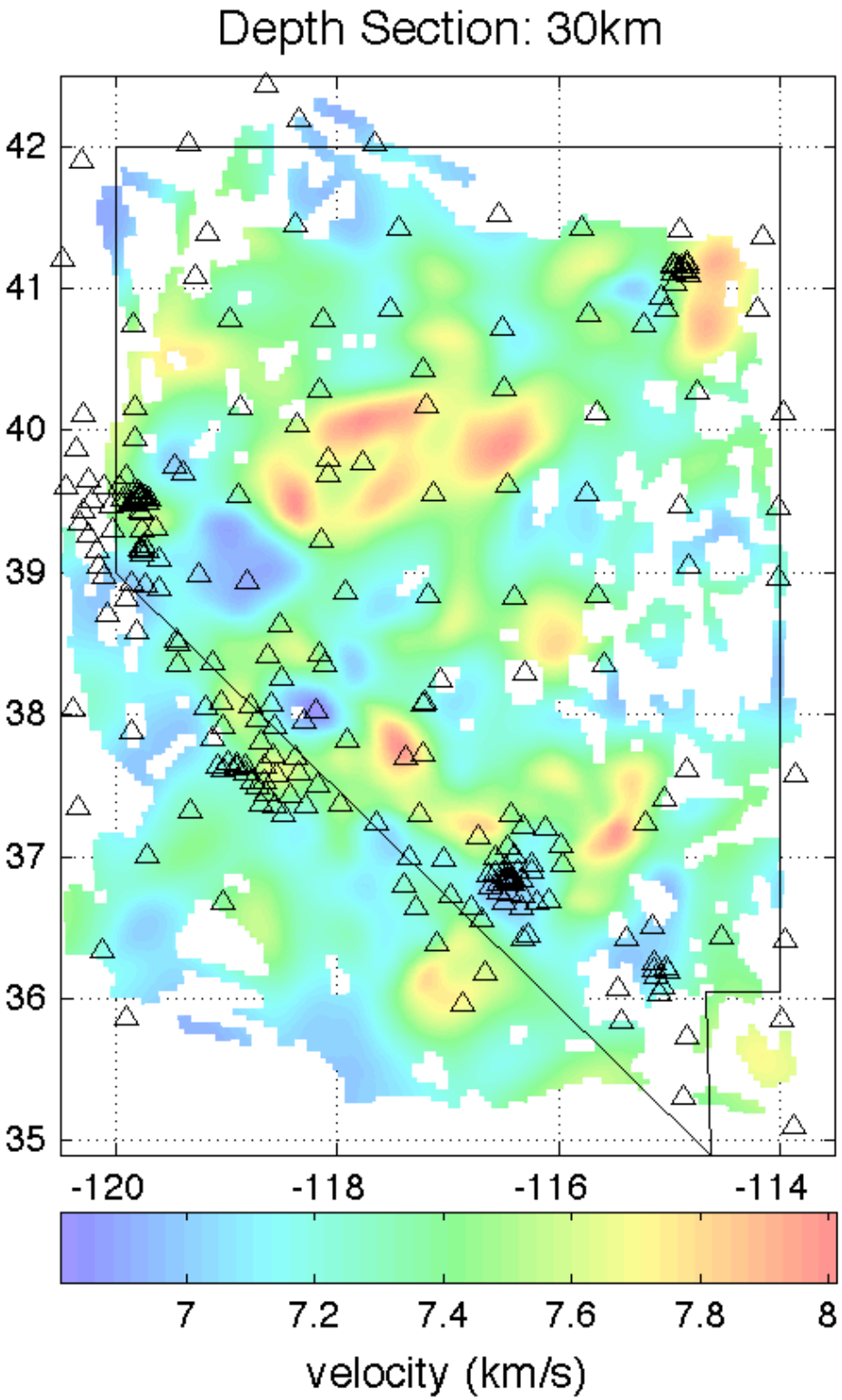
Depth Section: 30km
42
41
40
39
38
37
36
35
-120
-118
-116
-114
7
7.2
7.4
7.6
7.8
8
velocity (km/s)

Figure 9

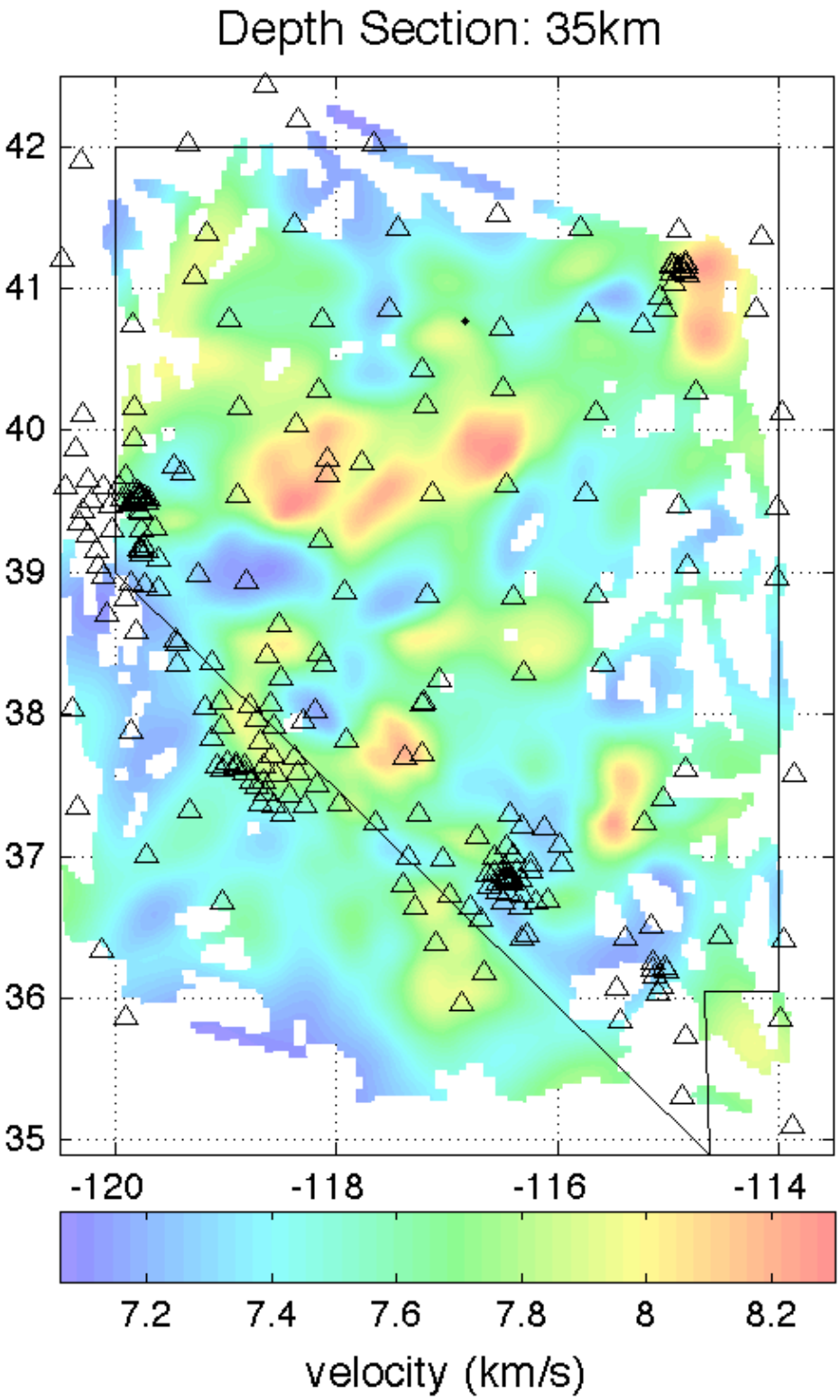
Depth Section: 35km
42
41
40
39
38
37
36
35
-120
-118
-116
-114
7.2
7.4
7.6
7.8
8
8.2
velocity (km/s)

Figure 10

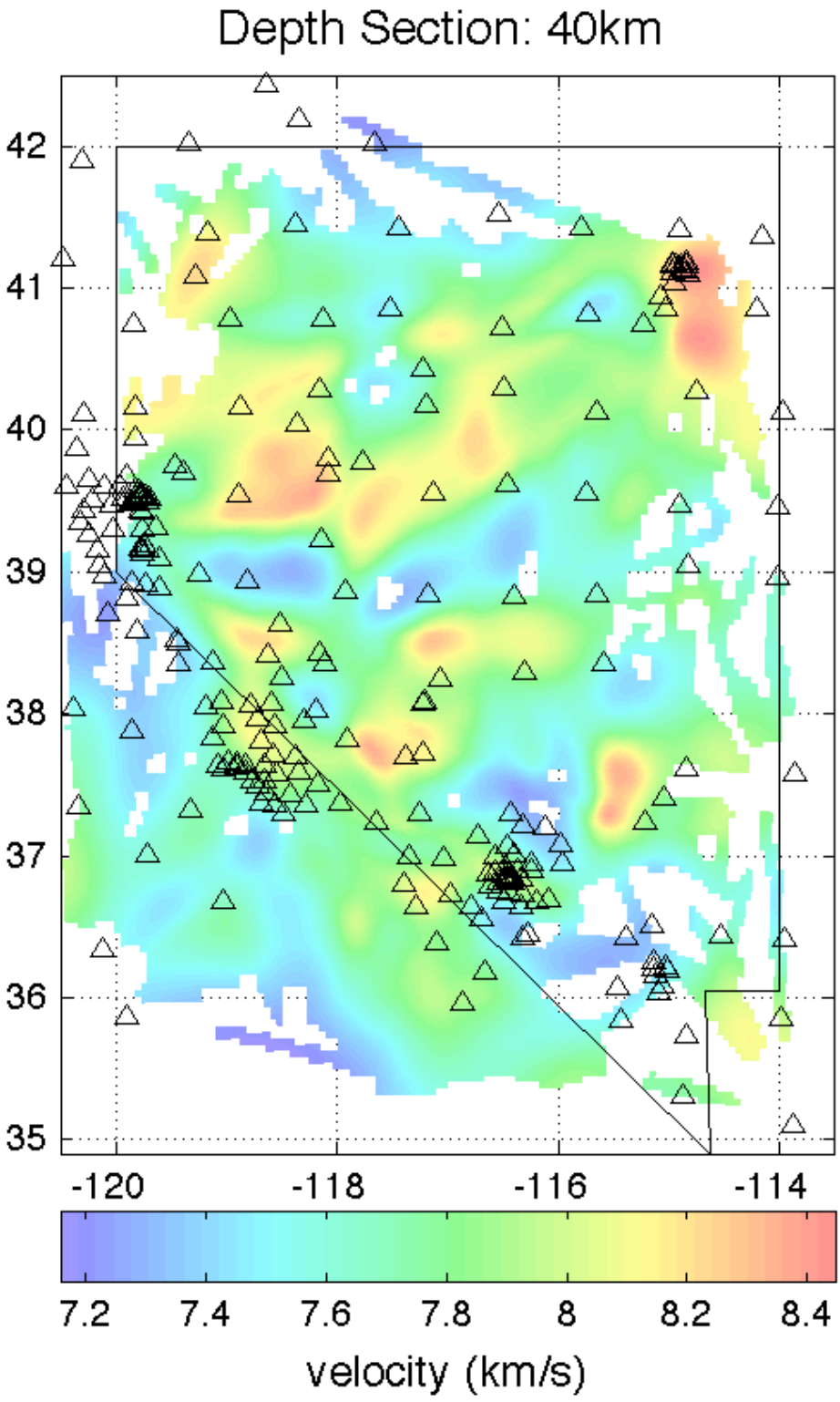
Depth Section: 40km
42
41
40
39
38
37
36
35
-120
-118
-116
-114
7.2
7.4
7.6
7.8
8
8.2
8.4
velocity (km/s)

Figure 11

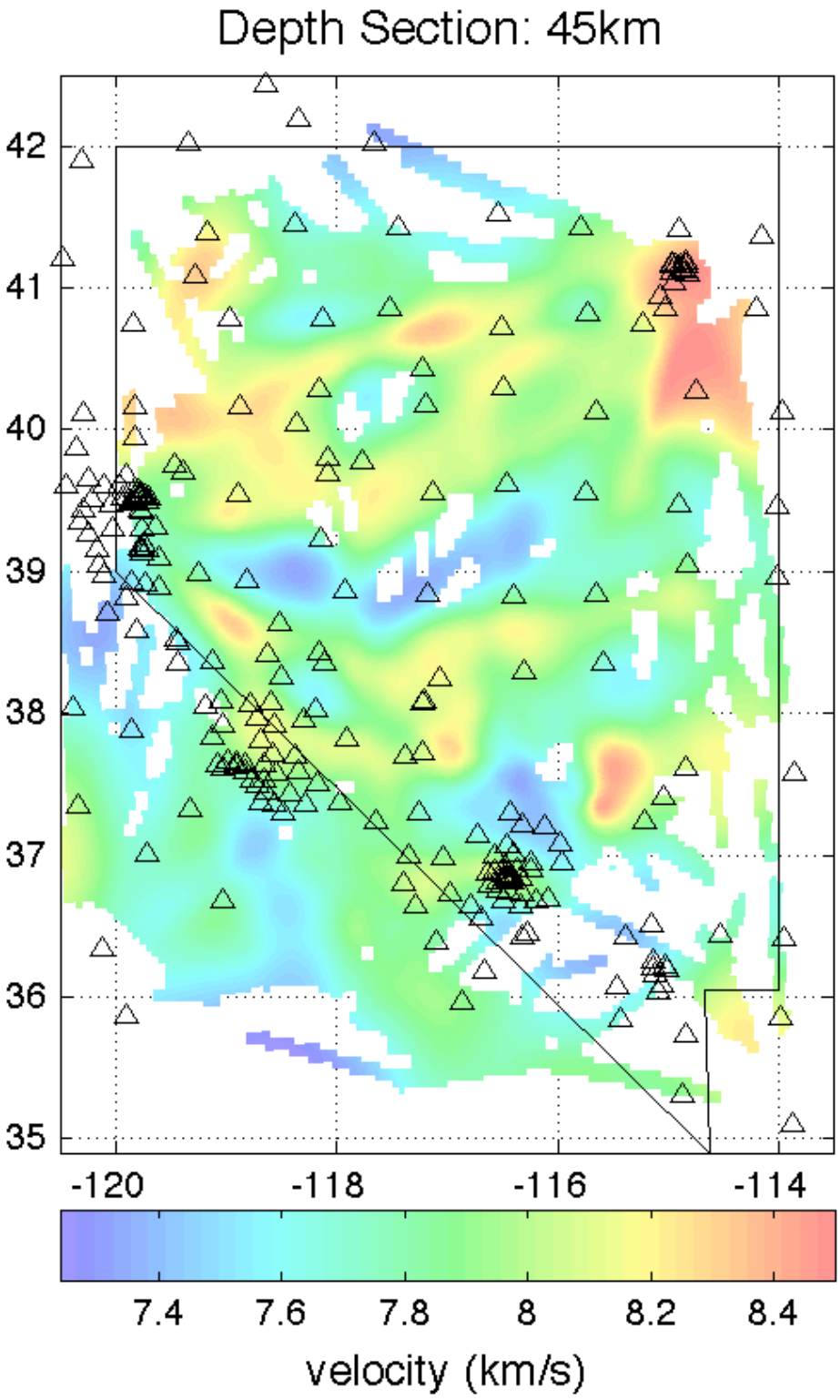
Depth Section: 45km
42
41
40
39
38
37
36
35
-120
-118
-116
-114
7.4
7.6
7.8
8
8.2
8.4
velocity (km/s)

## 11. Vp/Vs Depth Sections

Figures 12-19 are the Vp/Vs images in depth sections from 0 km (sea level) to 35 km depth in 5 km increments. Latitude and longitude are the plot coordinates. The color bar at the bottom of each figure gives the color scale. Note that the color scale changes with each depth. Stations are shown as triangles in all sections for reference. Black dots are earthquakes that locate within ±2.5 km of the given depth.

Figure 12

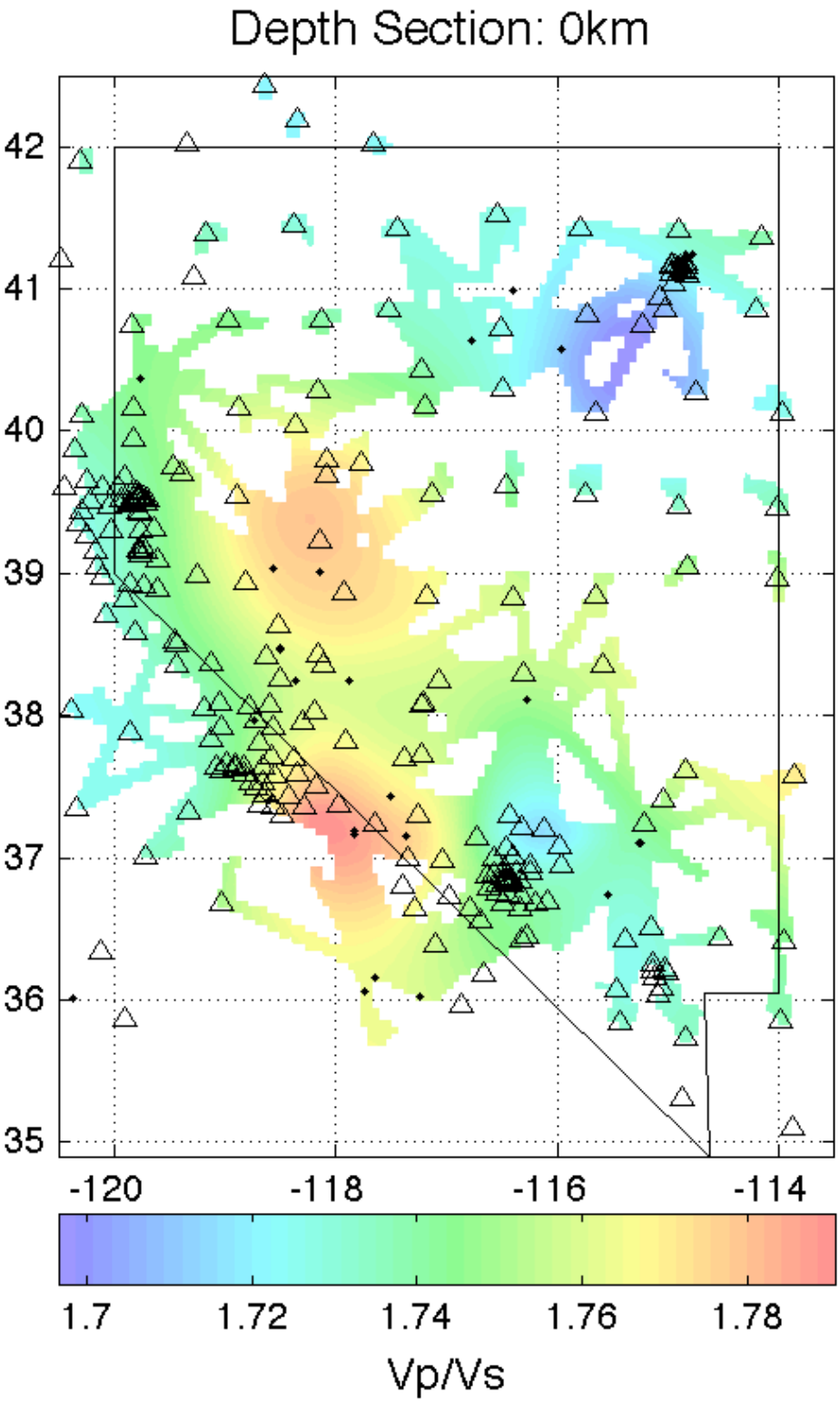
Depth Section: 0km
42
41
40
39
38
37
36
35
-120
-118
-116
-114
1.7
1.72
1.74
1.76
1.78
Vp/Vs

Figure 13

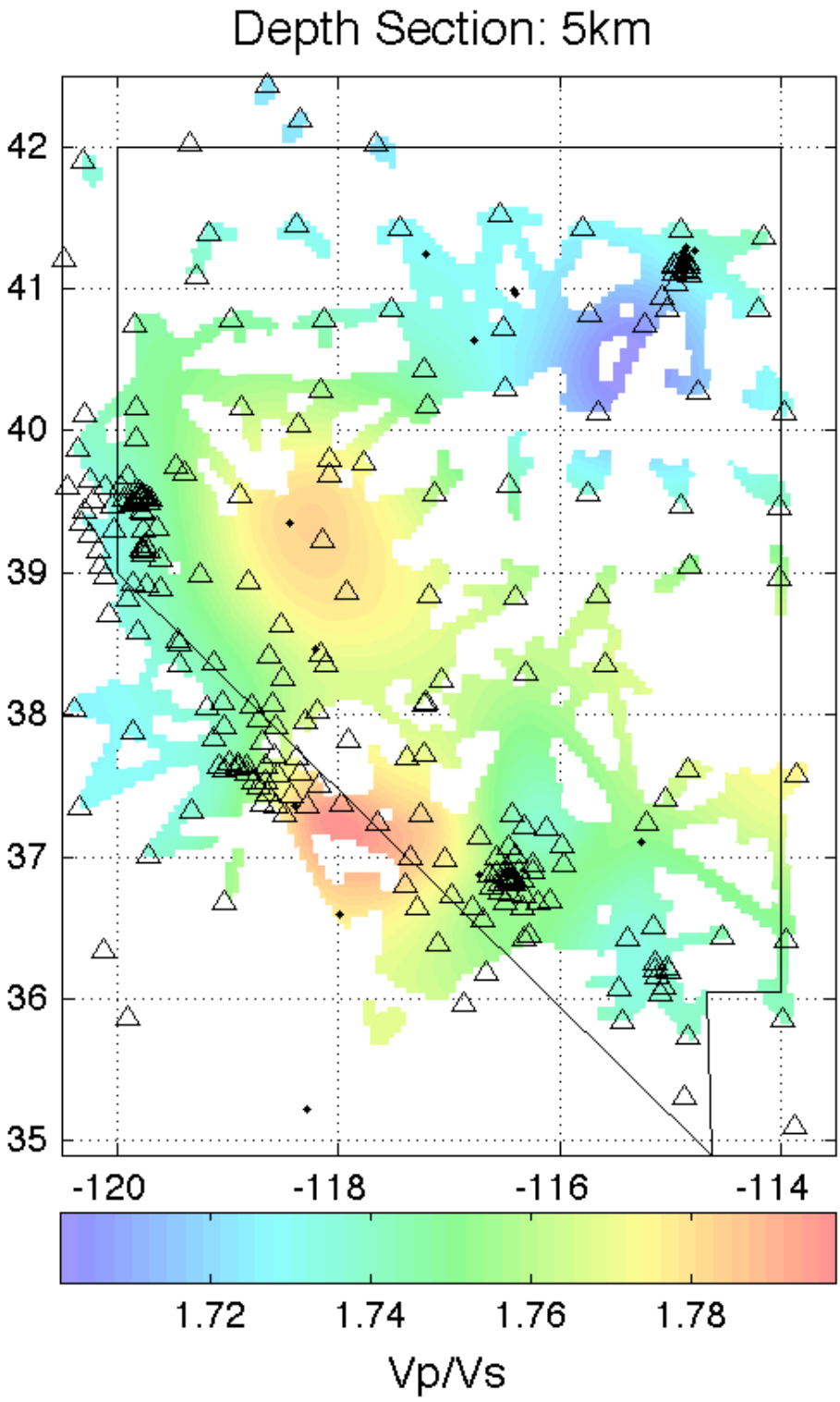
Depth Section: 5km
42
41
40
39
38
37
36
35
-120
-118
-116
-114
1.72
1.74
1.76
1.78
Vp/Vs

Figure 14

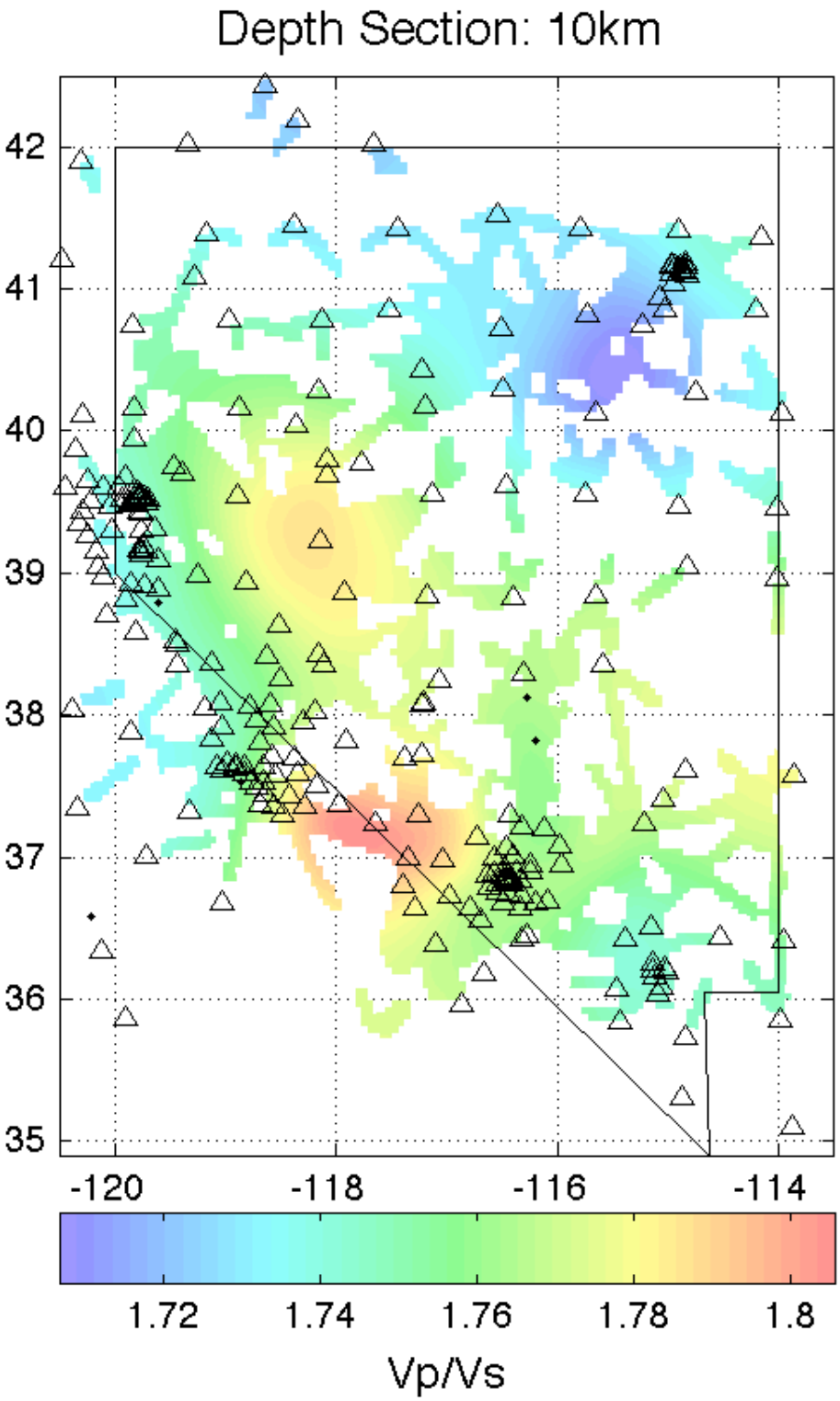
Depth Section: 10km
42
41
40
39
38
37
36
35
-120
-118
-116
-114
1.72
1.74
1.76
1.78
1.8
Vp/Vs

Figure 15

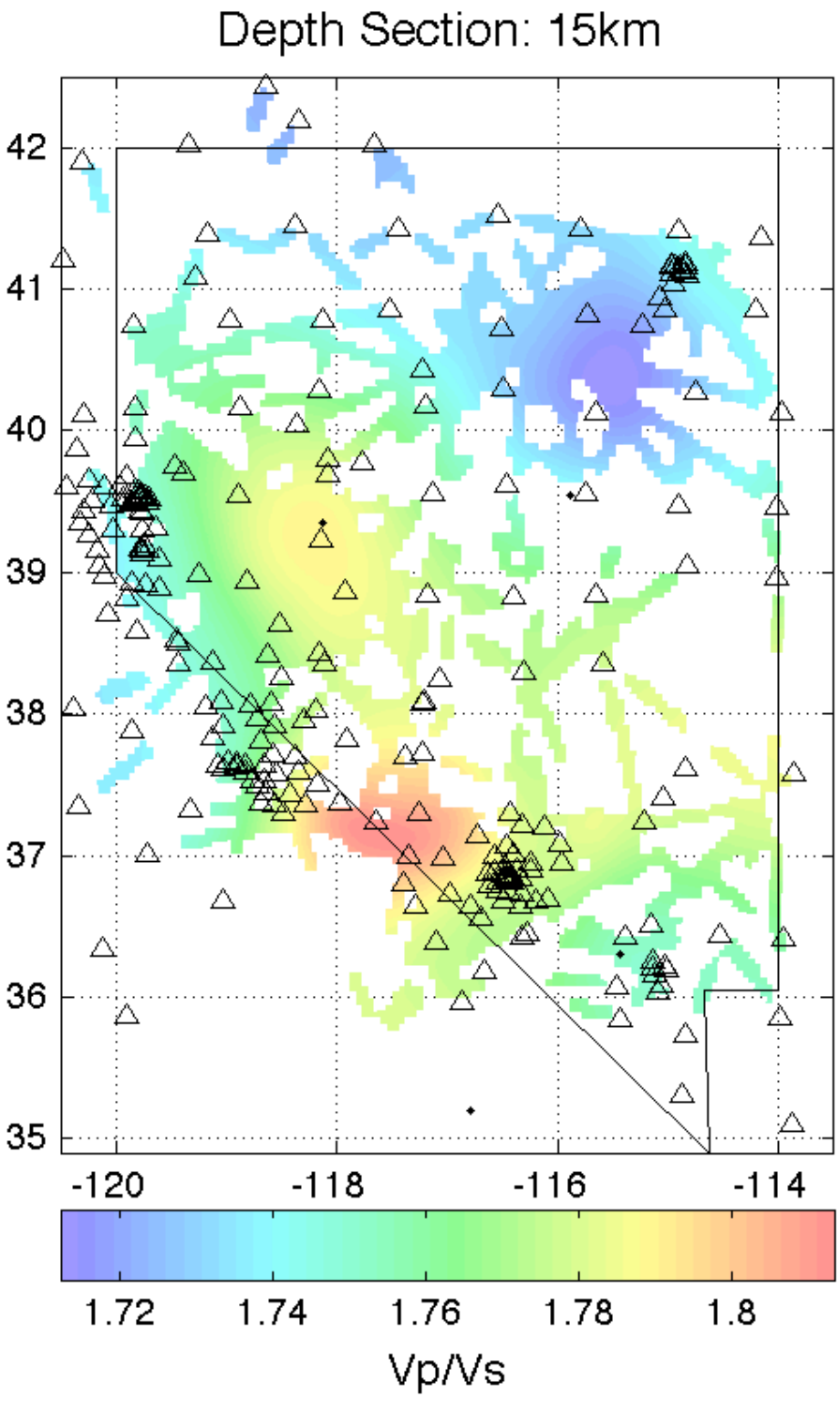
Depth Section: 15km
42
41
40
39
38
37
36
35
-120
-118
-116
-114
1.72
1.74
1.76
1.78
1.8
Vp/Vs

Figure 16

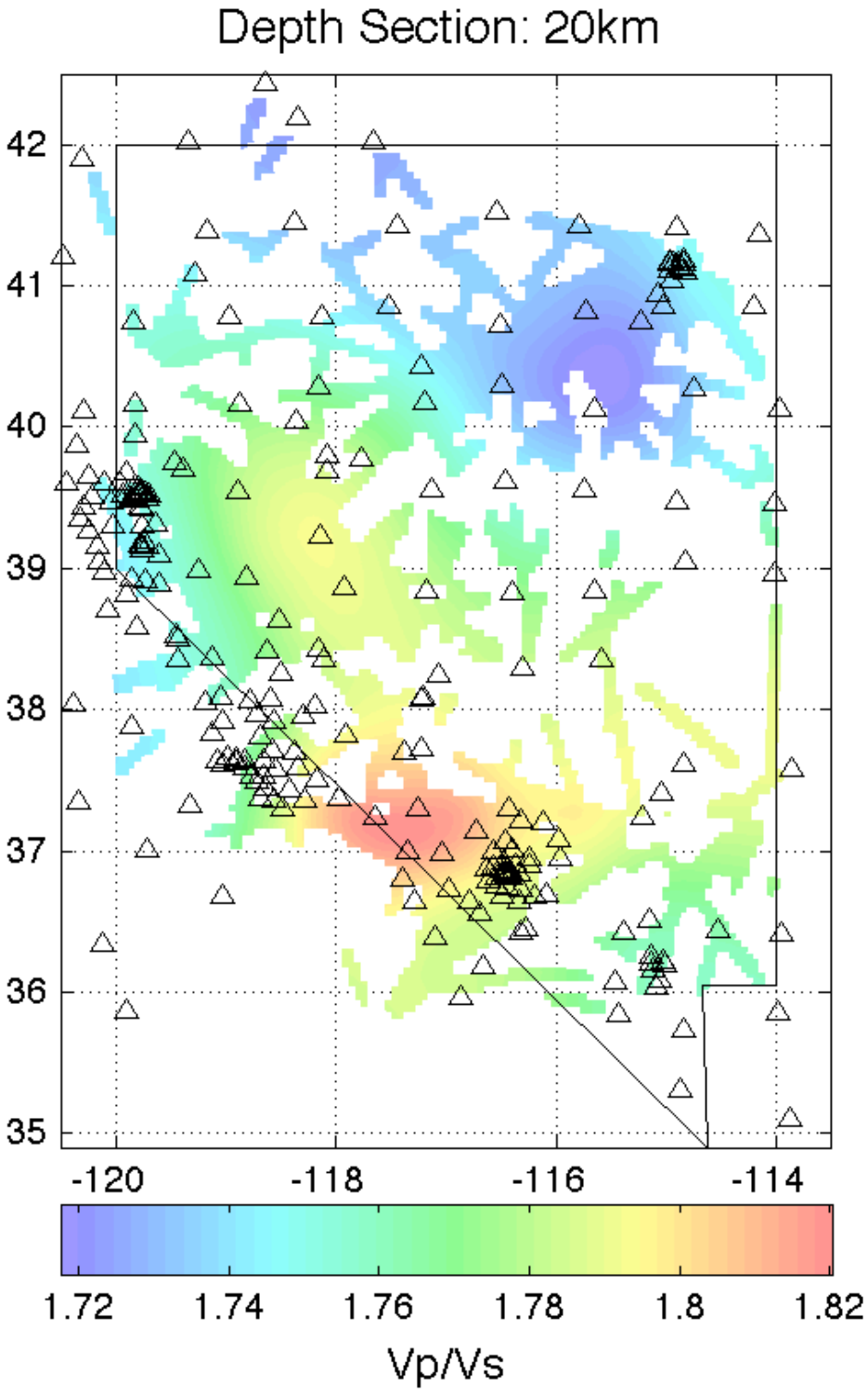
Depth Section: 20km
42
41
40
39
38
37
36
35
-120
-118
-116
-114
1.72
1.74
1.76
1.78
1.8
1.82
Vp/Vs

Figure 17

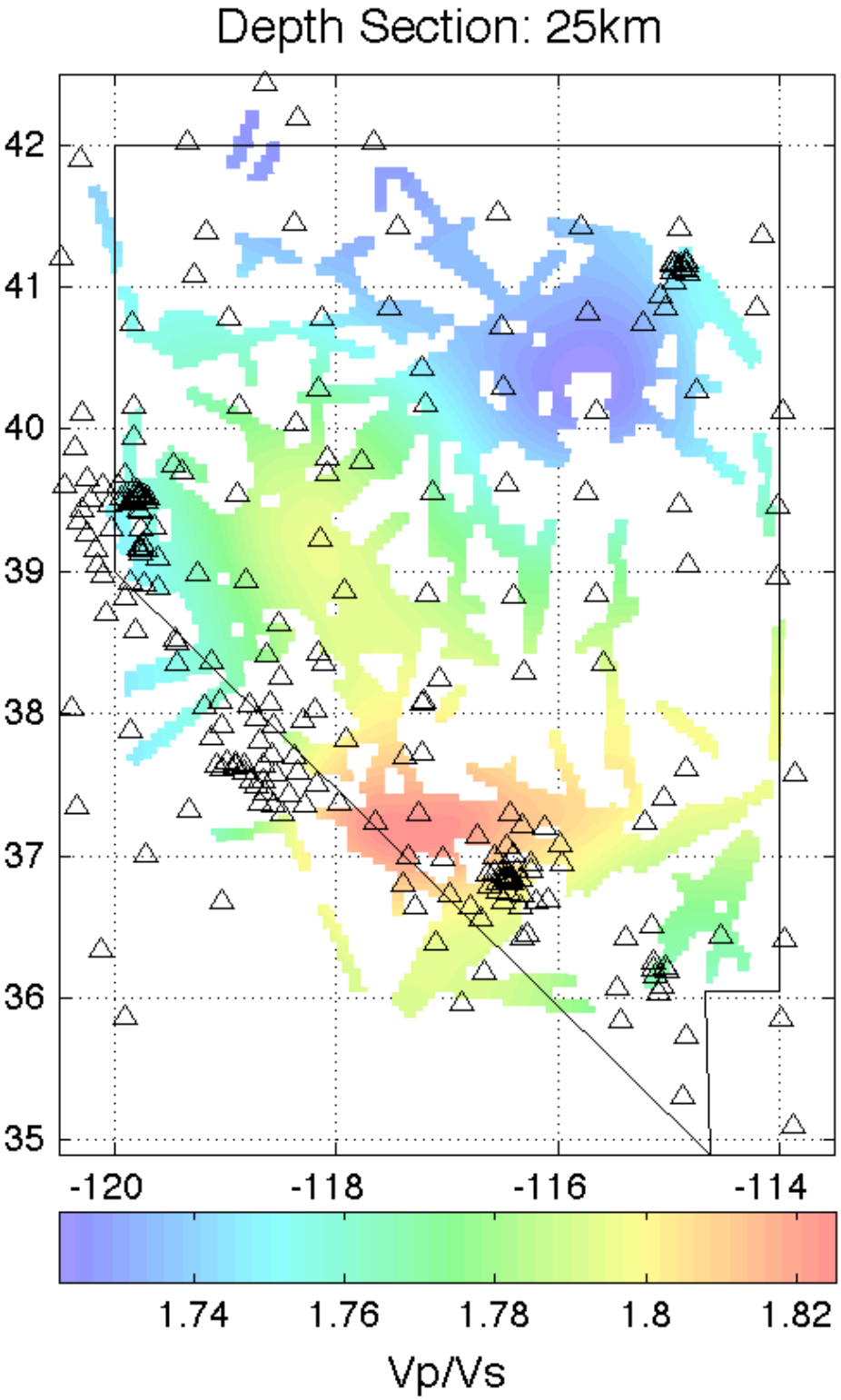
Depth Section: 25km
42
41
40
39
38
37
36
35
-120
-118
-116
-114
1.74
1.76
1.78
1.8
1.82
Vp/Vs

Figure 18

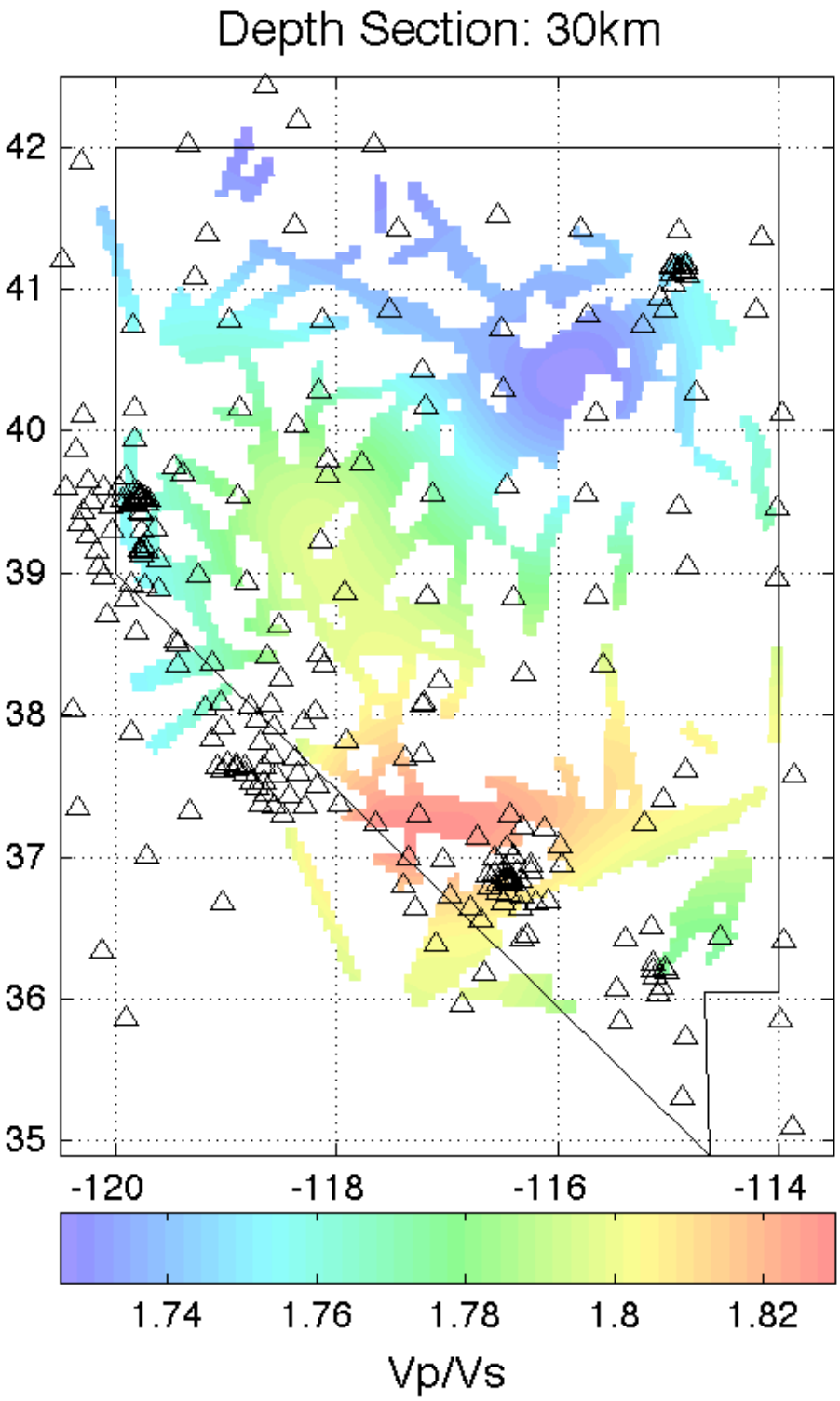
Depth Section: 30km
42
41
40
39
38
37
36
35
-120
-118
-116
-114
1.74
1.76
1.78
1.8
1.82
Vp/Vs

Figure 19

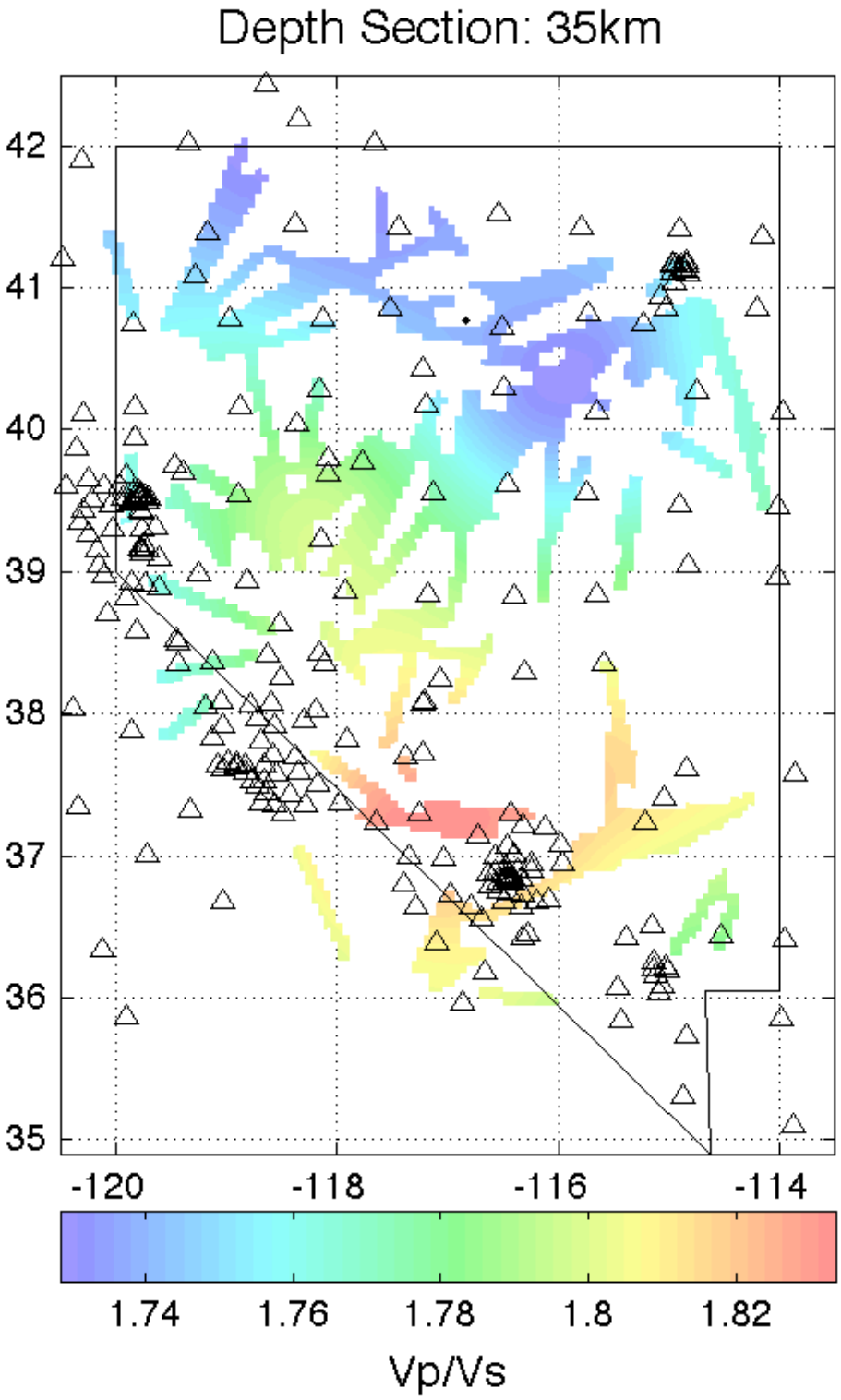
Depth Section: 35km
42
41
40
39
38
37
36
35
-120
-118
-116
-114
1.74
1.76
1.78
1.8
1.82
Vp/Vs

## 12. Checkerboard Tests

Figures 20-55 show the checkerboard test results in depth sections from 0 km (sea level) to 45 km depth in 5 km increments. Latitude and longitude are the plot coordinates. The color bar at the bottom of each figure gives the color scale. Stations are shown as triangles in all sections for reference. Black dots are earthquakes that locate within ±2.5 km of the given depth. Checkerboard tests for 50 by 50 km and 100 by 100 km are shown for P-waves and 100 by 100 km and 200 by 200 km for Vp/Vs (Vp/Vs is only shown to 35 km depth).

Figure 20

**50 x 50 km Vp checkerboard**

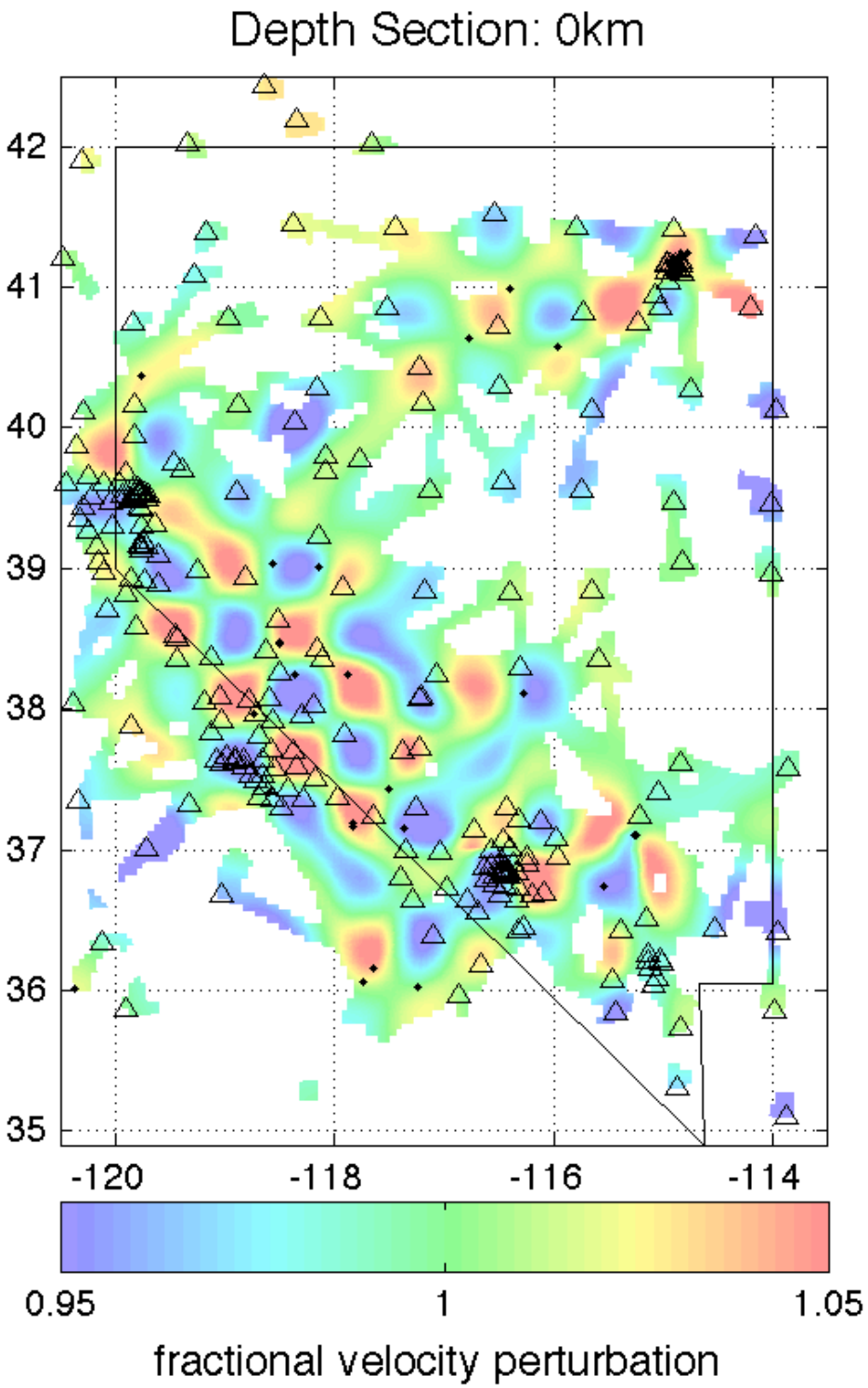

Figure 21 **50 x 50 km Vp checkerboard**

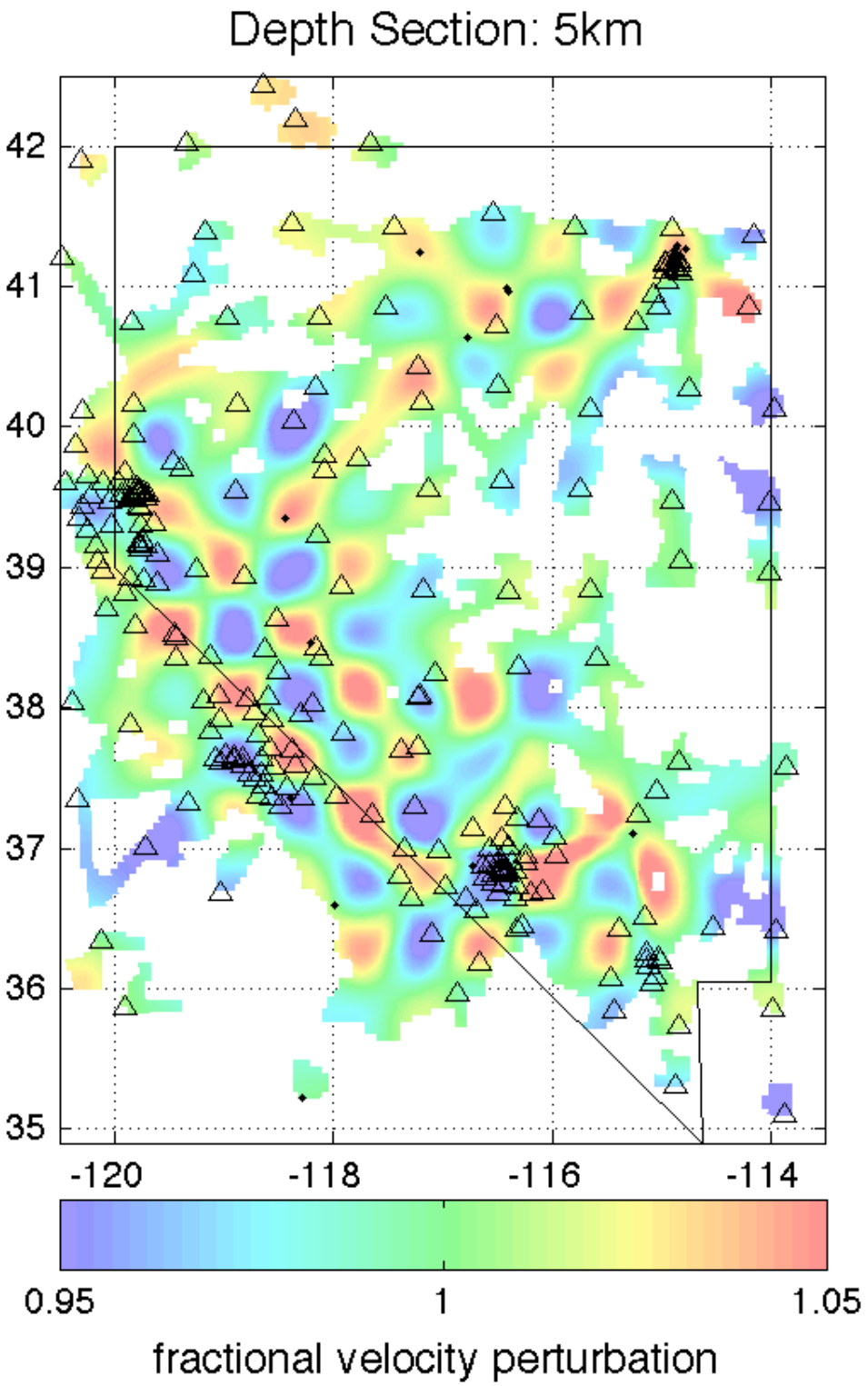

Figure 22 **50 x 50 km Vp checkerboard**

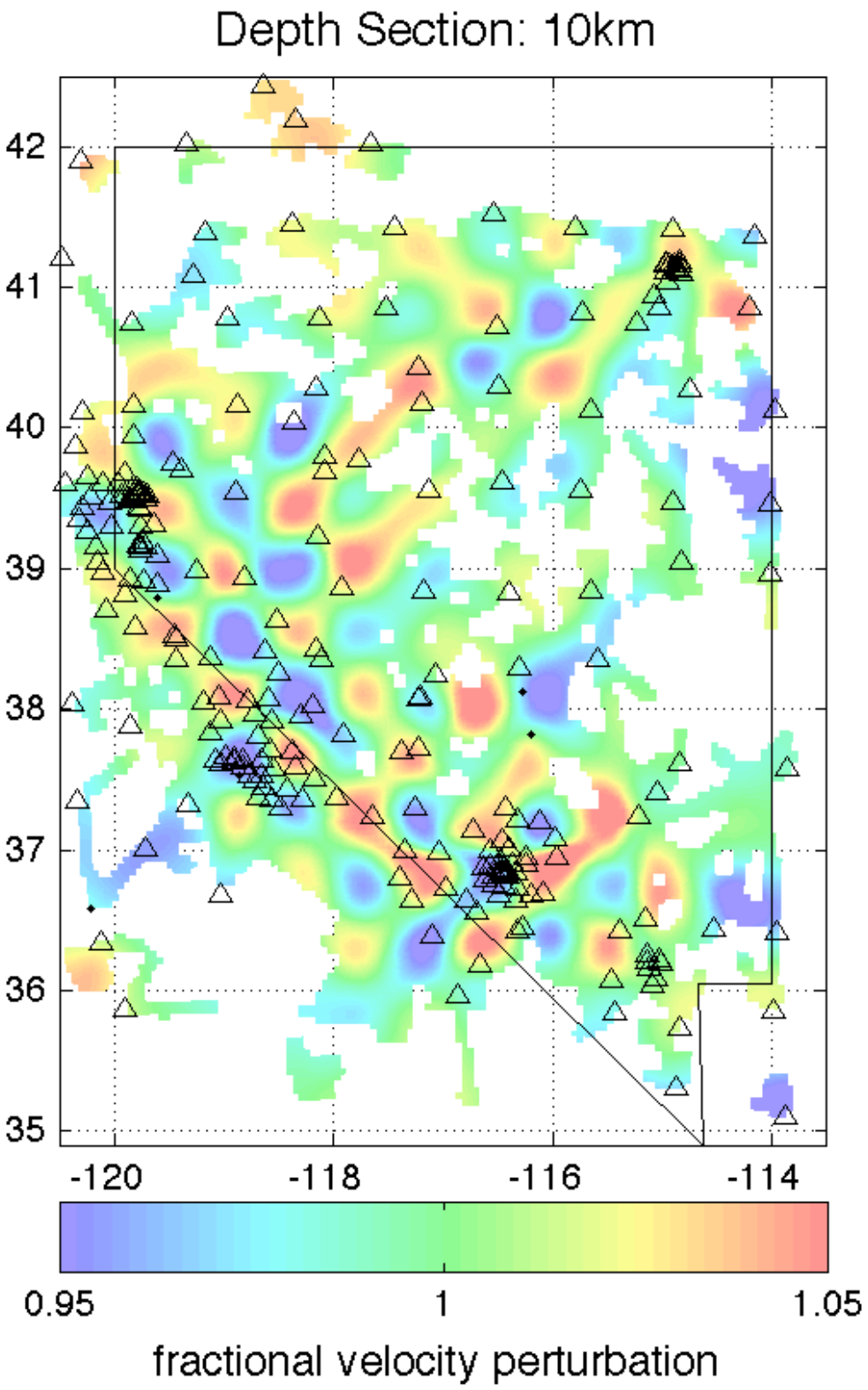

Figure 23 **50 x 50 km Vp checkerboard**

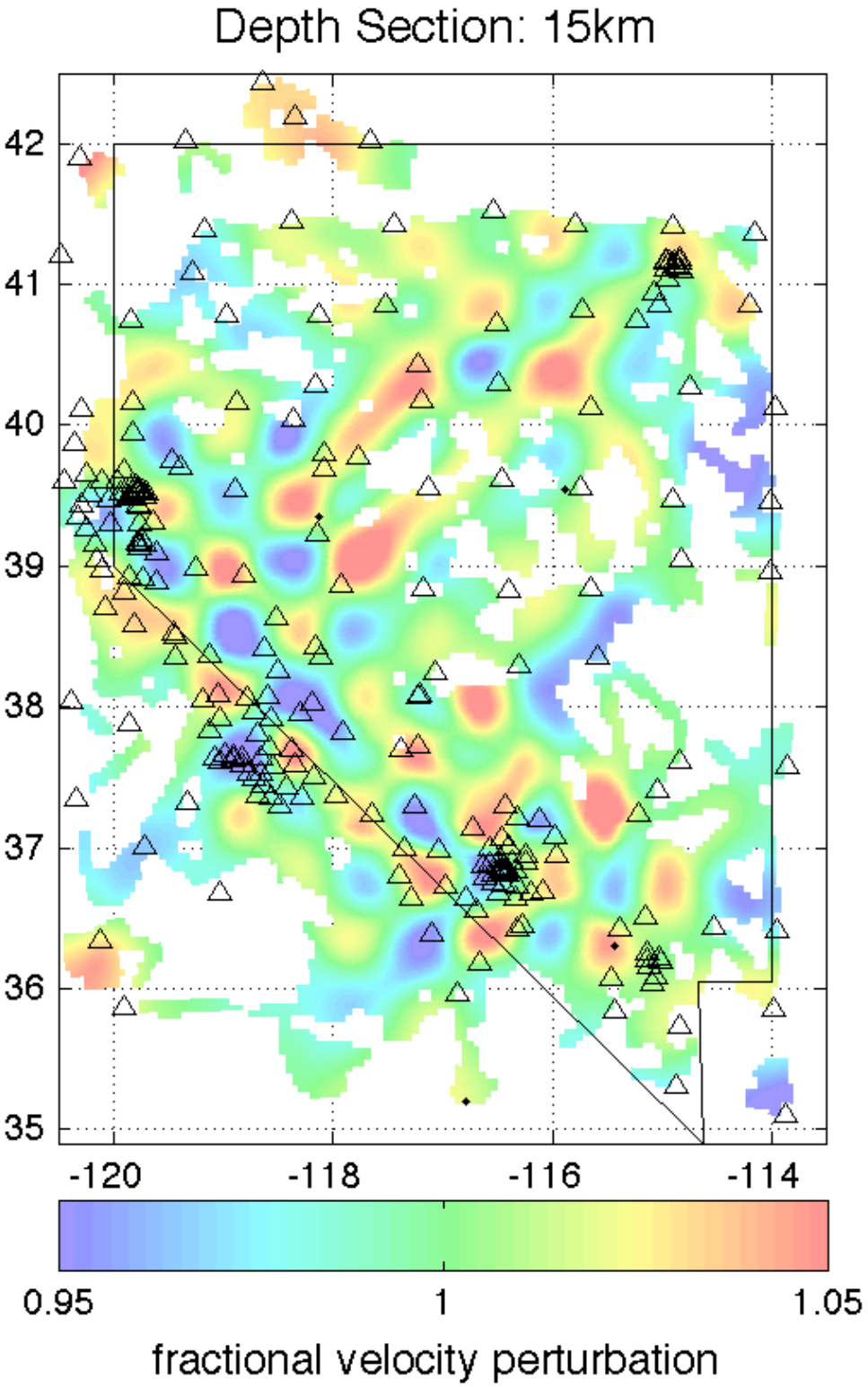

Figure 24 **50 x 50 km Vp checkerboard**

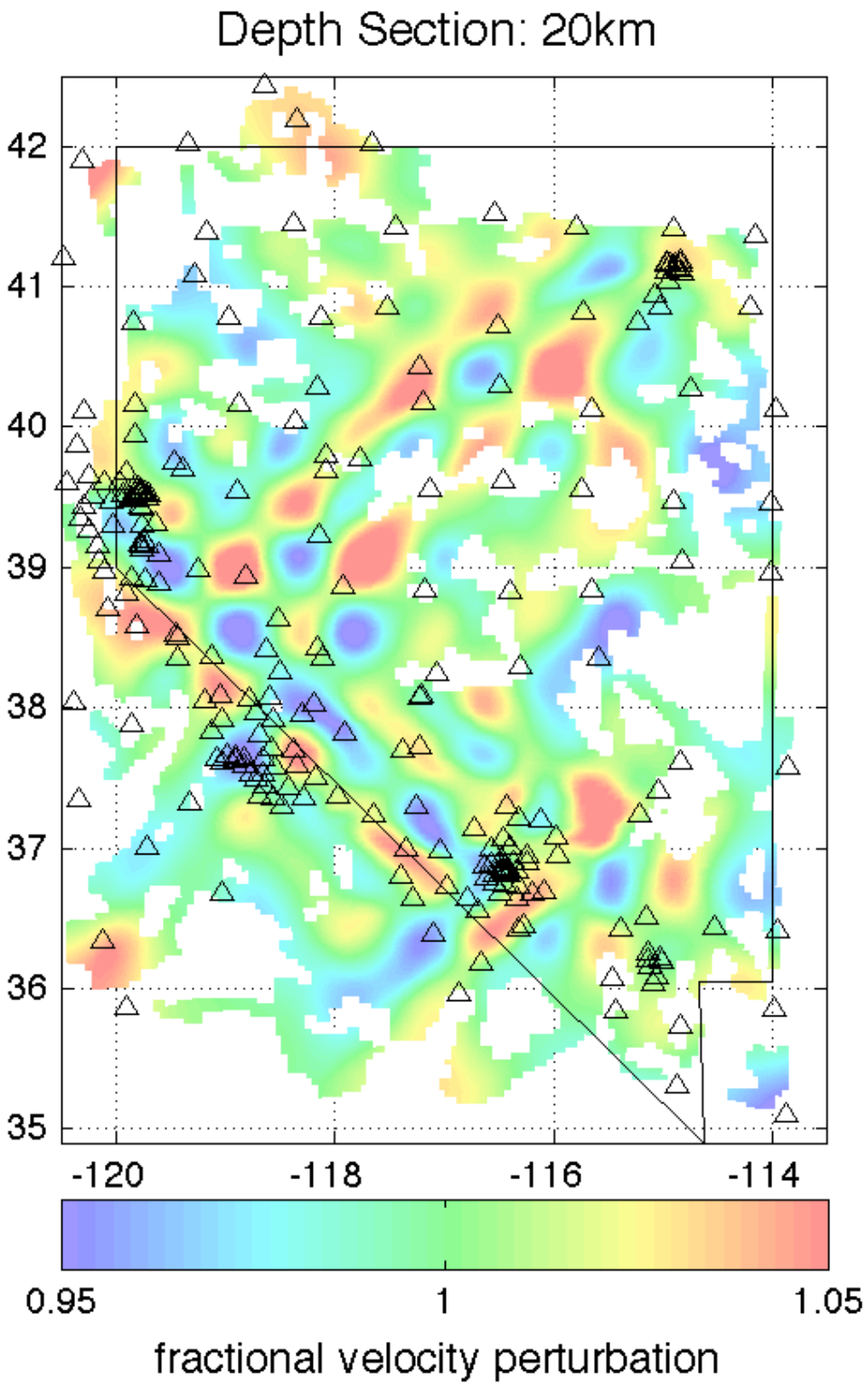

Figure 25 **50 x 50 km Vp checkerboard**

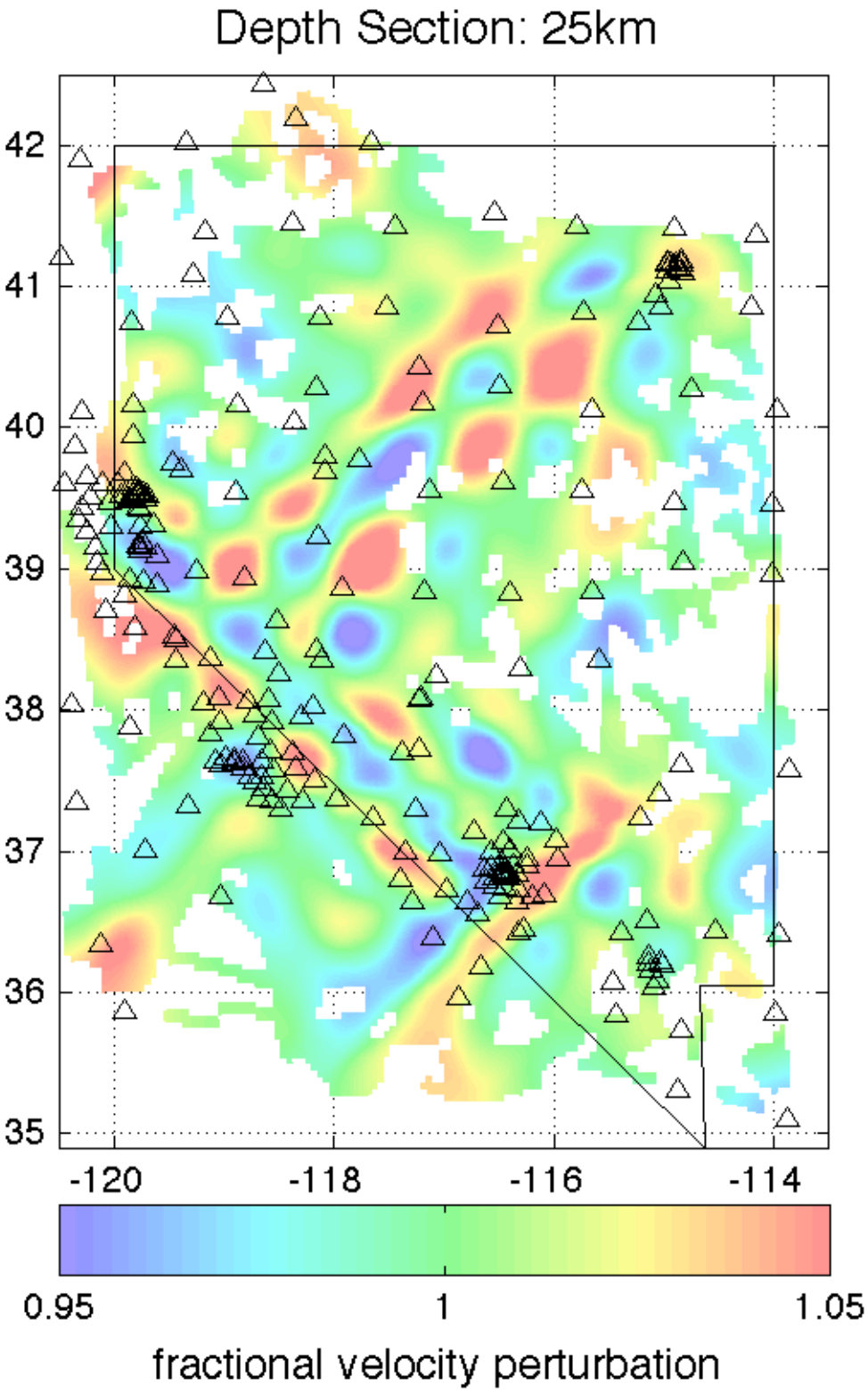

Figure 26

**50 x 50 km Vp checkerboard**

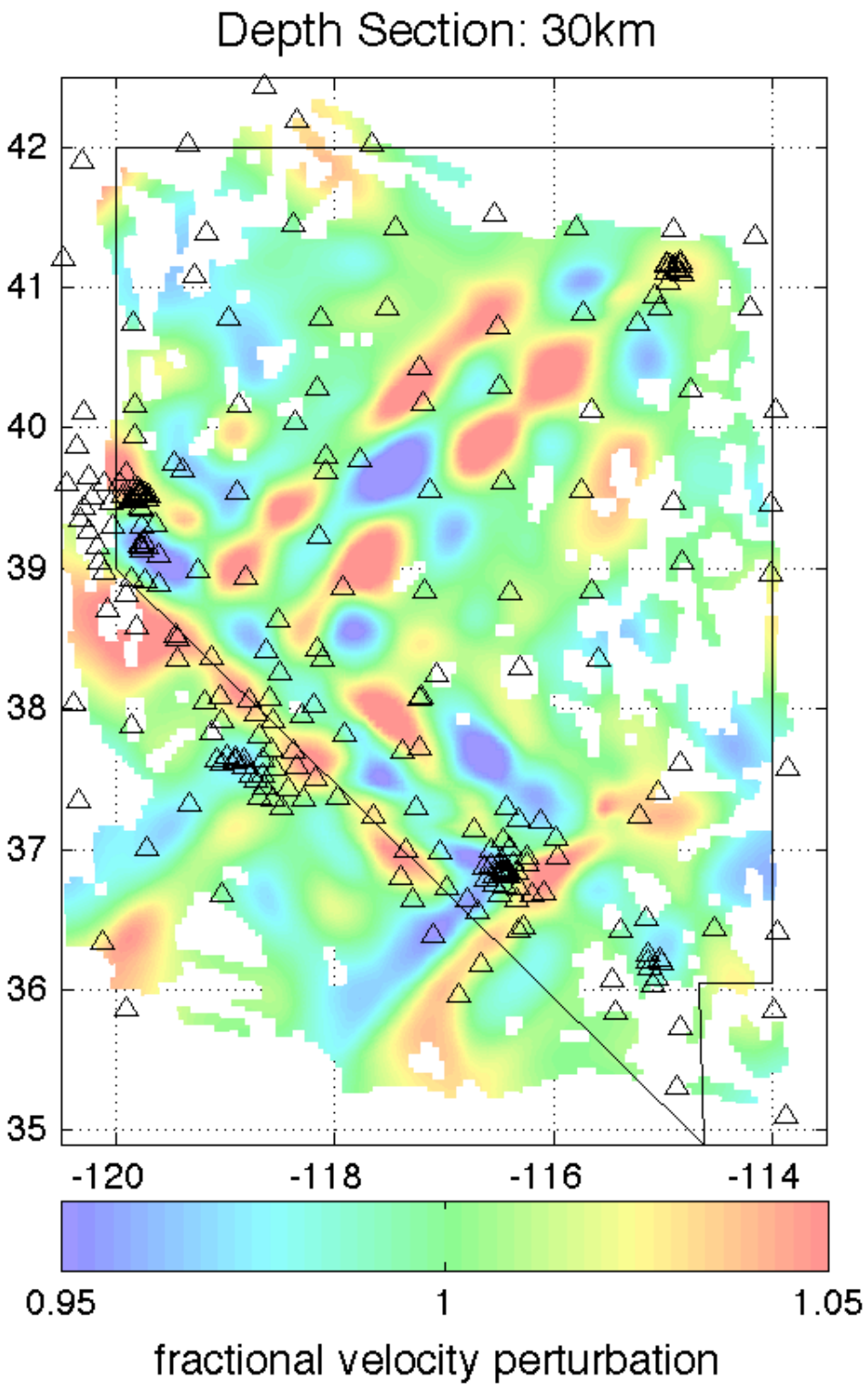

Figure 27 **50 x 50 km Vp checkerboard**

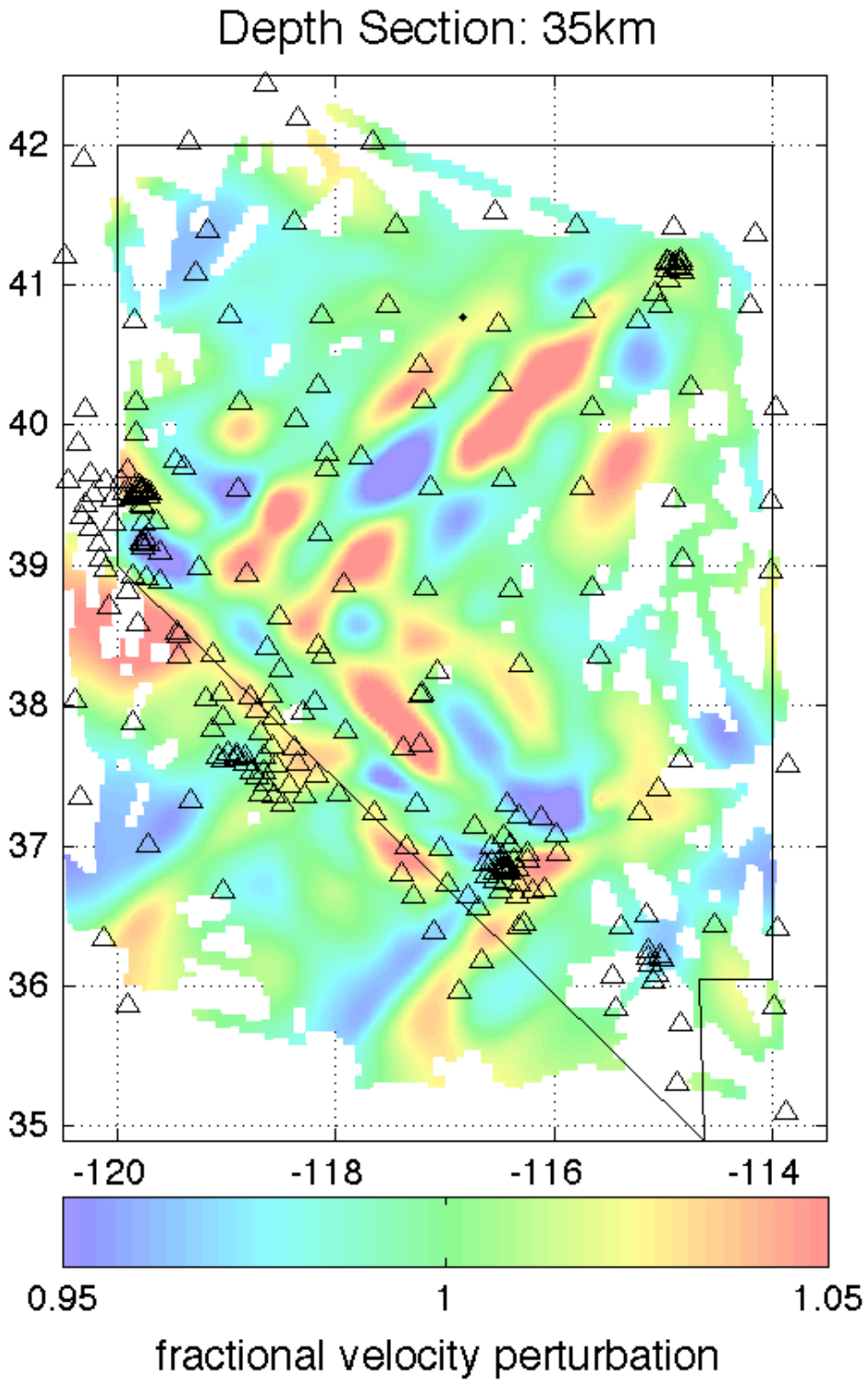

Figure 28 **50 x 50 km Vp checkerboard**

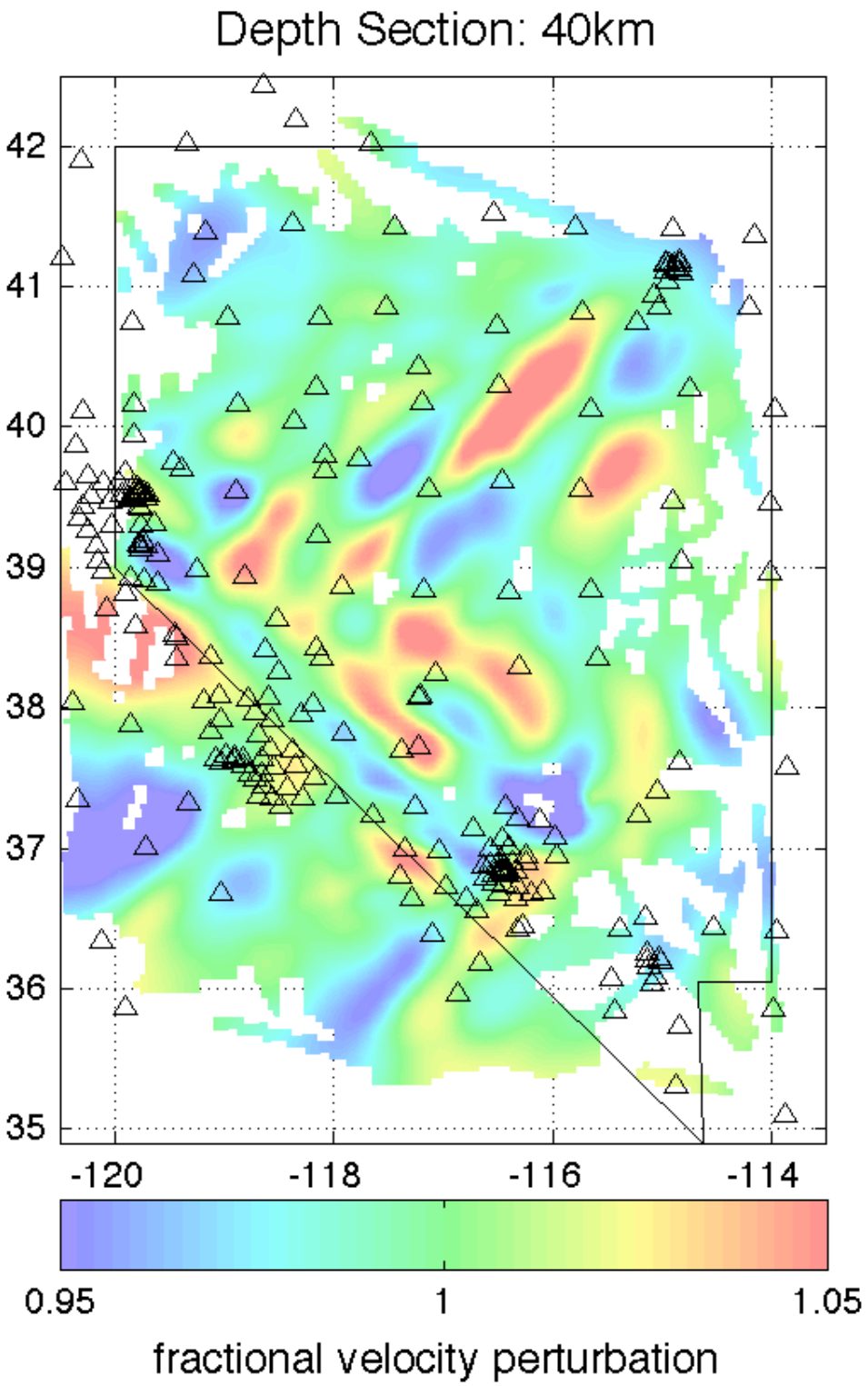

Figure 29 **50 x 50 km Vp checkerboard**

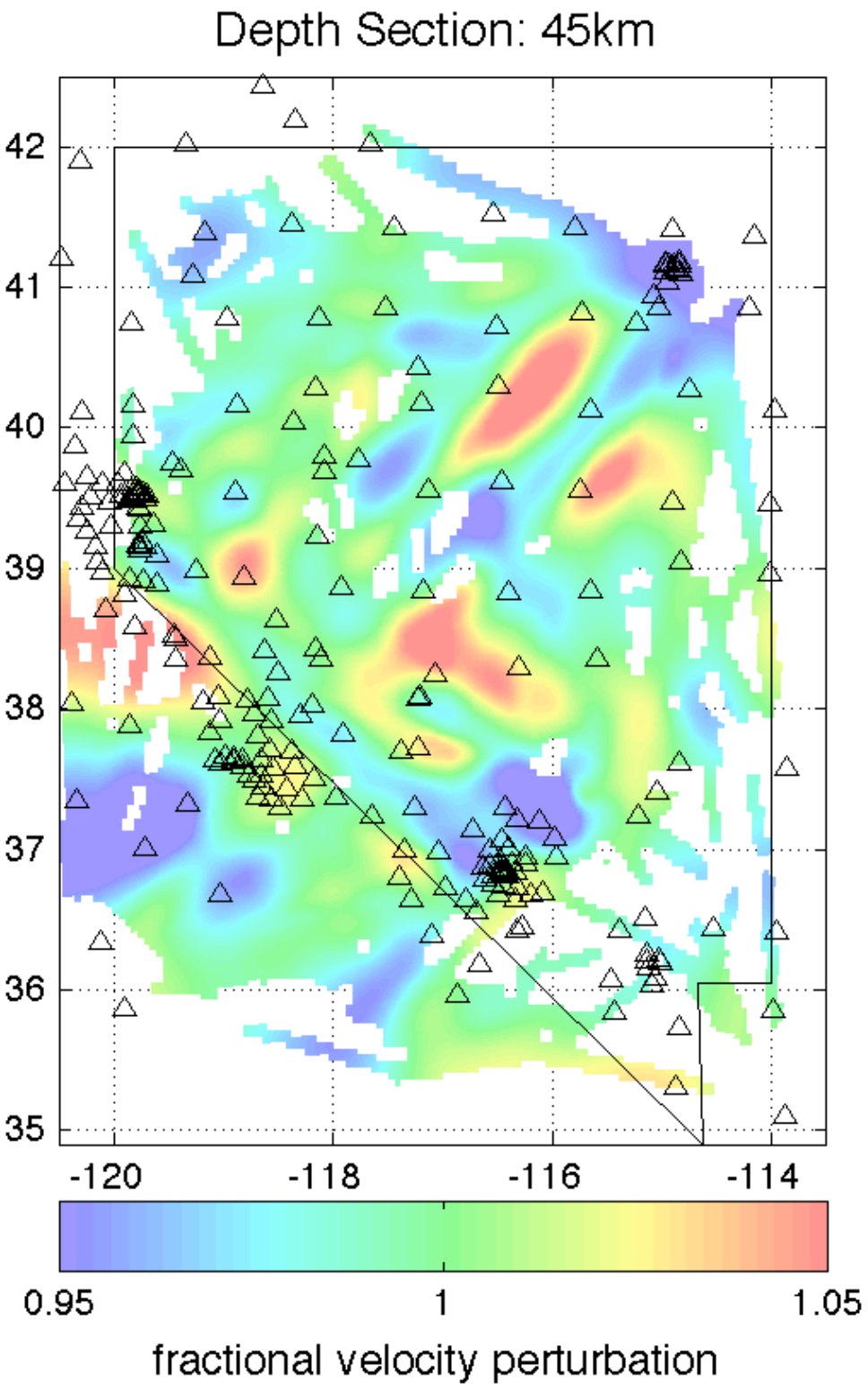

Figure 30

**100 x 100 km Vp checkerboard**

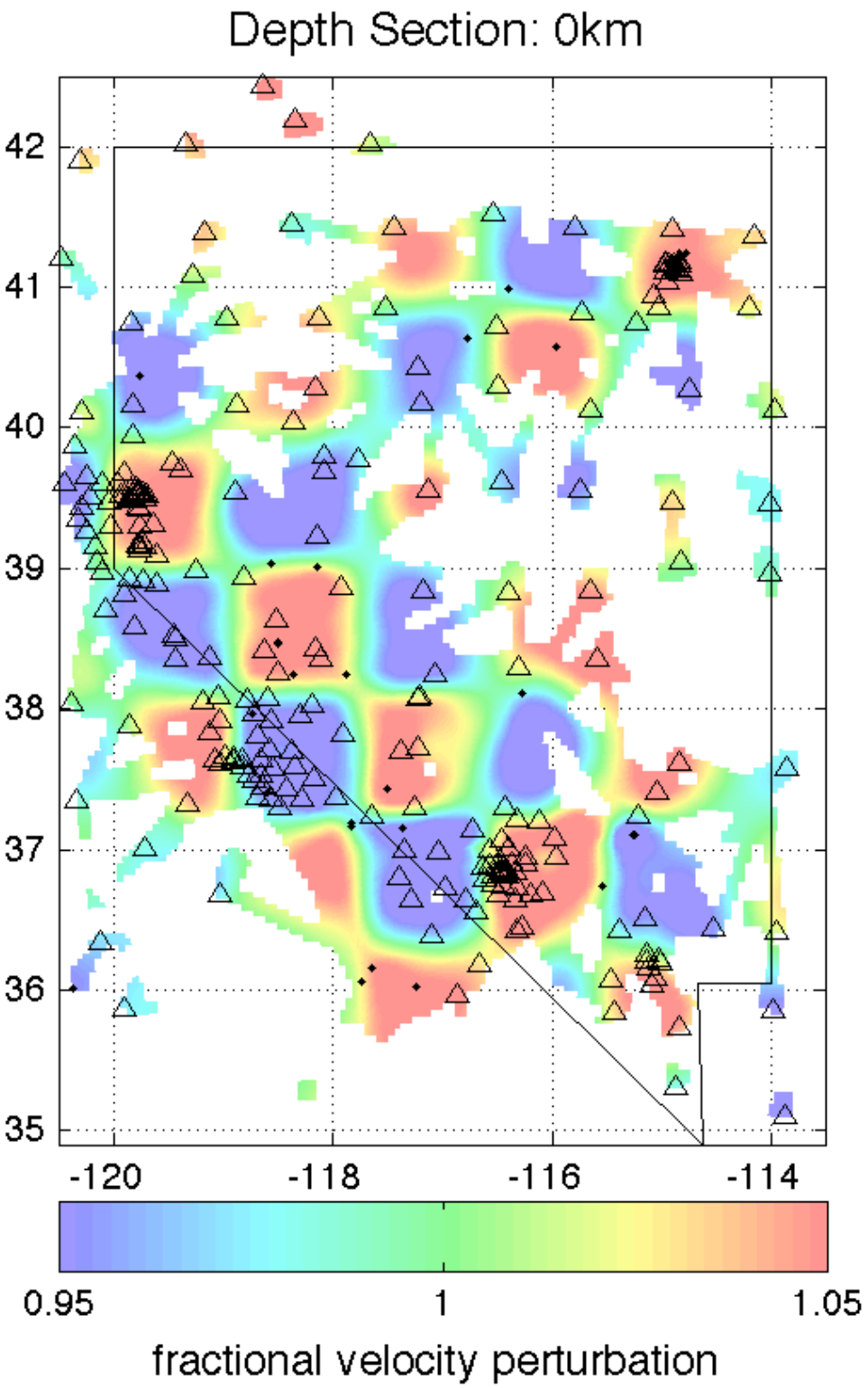

Figure 31

**100 x 100 km Vp checkerboard**

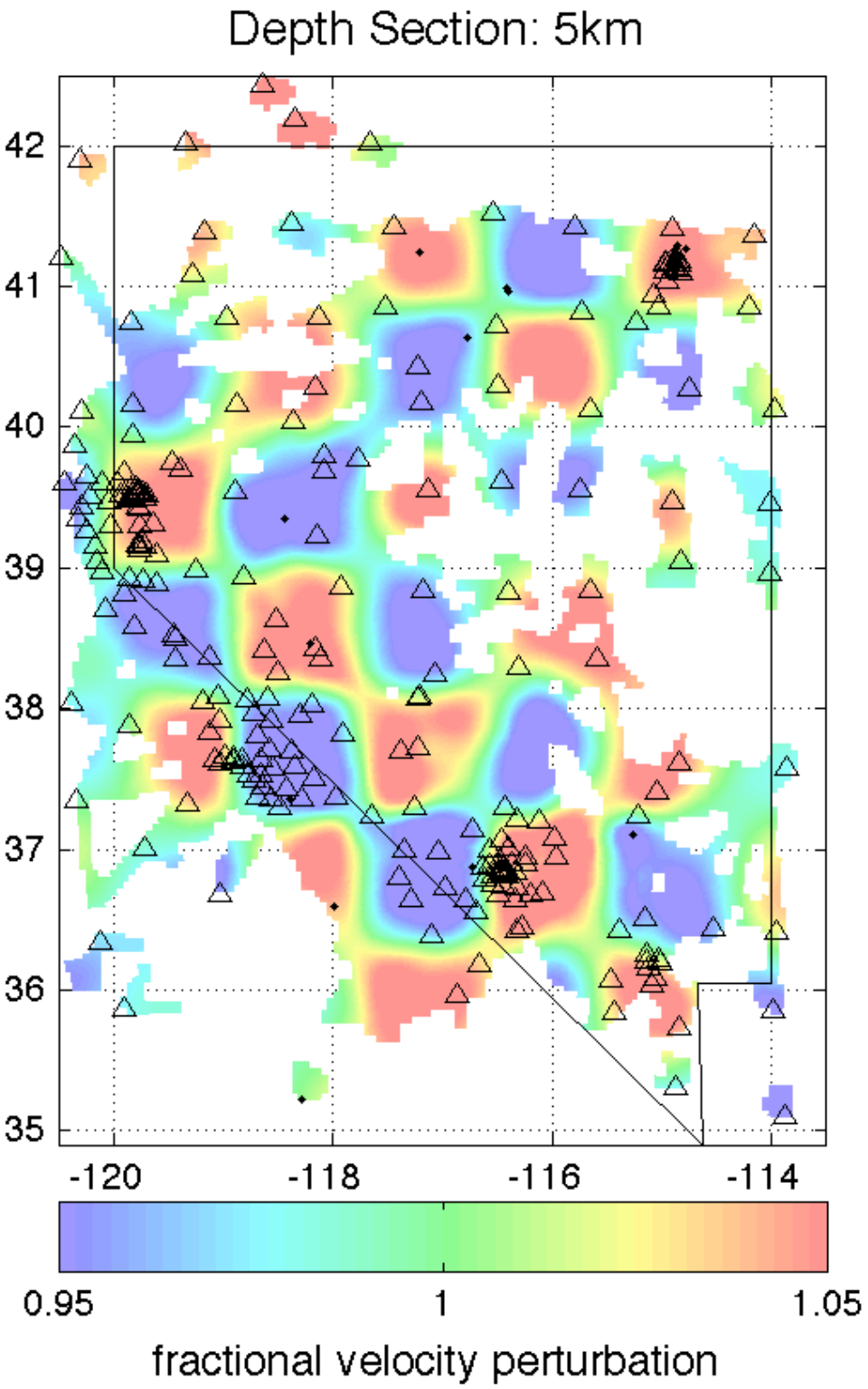

Figure 32

**100 x 100 km Vp checkerboard**

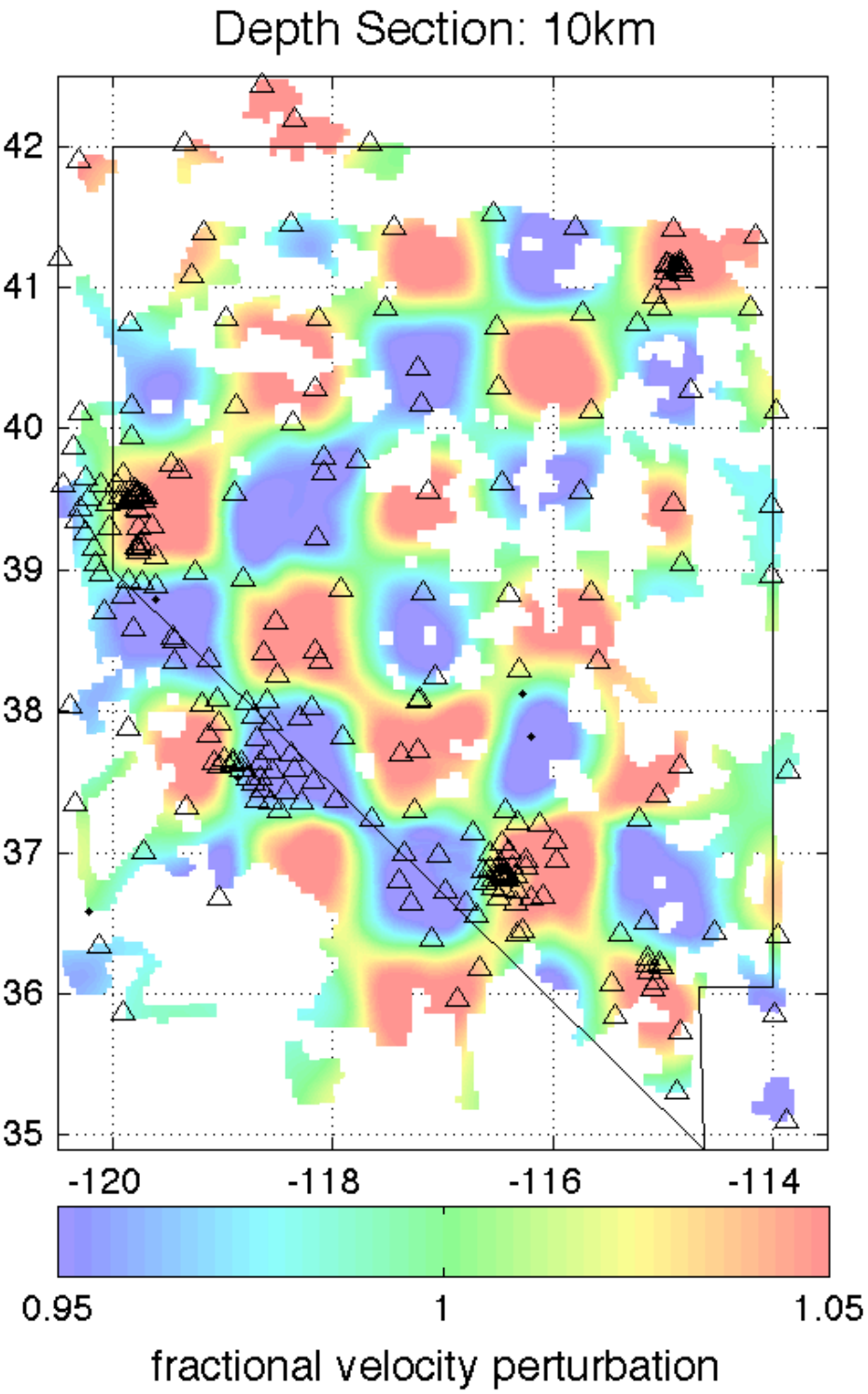

Figure 33

**100 x 100 km Vp checkerboard**

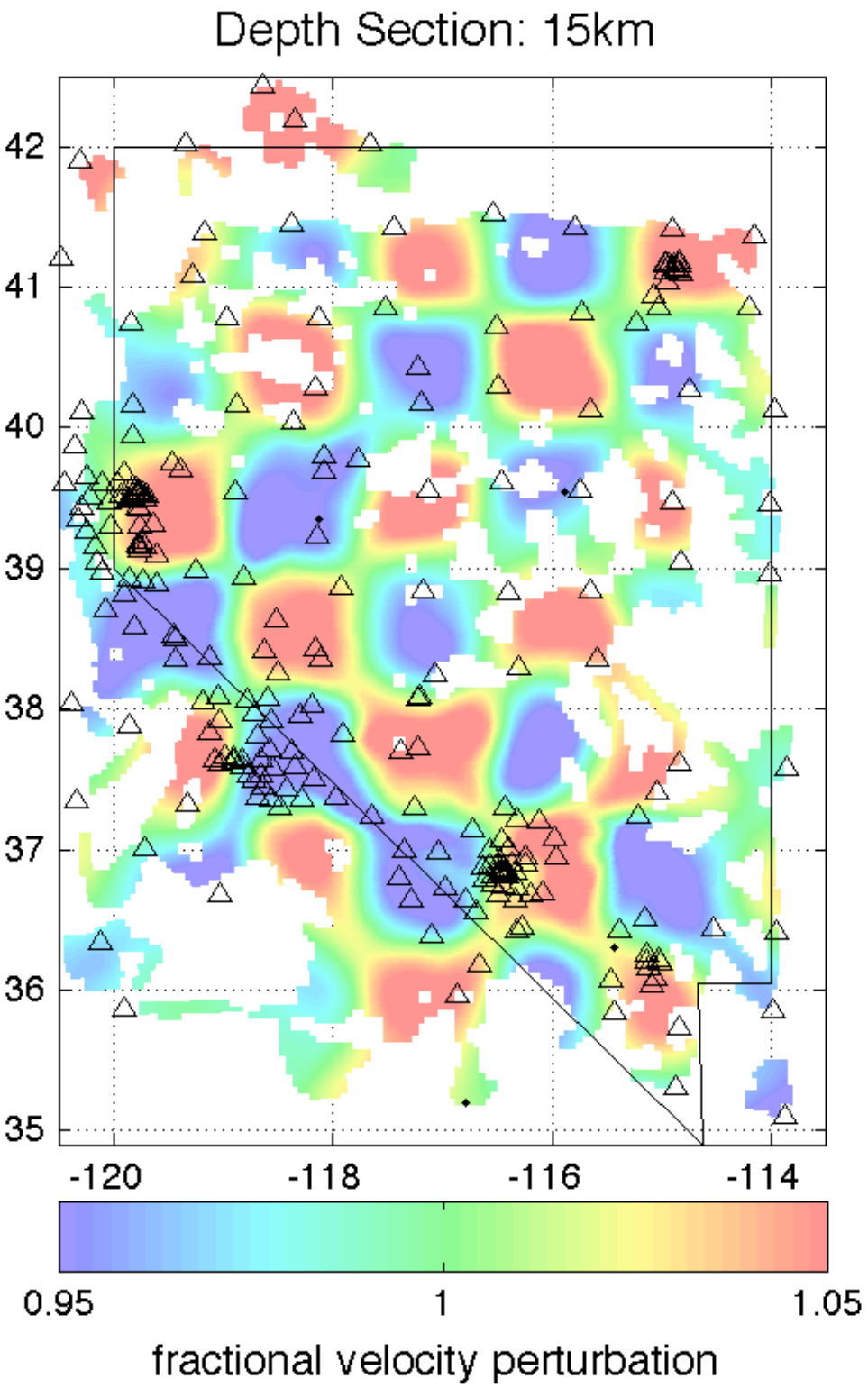

Figure 34

**100 x 100 km Vp checkerboard**

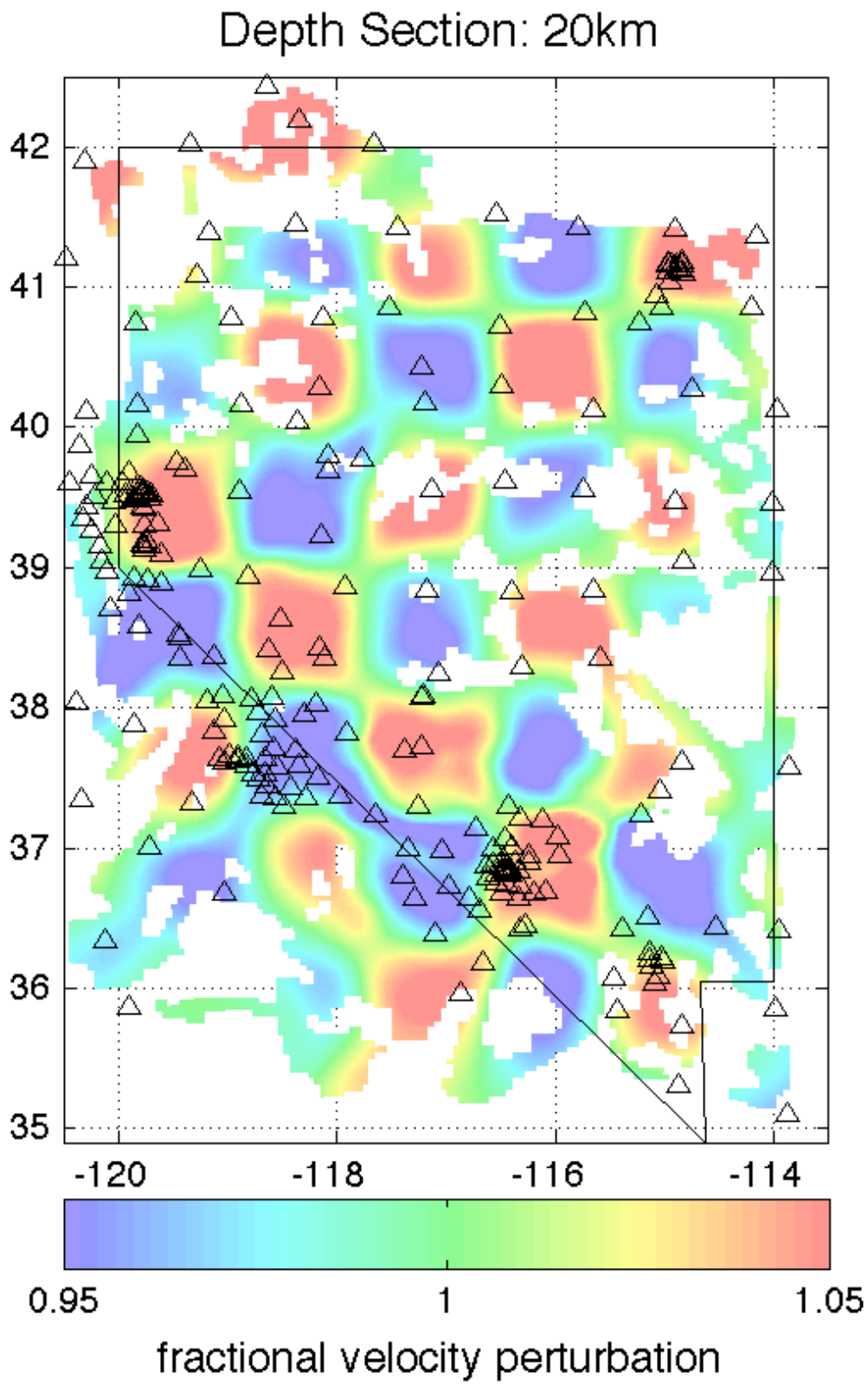

Figure 35

**100 x 100 km Vp checkerboard**

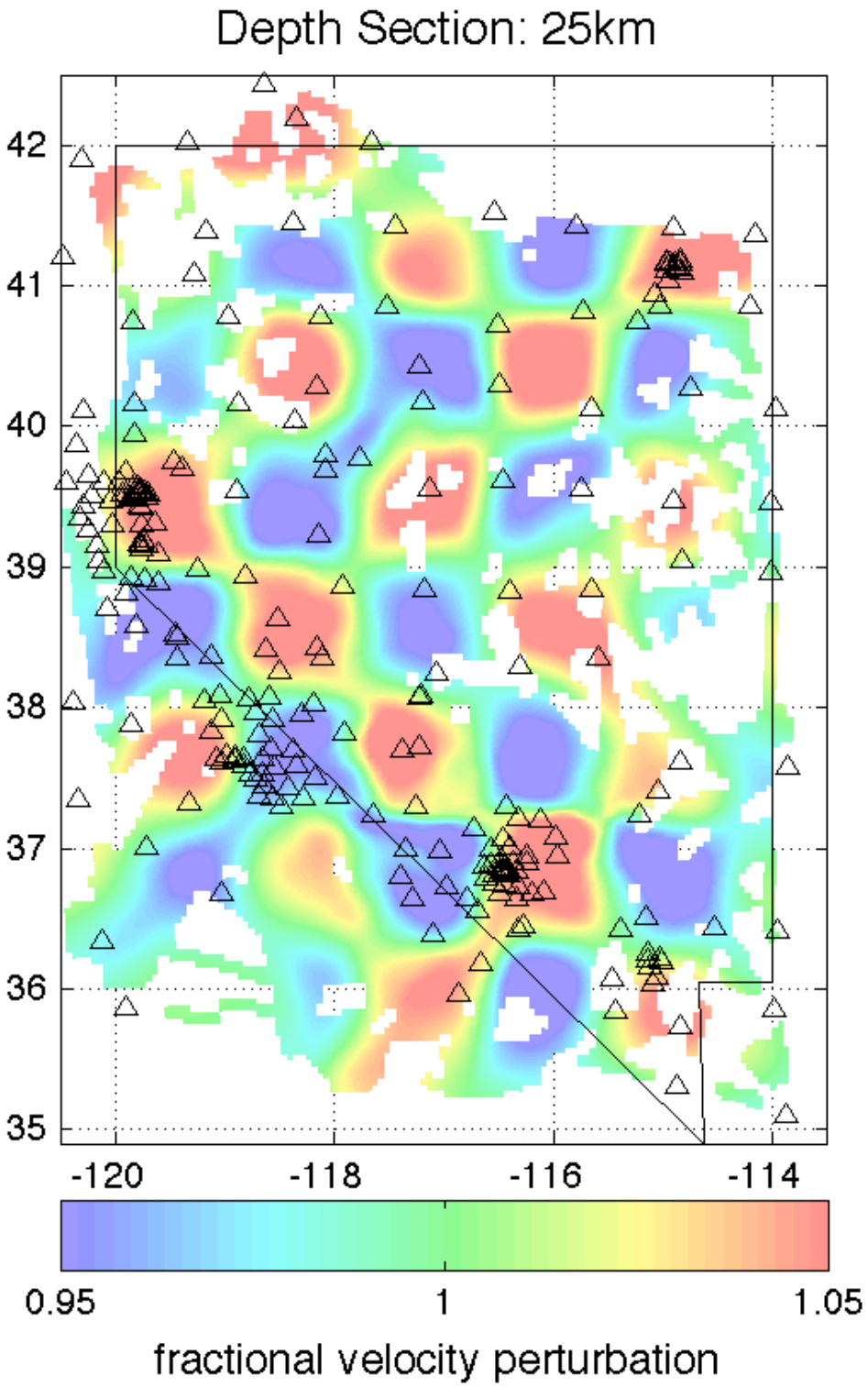

Figure 36

**100 x 100 km Vp checkerboard**

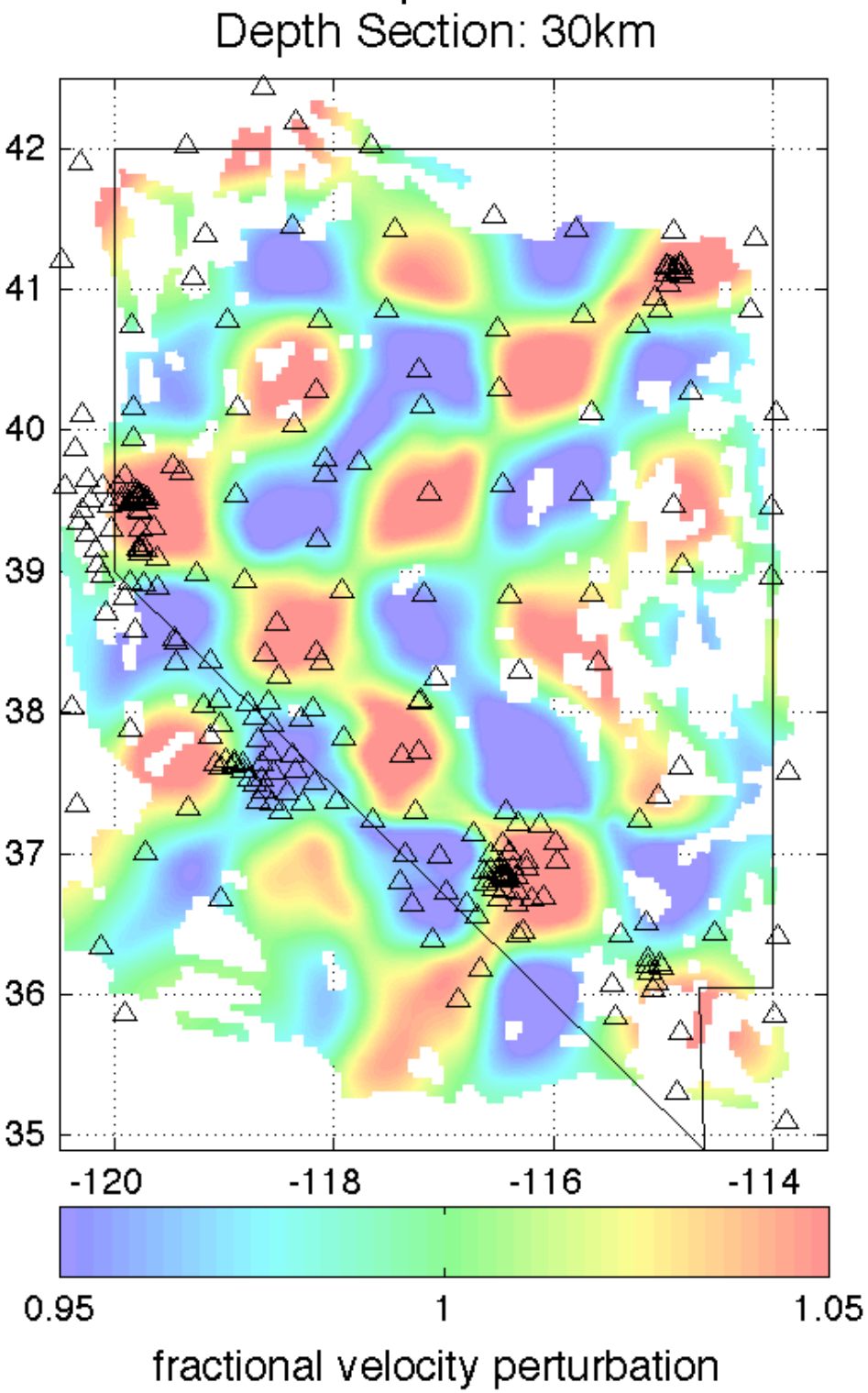

Figure 37

**100 x 100 km Vp checkerboard**

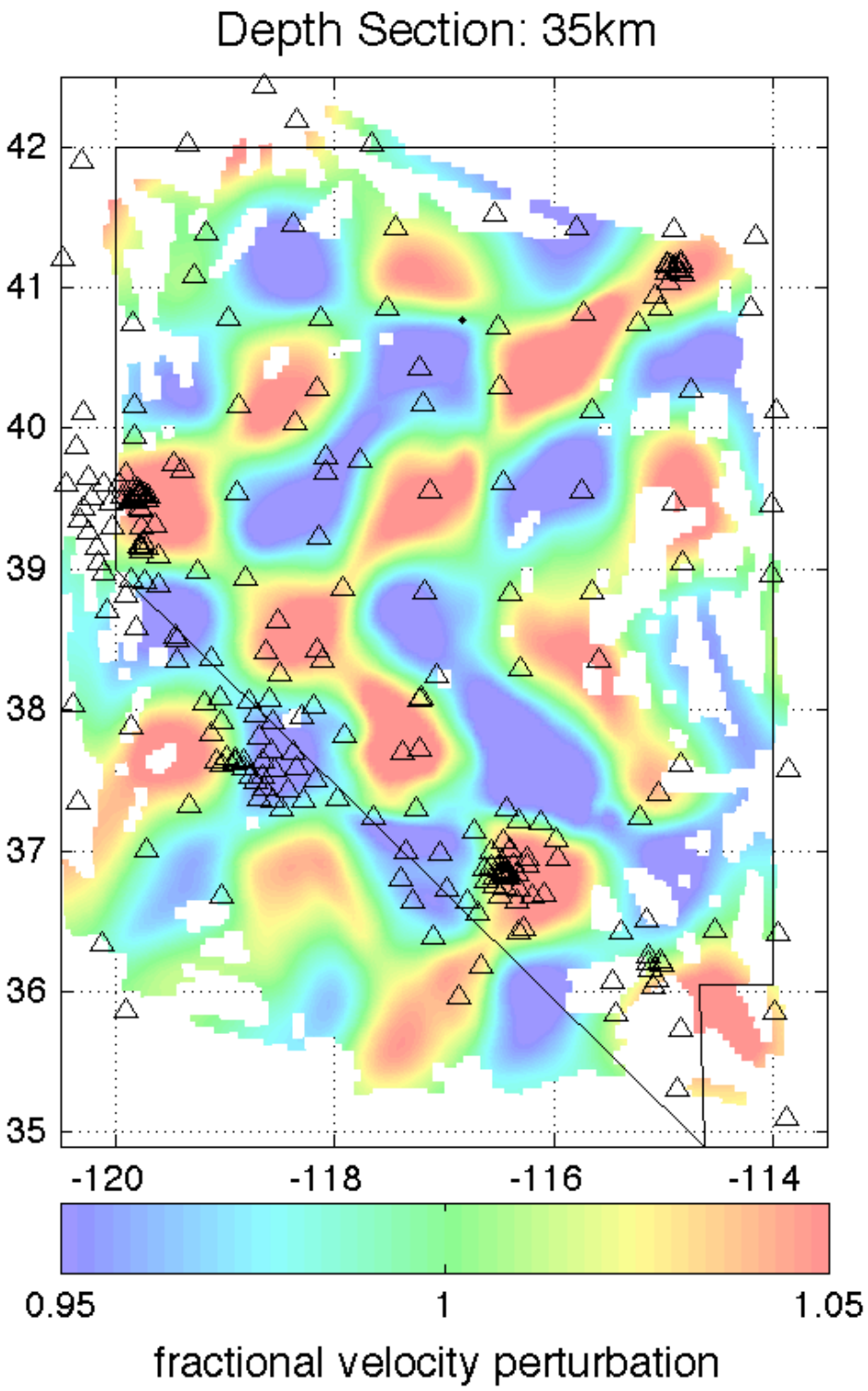

Figure 38

**100 x 100 km Vp checkerboard**

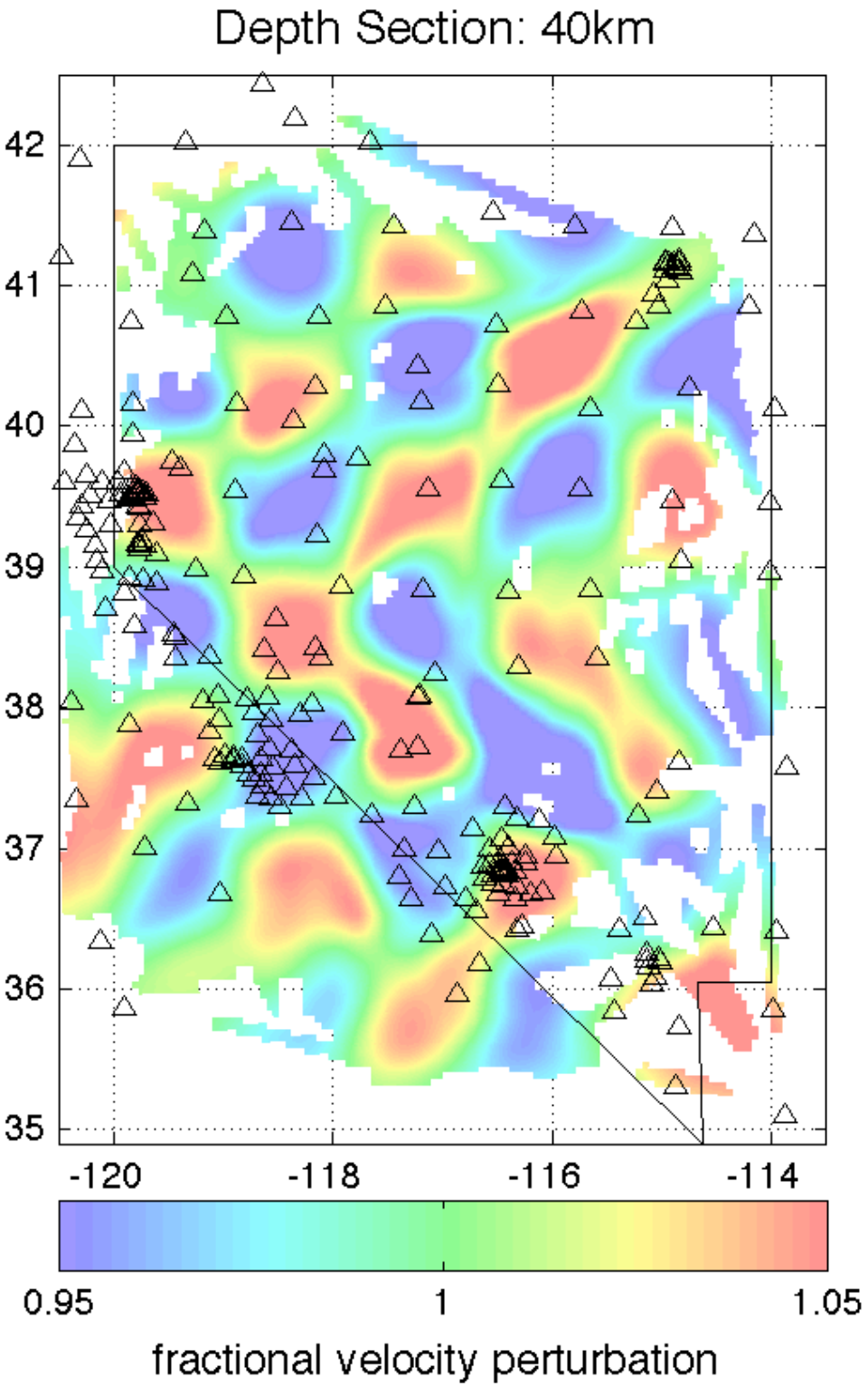

Figure 39

**100 x 100 km Vp checkerboard**

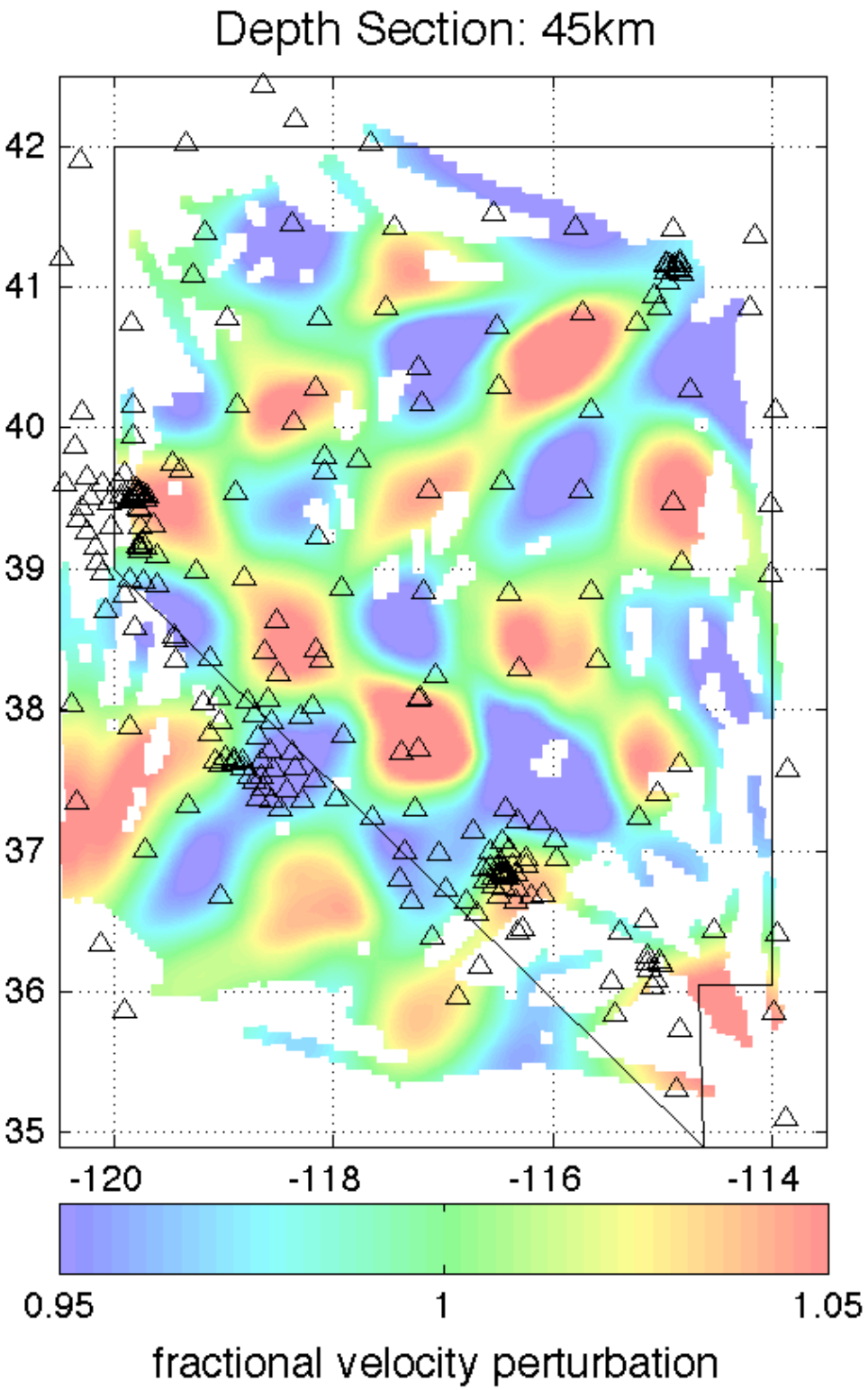

Figure 40 **100 x 100 km Vp/Vs checkerboard**

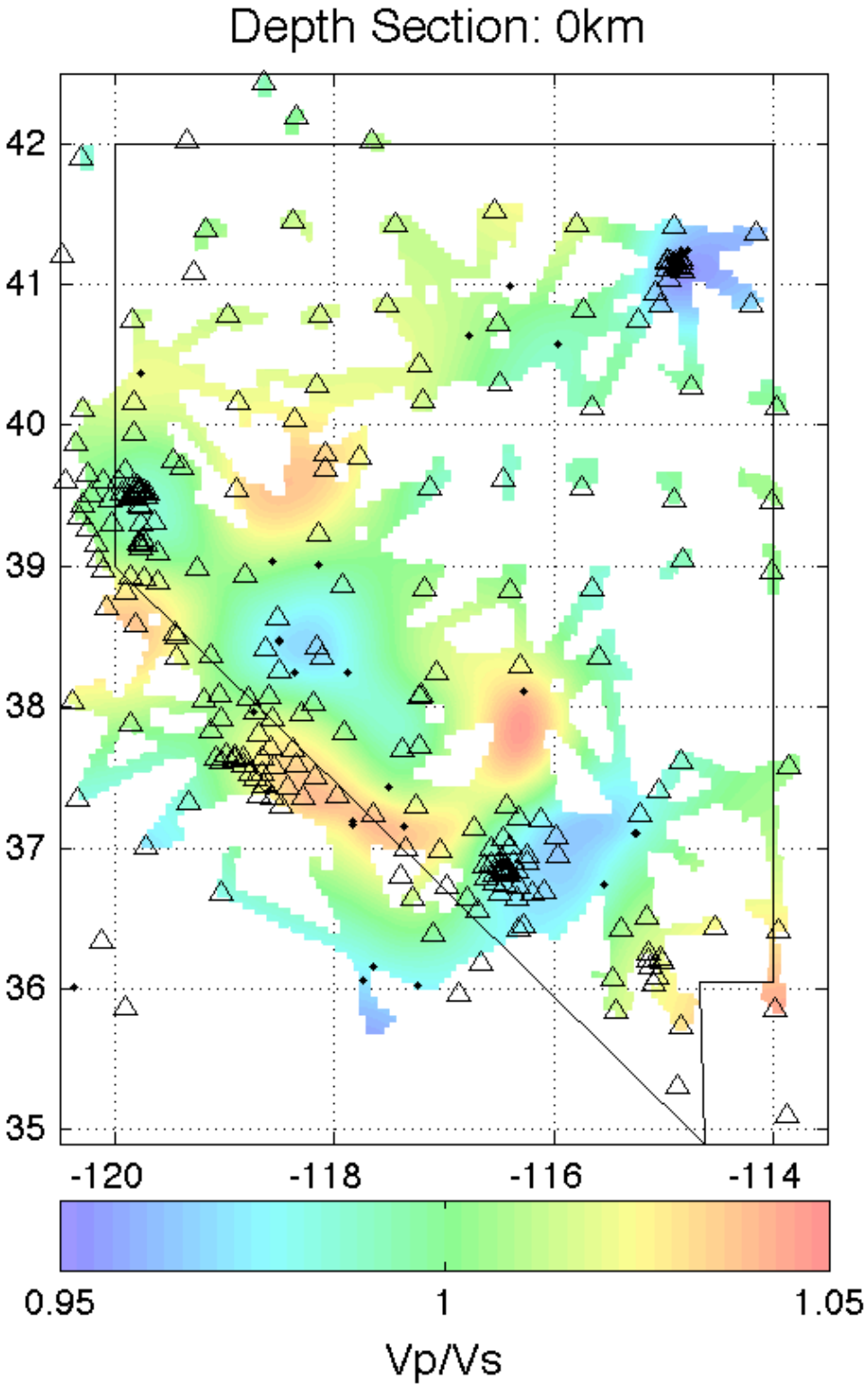

Figure 41 **100 x 100 km Vp/Vs checkerboard**

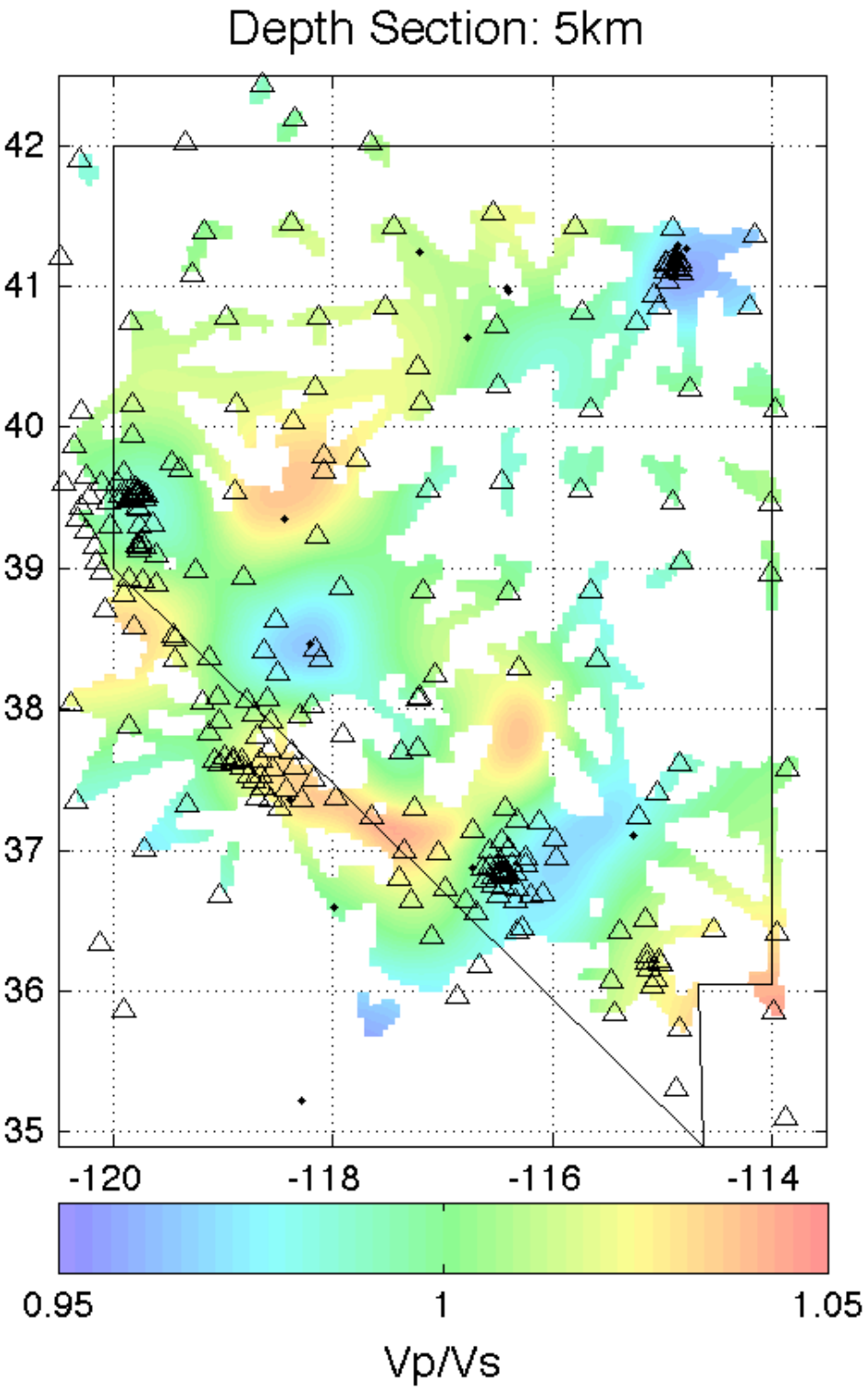

Figure 42 **100 x 100 km Vp/Vs checkerboard**

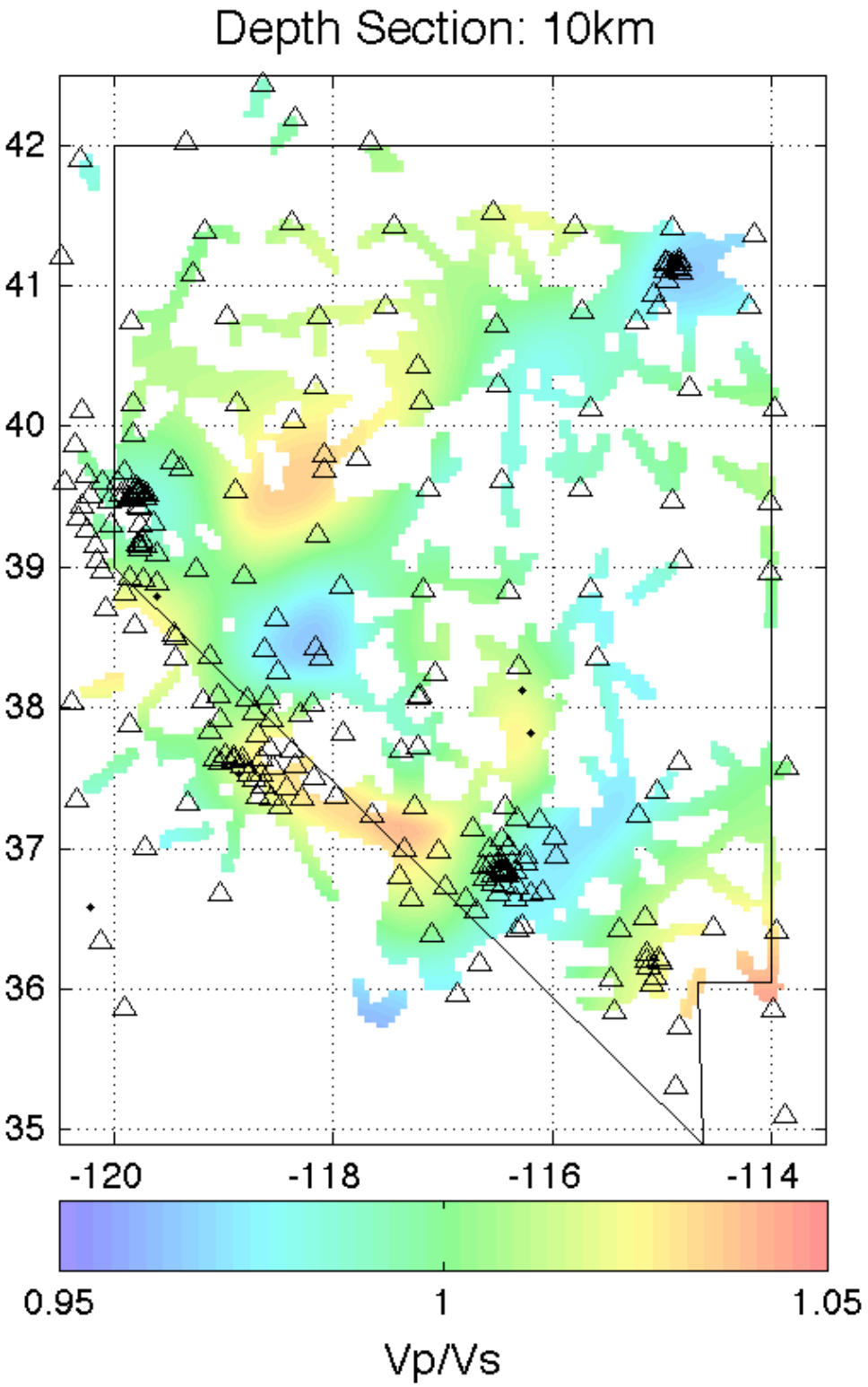

Figure 43 **100 x 100 km Vp/Vs checkerboard**

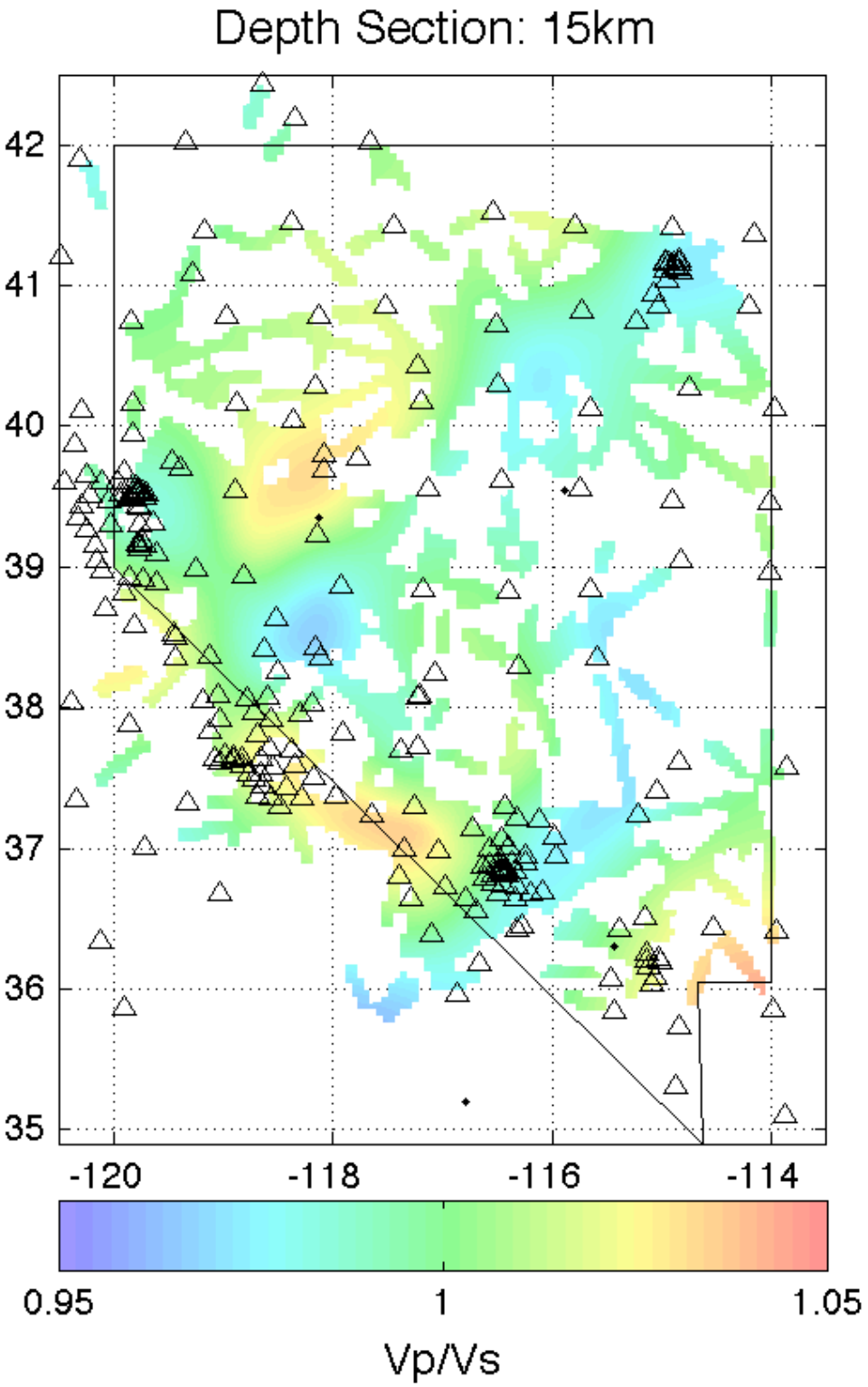

Figure 44 **100 x 100 km Vp/Vs checkerboard**

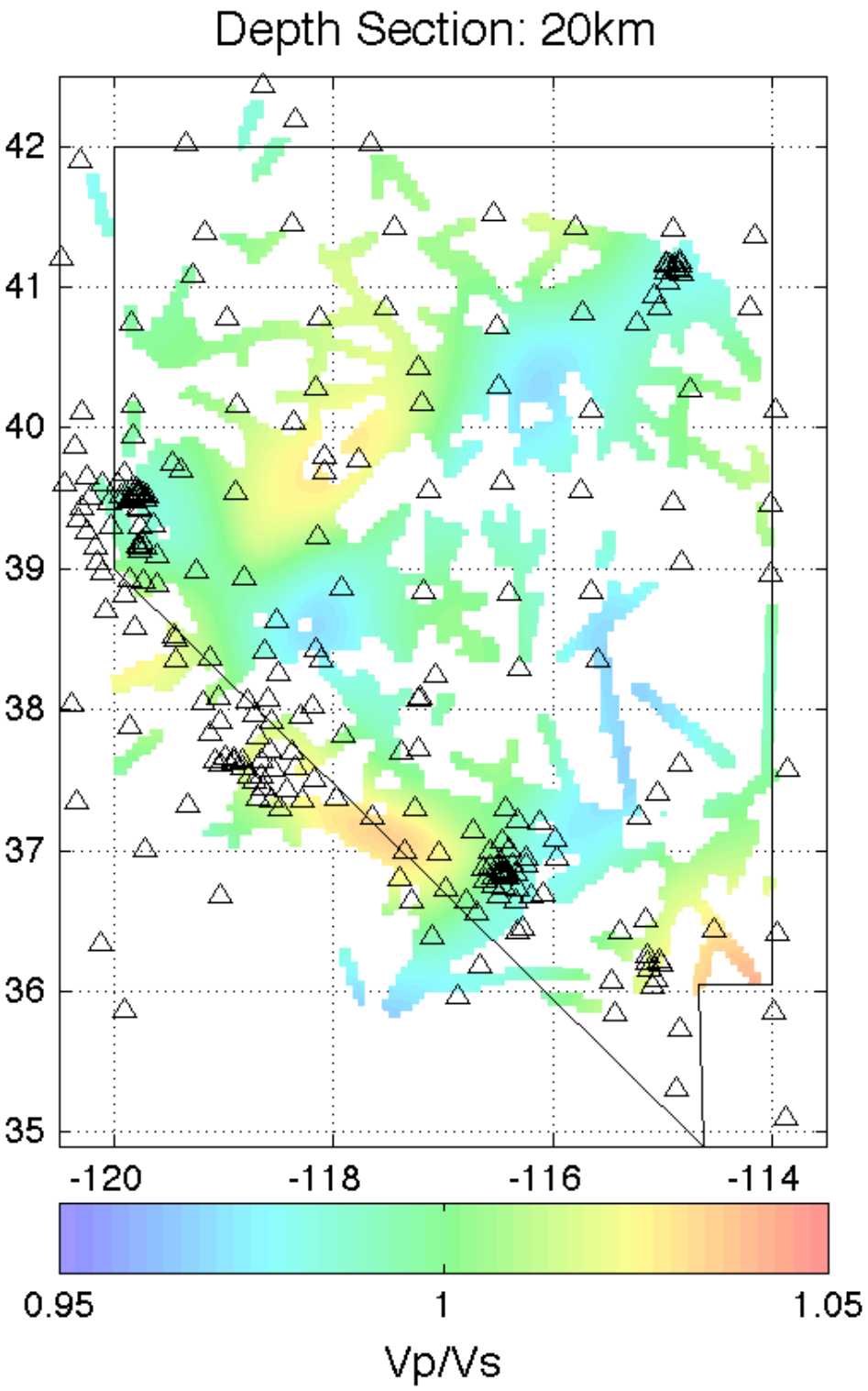

Figure 45 **100 x 100 km Vp/Vs checkerboard**

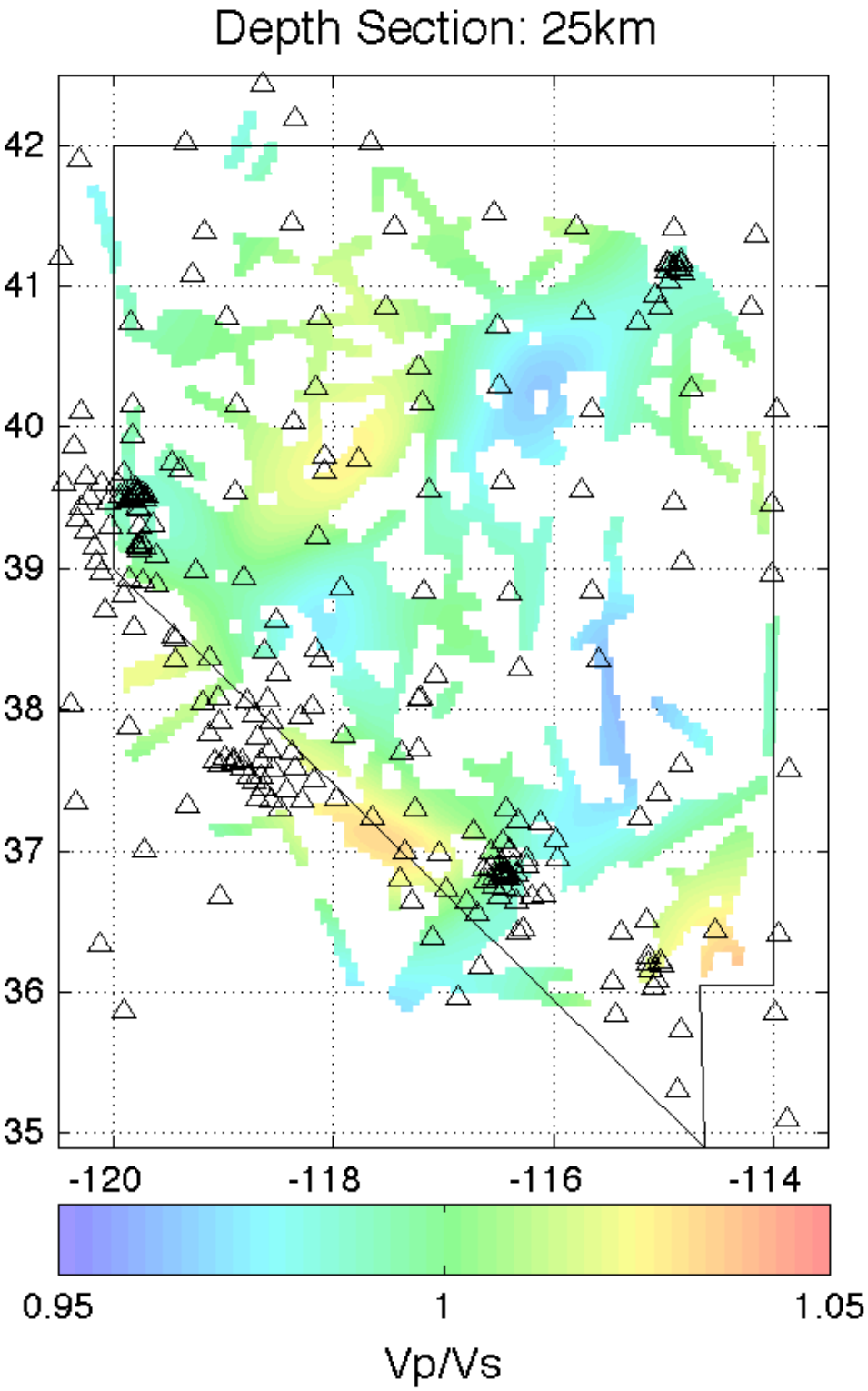

Figure 46 **100 x 100 km Vp/Vs checkerboard**

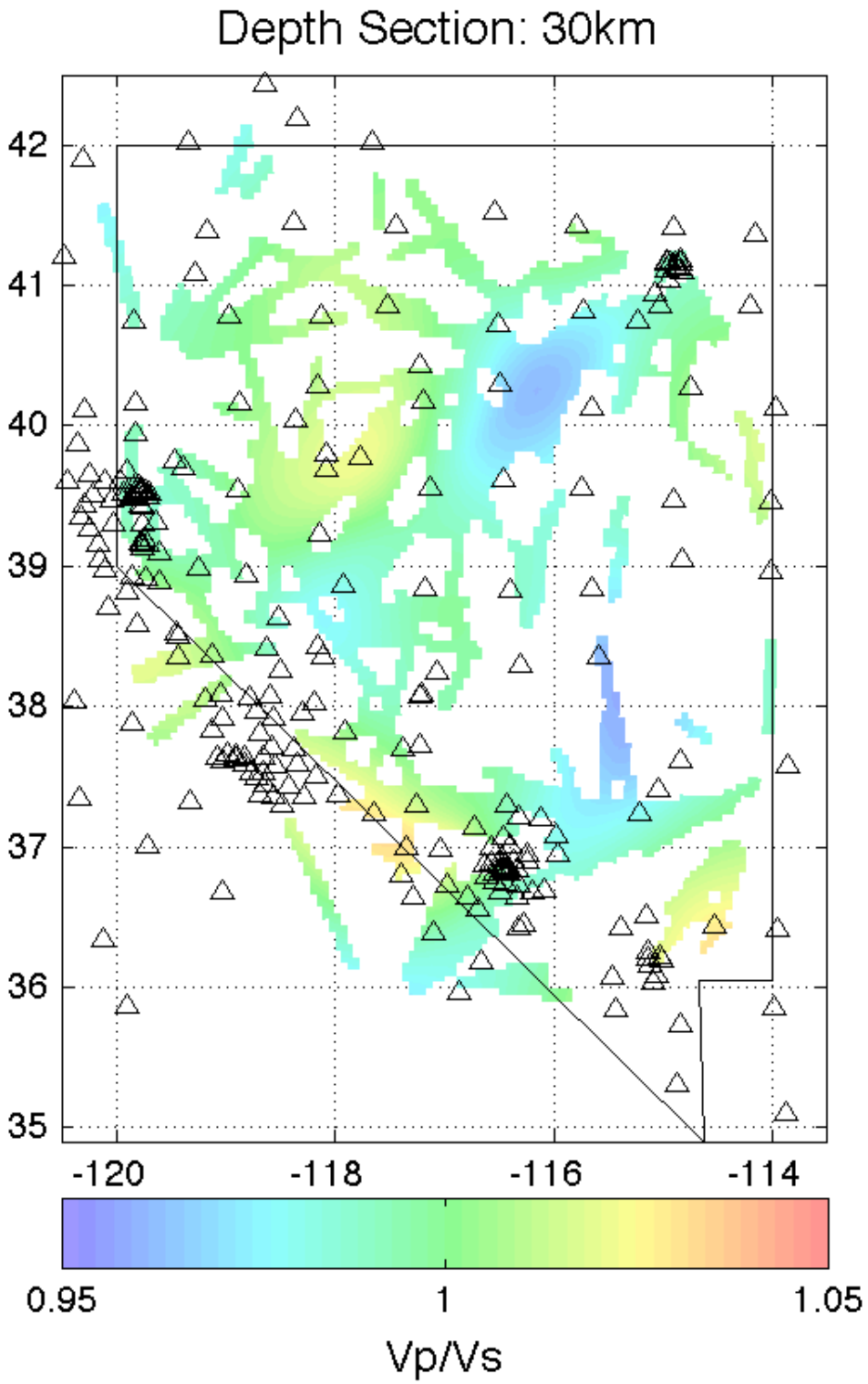

Figure 47 **100 x 100 km Vp/Vs checkerboard**

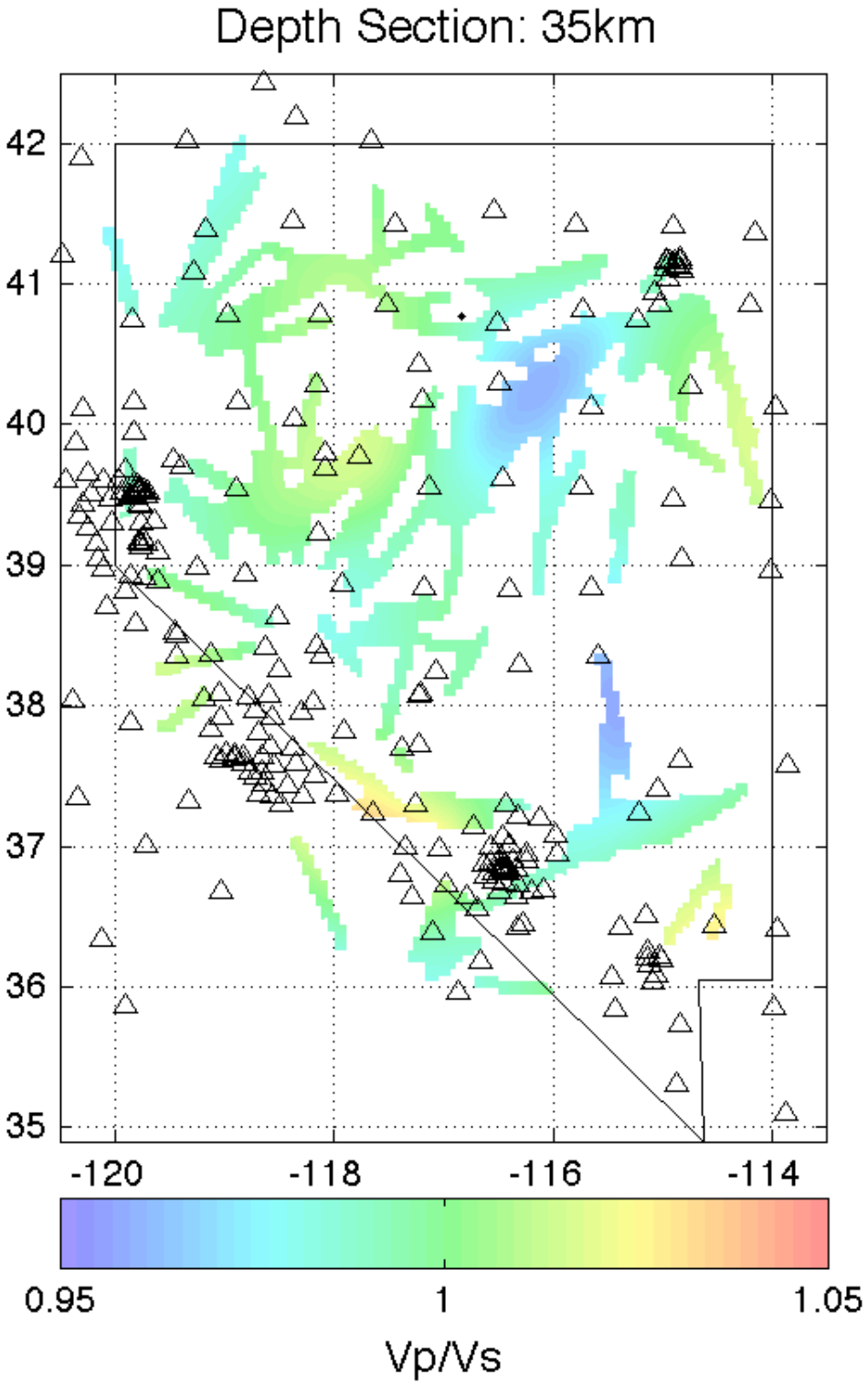

Figure 48 **200 x 200 km Vp/Vs checkerboard**

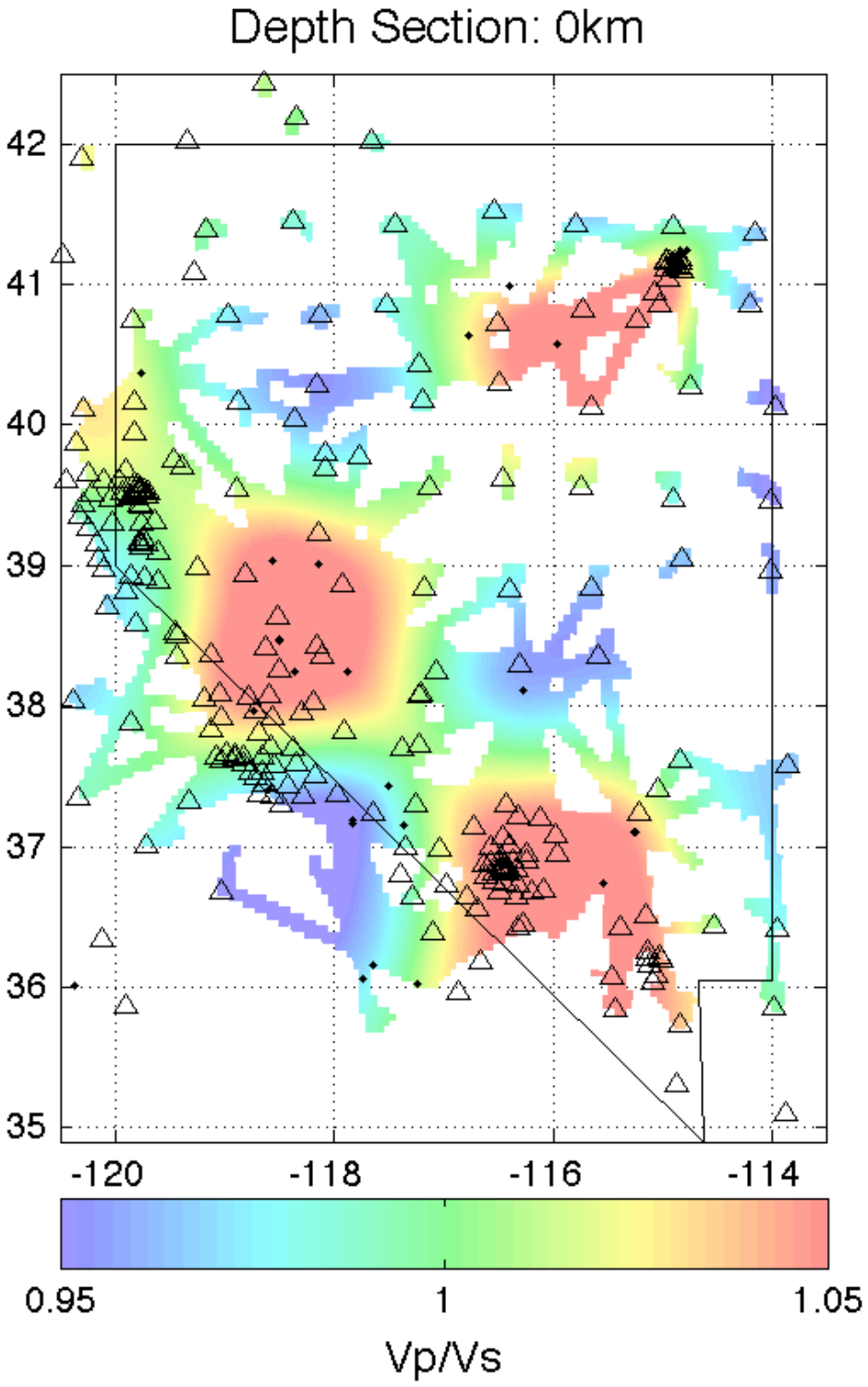

Figure 49 **200 x 200 km Vp/Vs checkerboard**

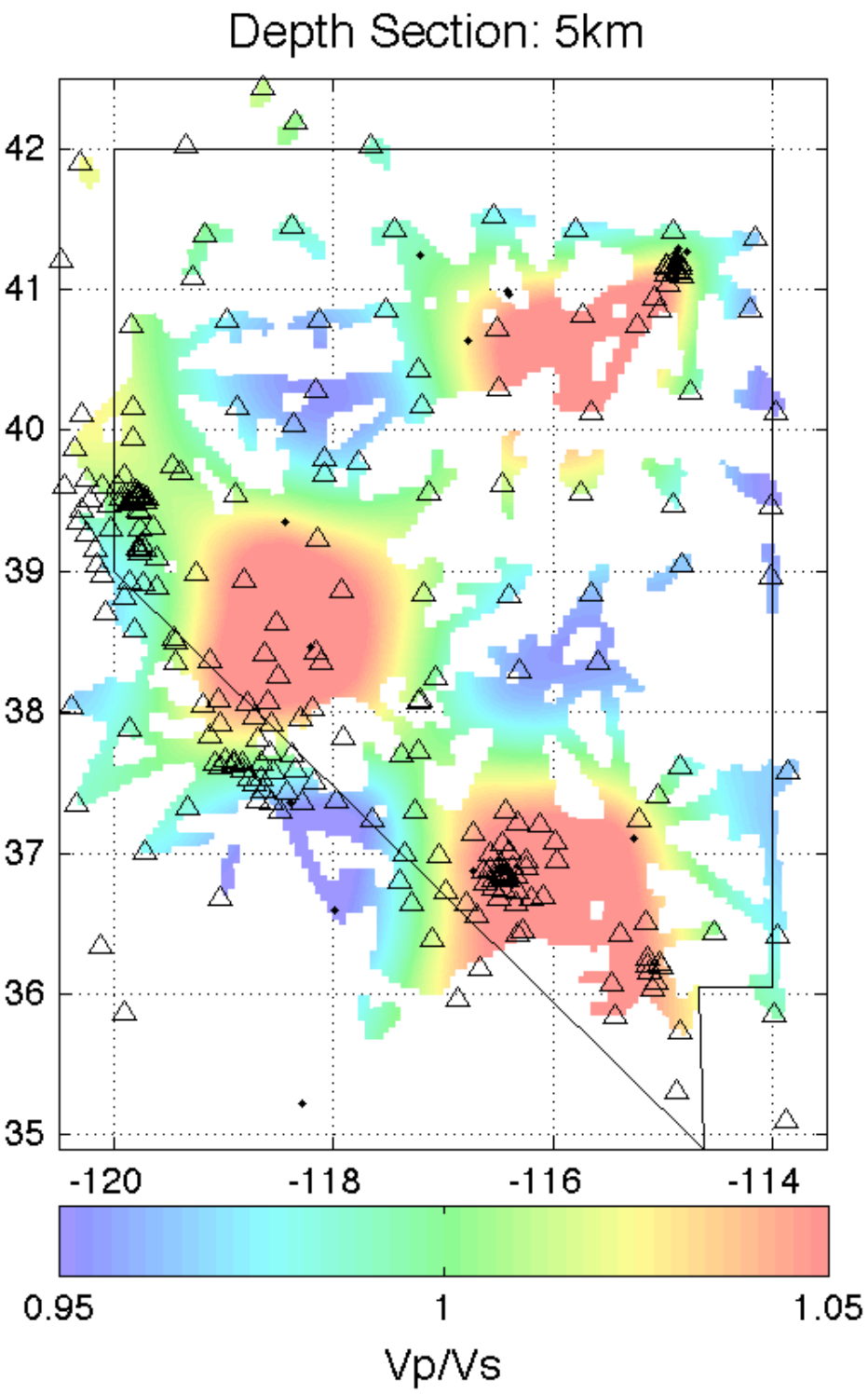

Figure 50 **200 x 200 km Vp/Vs checkerboard**

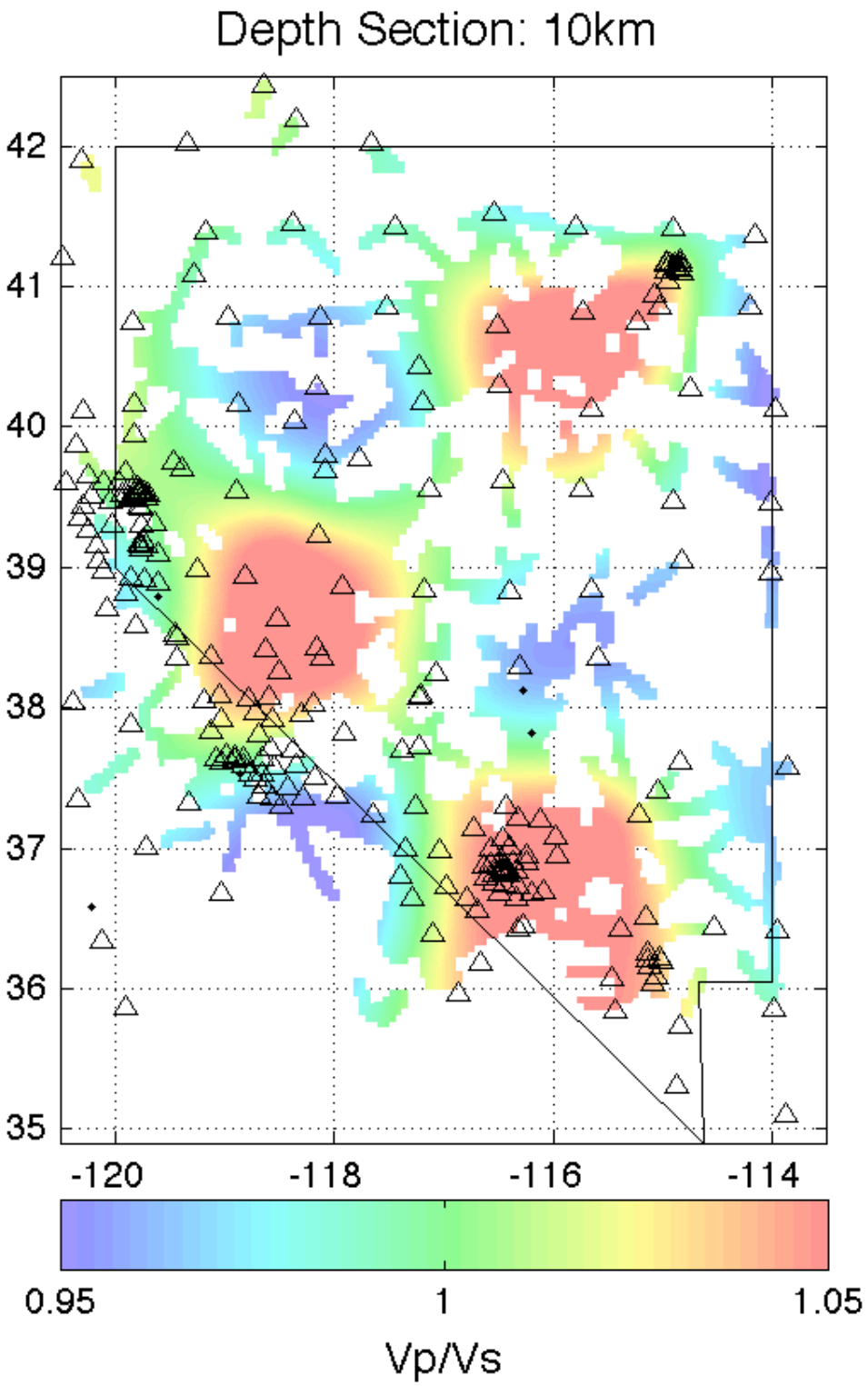

Figure 51 **200 x 200 km Vp/Vs checkerboard**

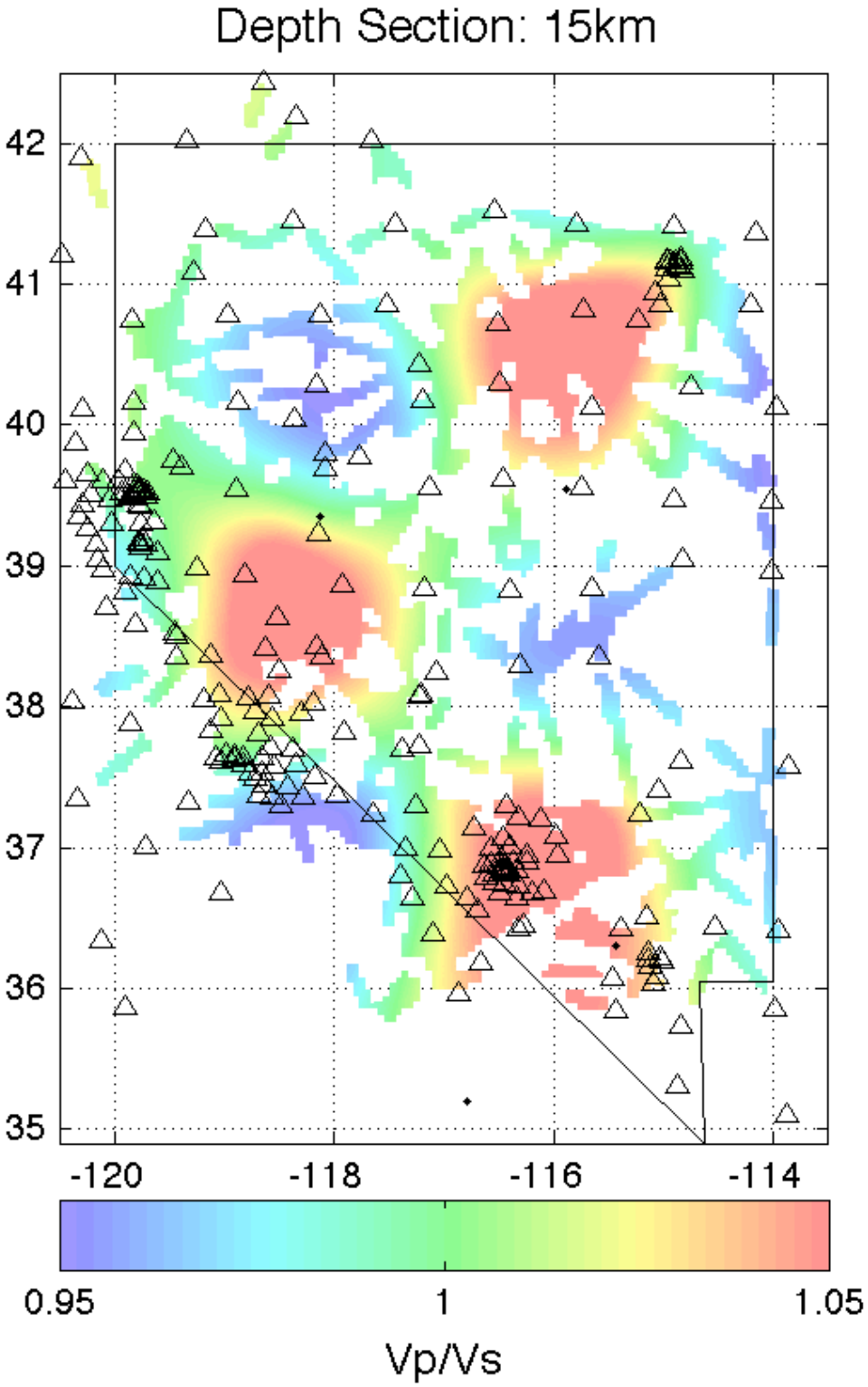

Figure 52 **200 x 200 km Vp/Vs checkerboard**

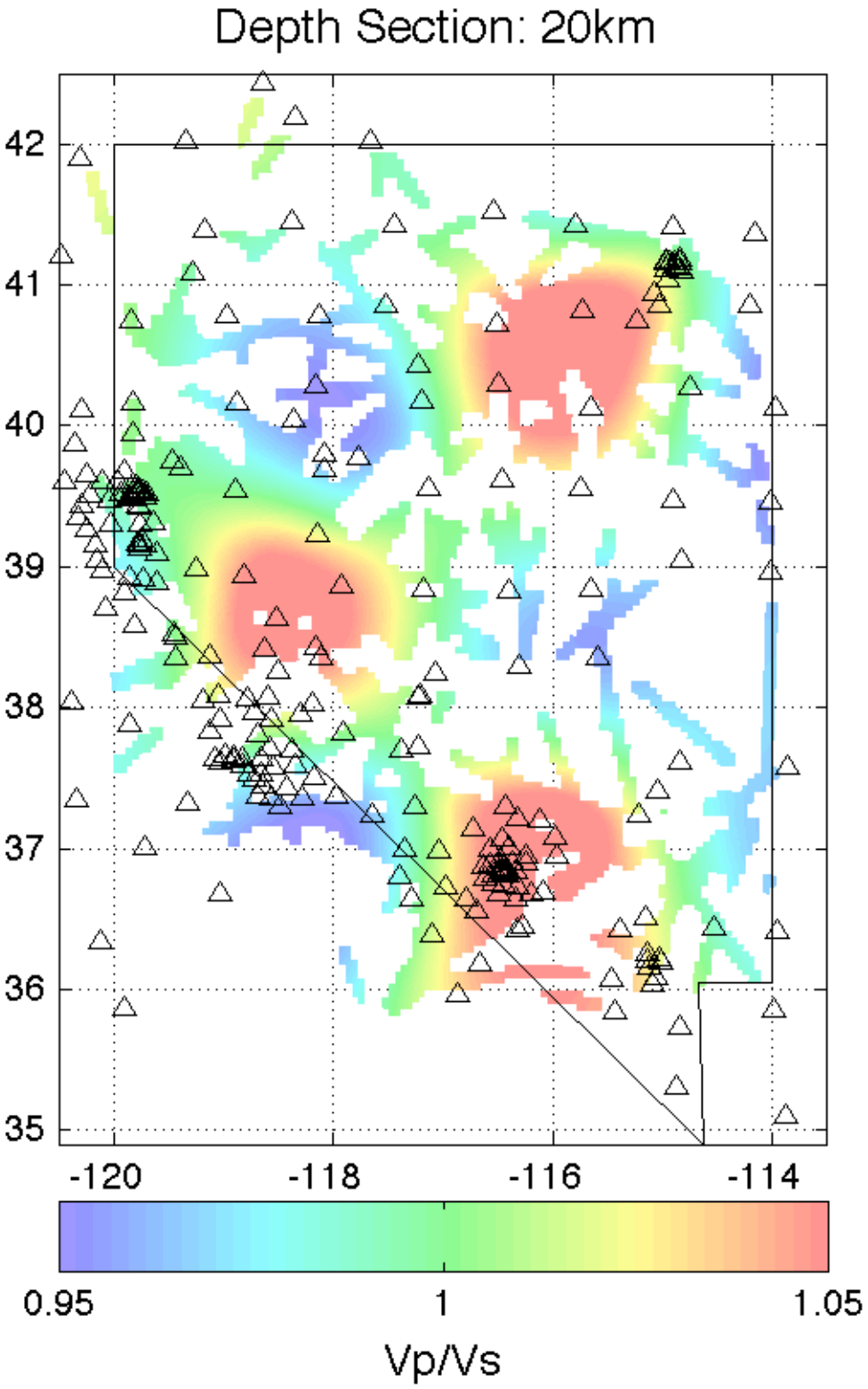

Figure 53 **200 x 200 km Vp/Vs checkerboard**

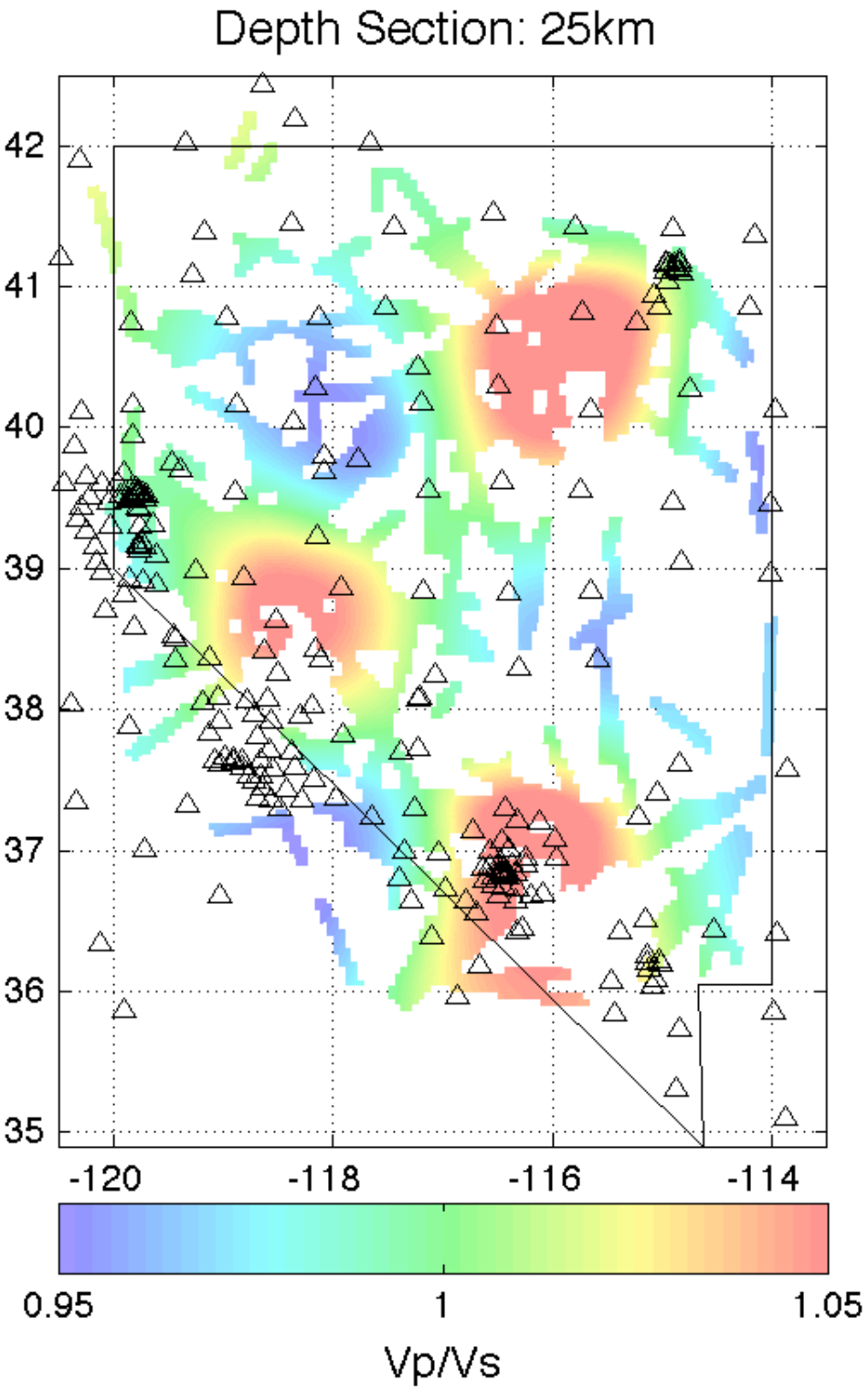

Figure 54 **200 x 200 km Vp/Vs checkerboard**

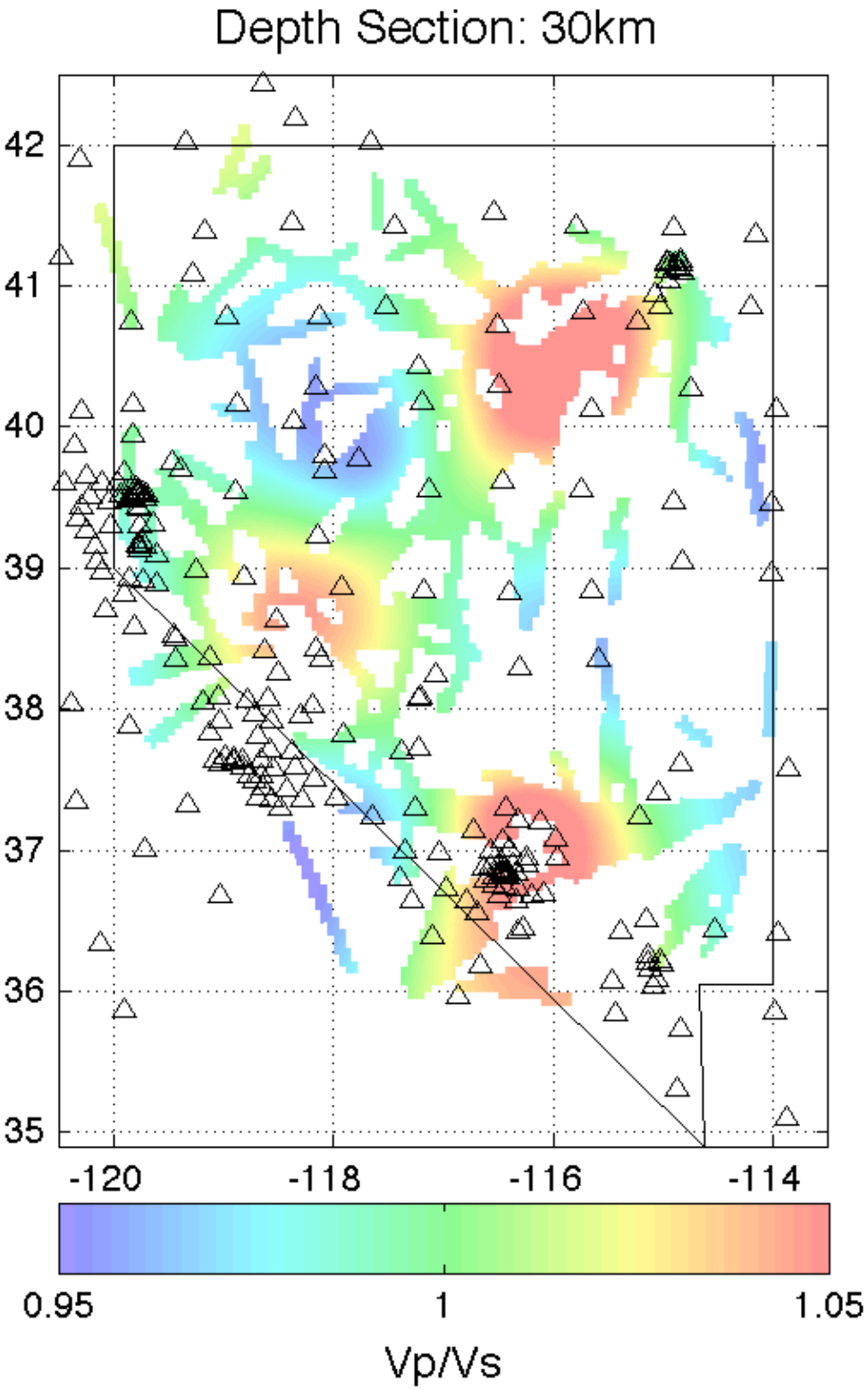

Figure 55 **200 x 200 km Vp/Vs checkerboard**

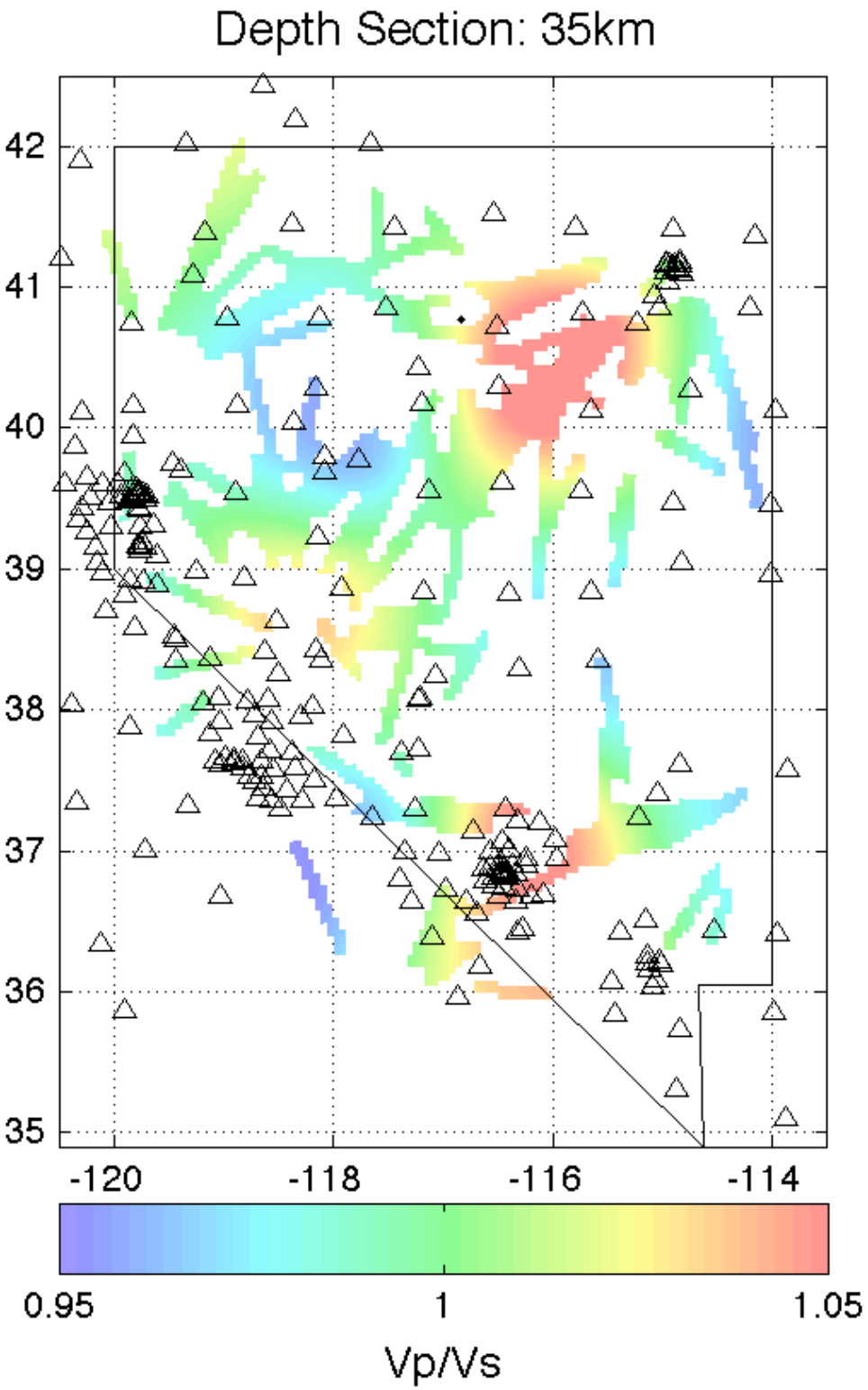

# 13. Jackknife Test Results

Figures 56-73 show the jackknife test results in depth sections from 0 km (sea level) to 45 km depth in 5 km increments. Latitude and longitude are the plot coordinates. The color bar at the bottom of each figure gives the color scale. Stations are shown as triangles in all sections for reference. Black dots are earthquakes that locate within ±2.5 km of the given depth. Vp/Vs is only shown to 35 km depth.

Figure 56 **Vp Jackknife**

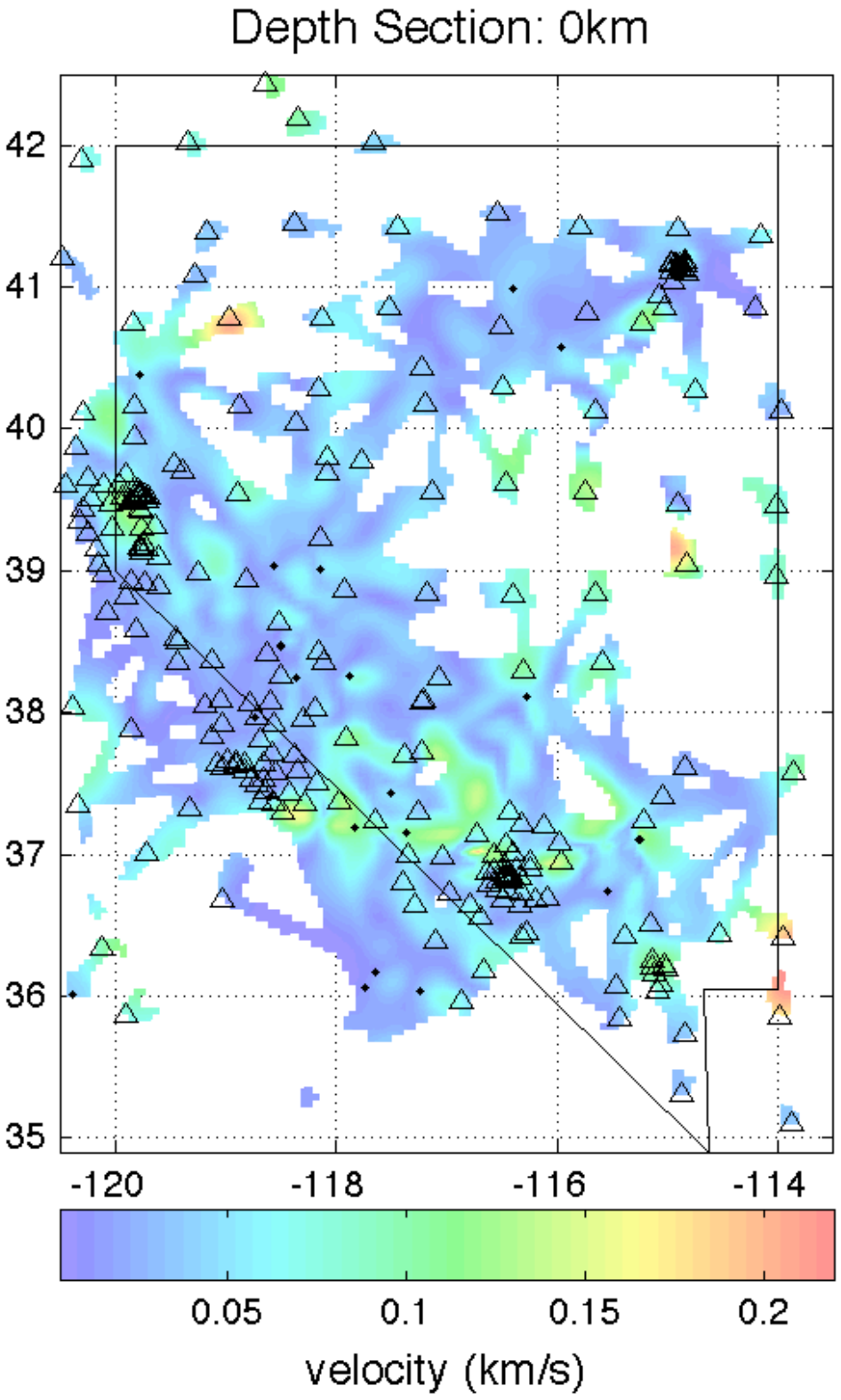

Figure 57 **Vp Jackknife**

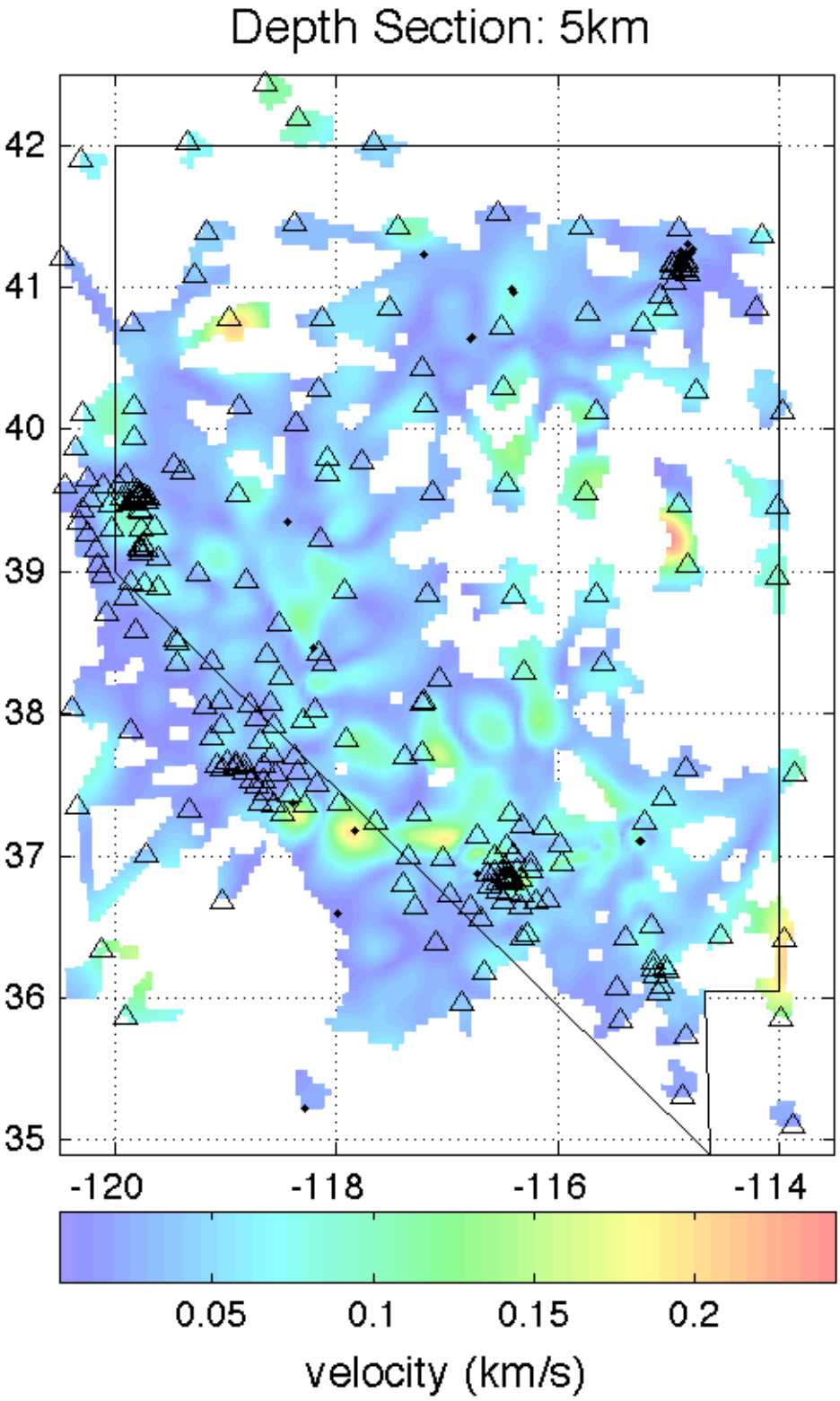

Figure 58 **Vp Jackknife**

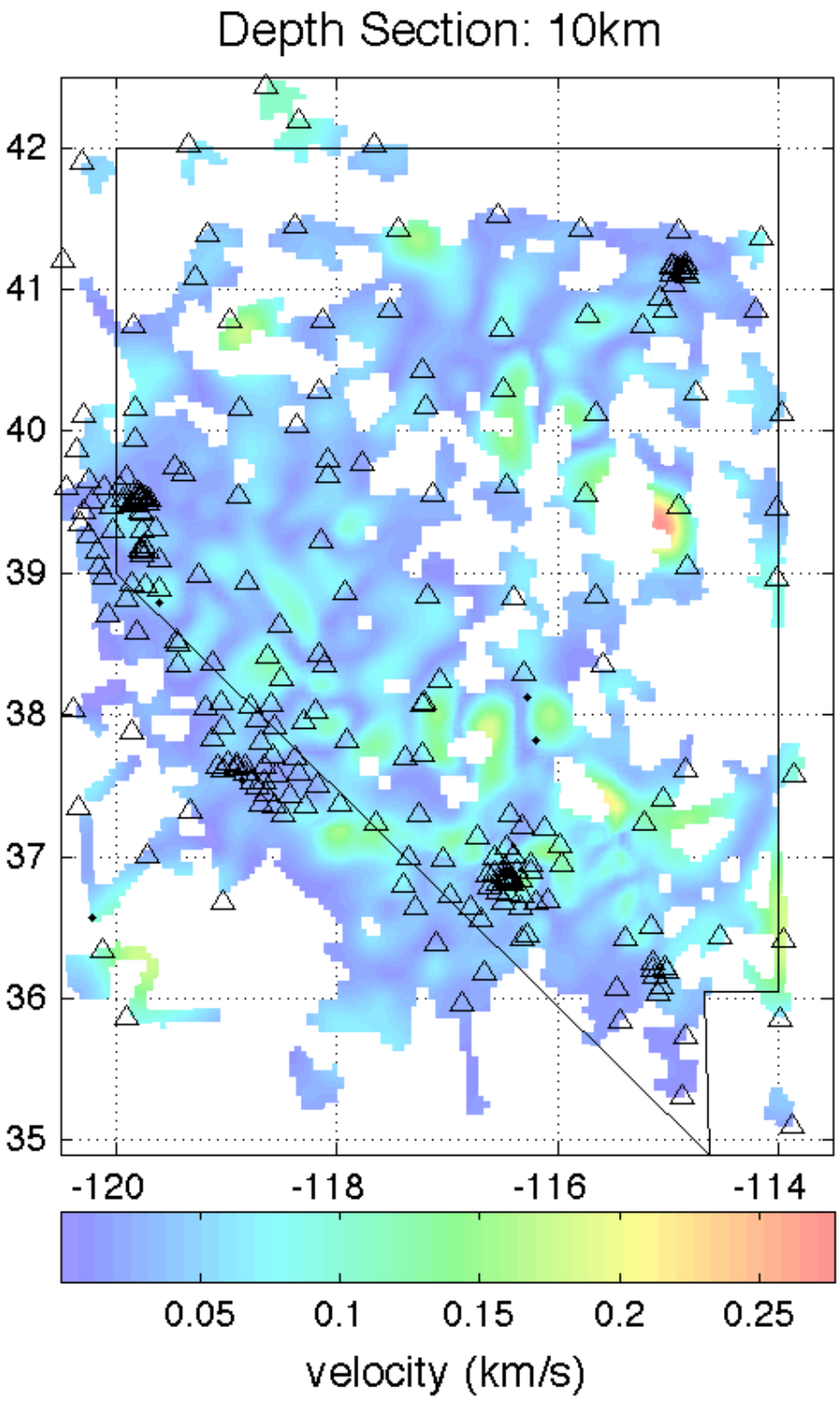

Figure 59 **Vp Jackknife**

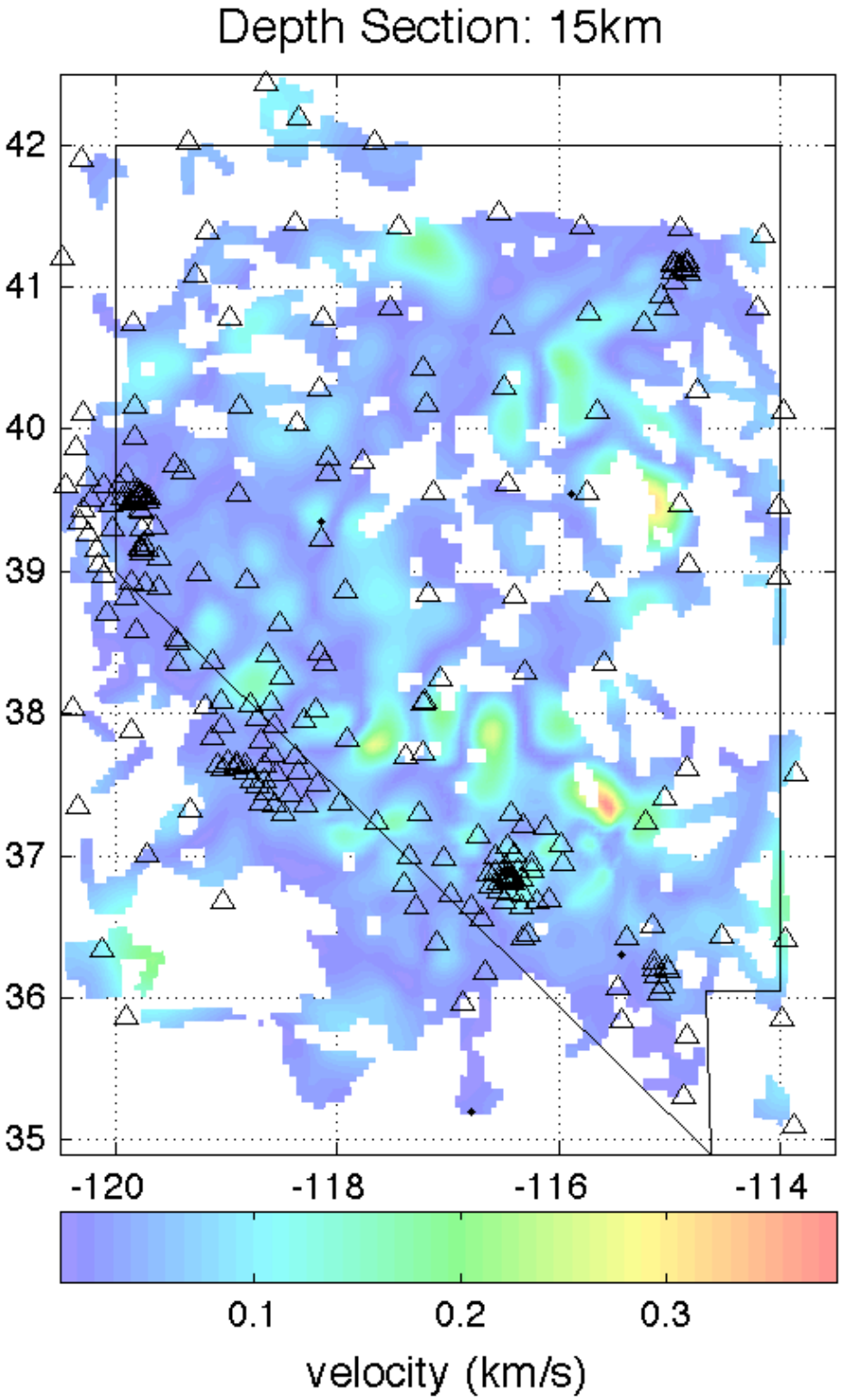

Figure 60 **Vp Jackknife**

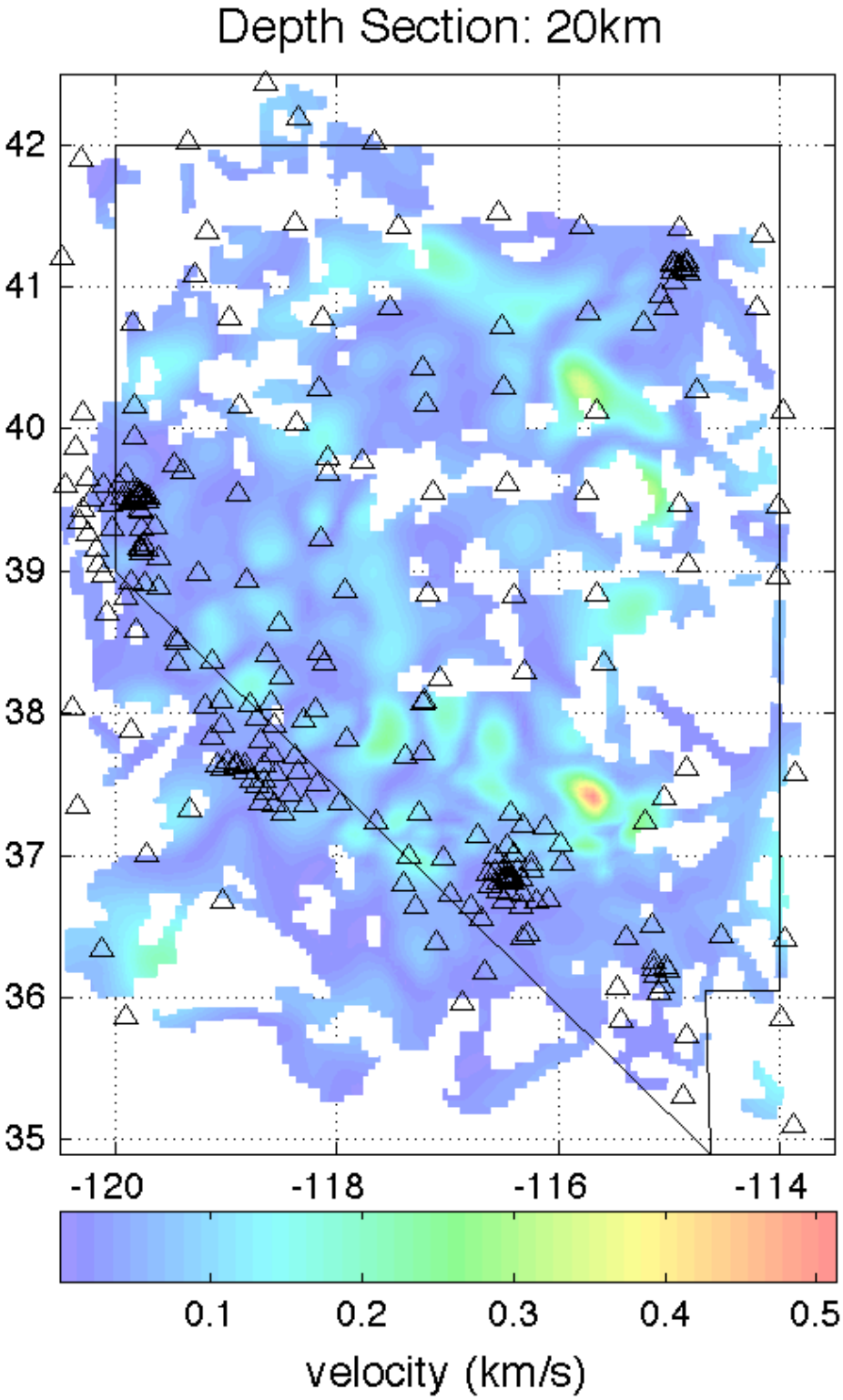

Figure 61 **Vp Jackknife**

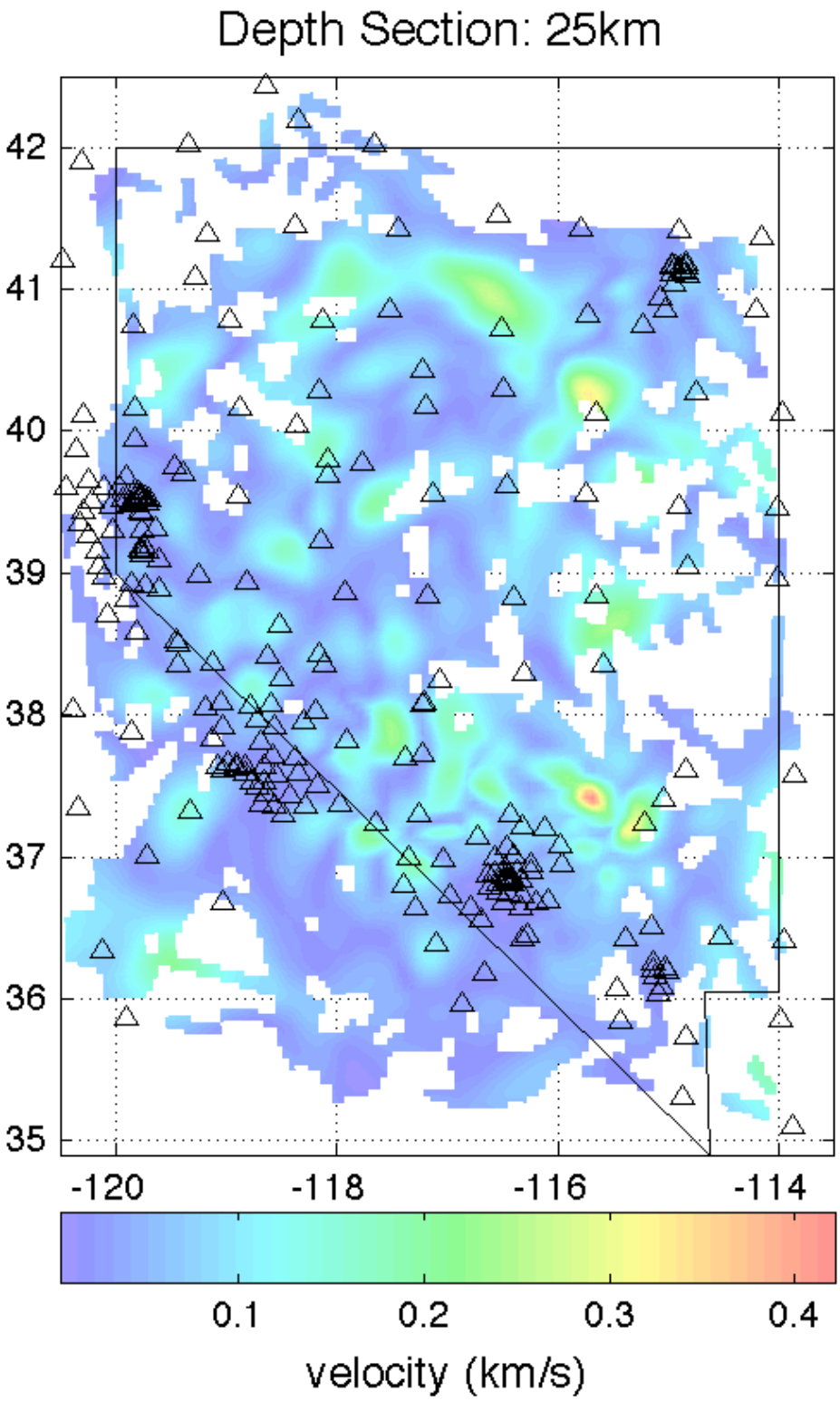

Figure 62 **Vp Jackknife**

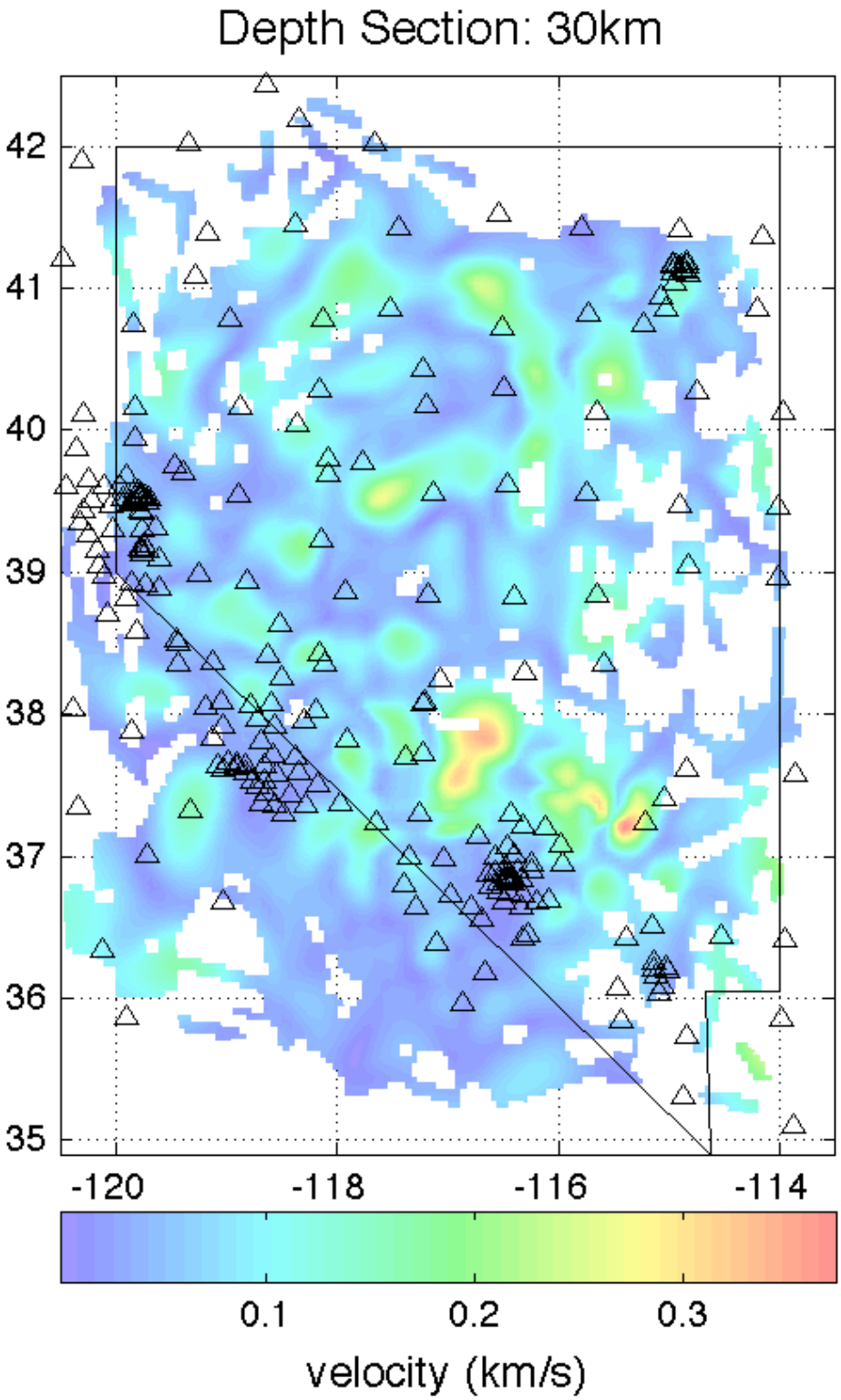

Figure 63 **Vp Jackknife**

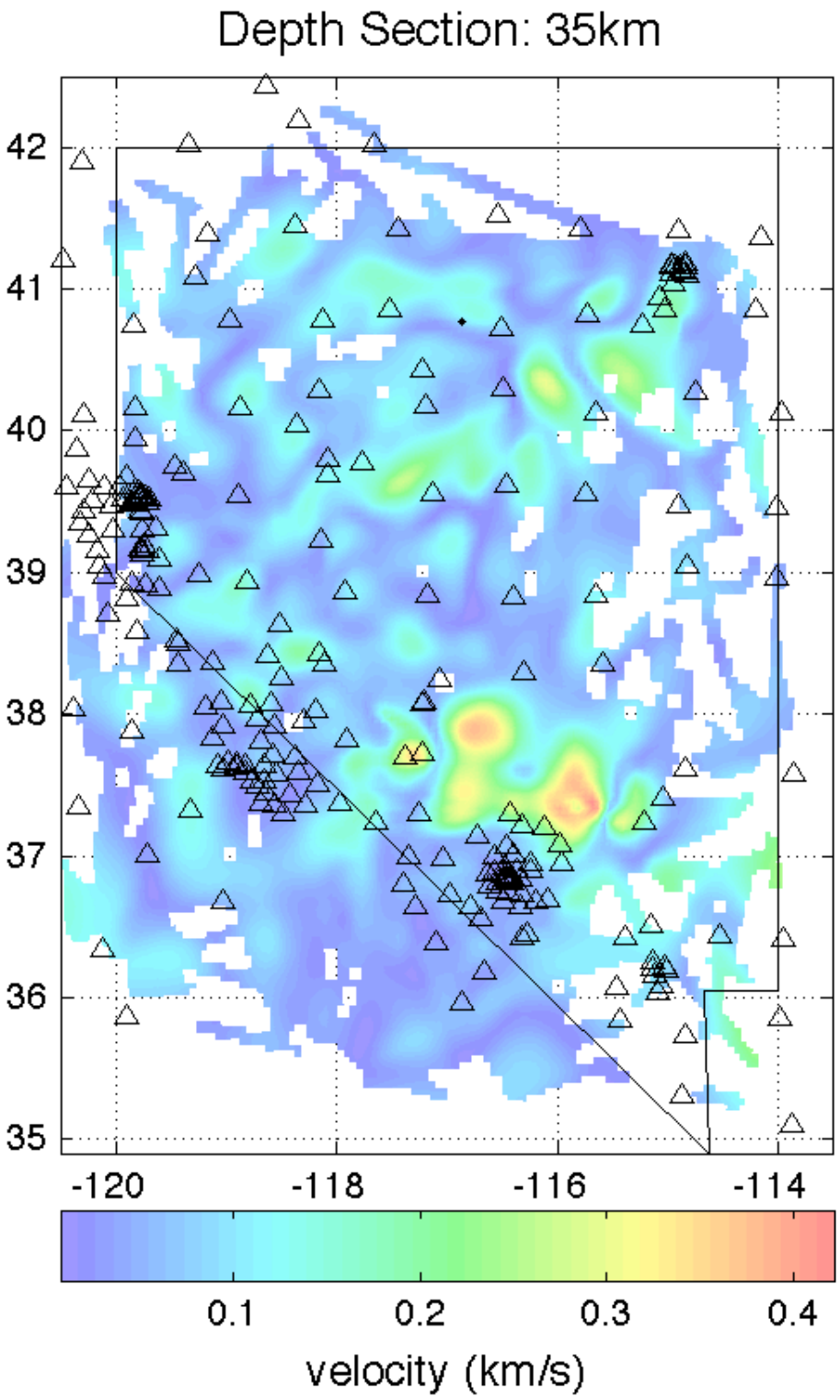

Figure 64 **Vp Jackknife**

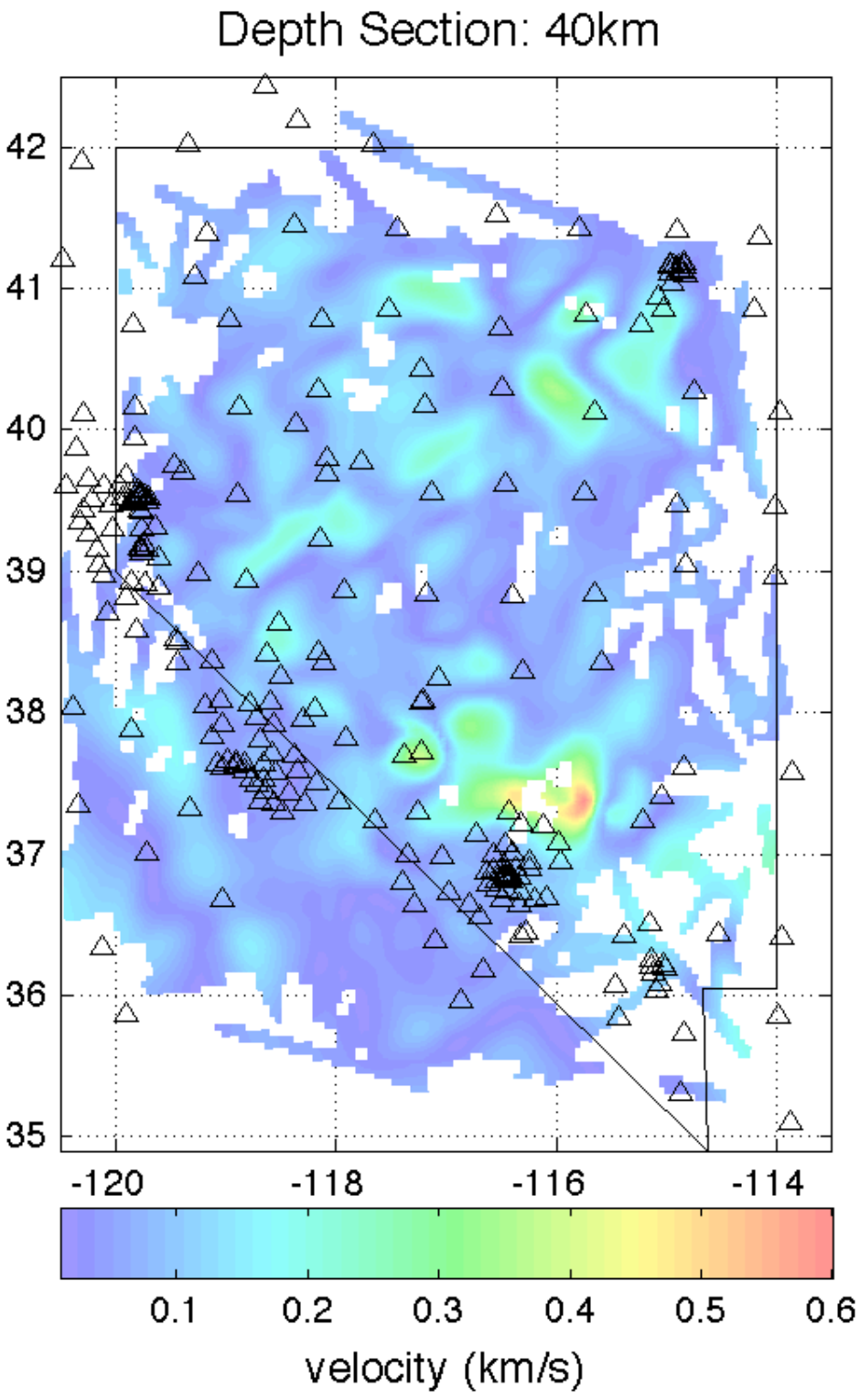

Figure 65 **Vp Jackknife**

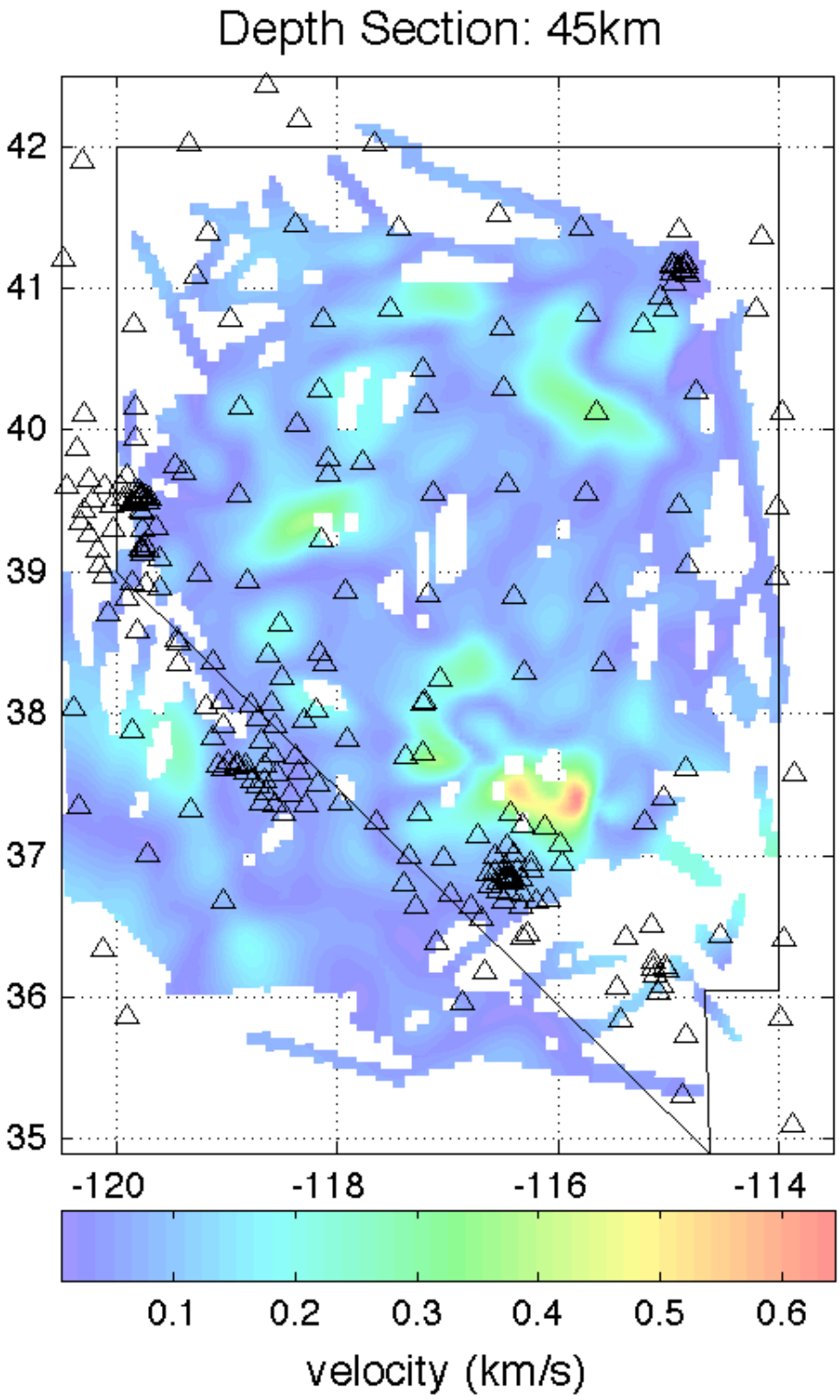

Figure 66

**Vp/Vs Jackknife**

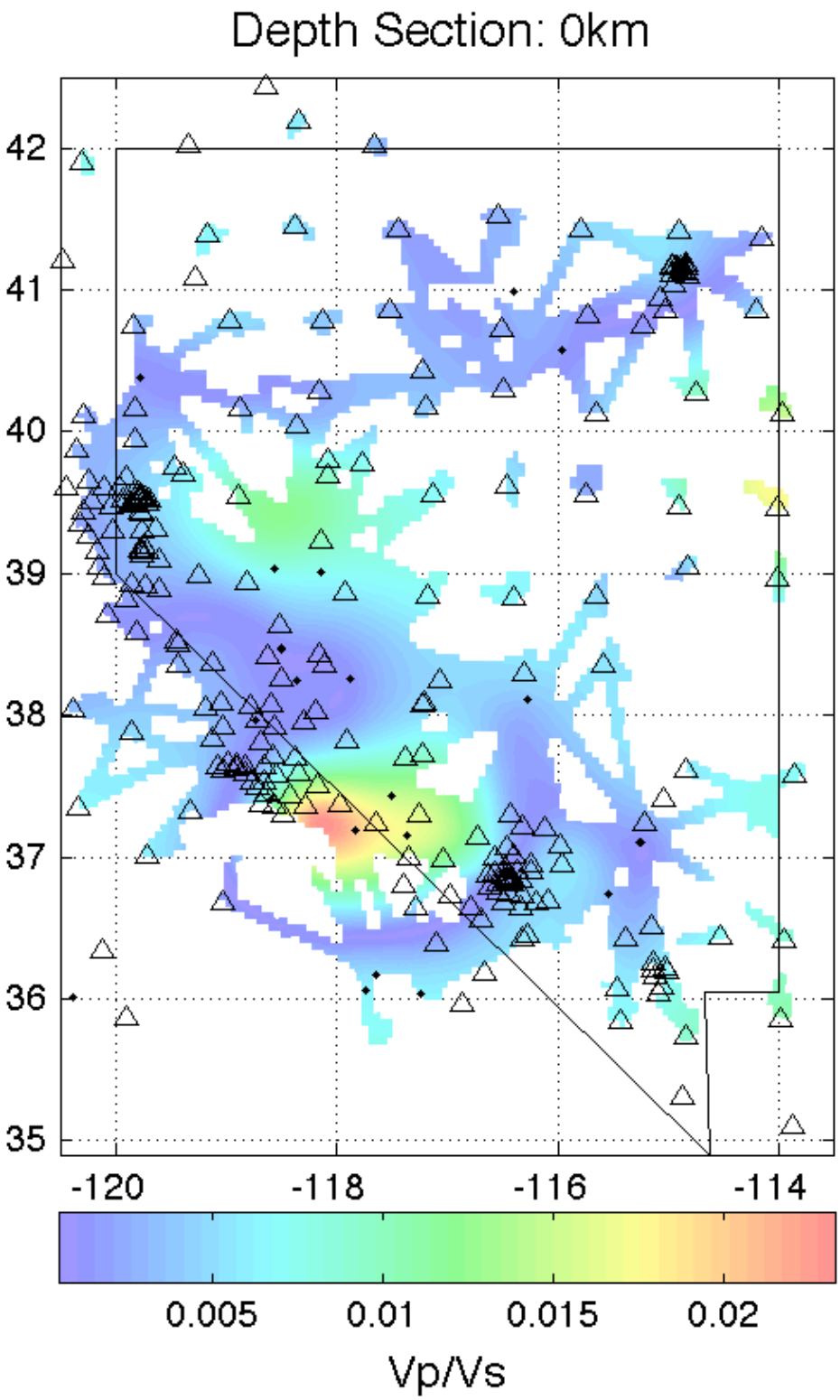

Figure 67

**Vp/Vs Jackknife**

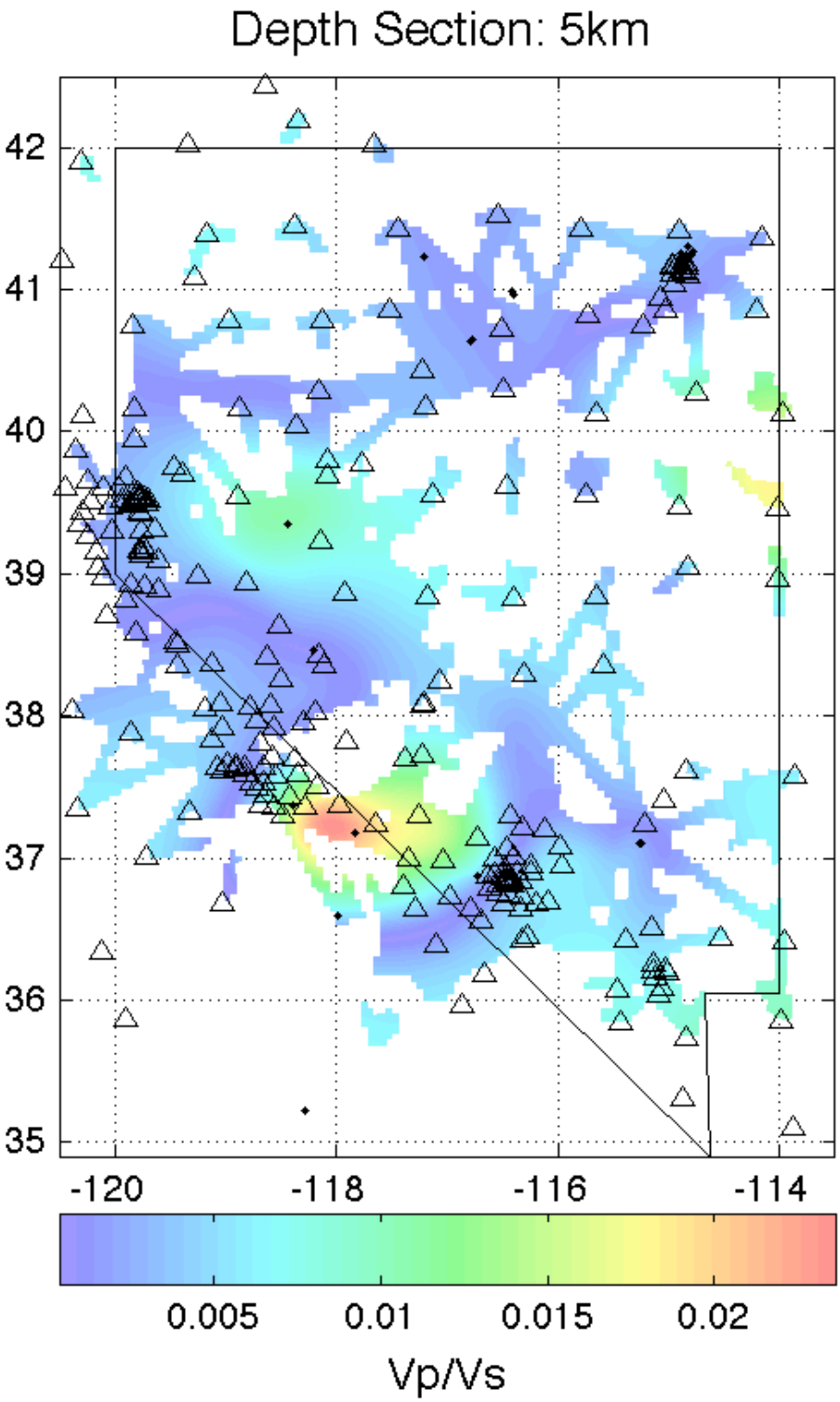

Figure 68

**Vp/Vs Jackknife**

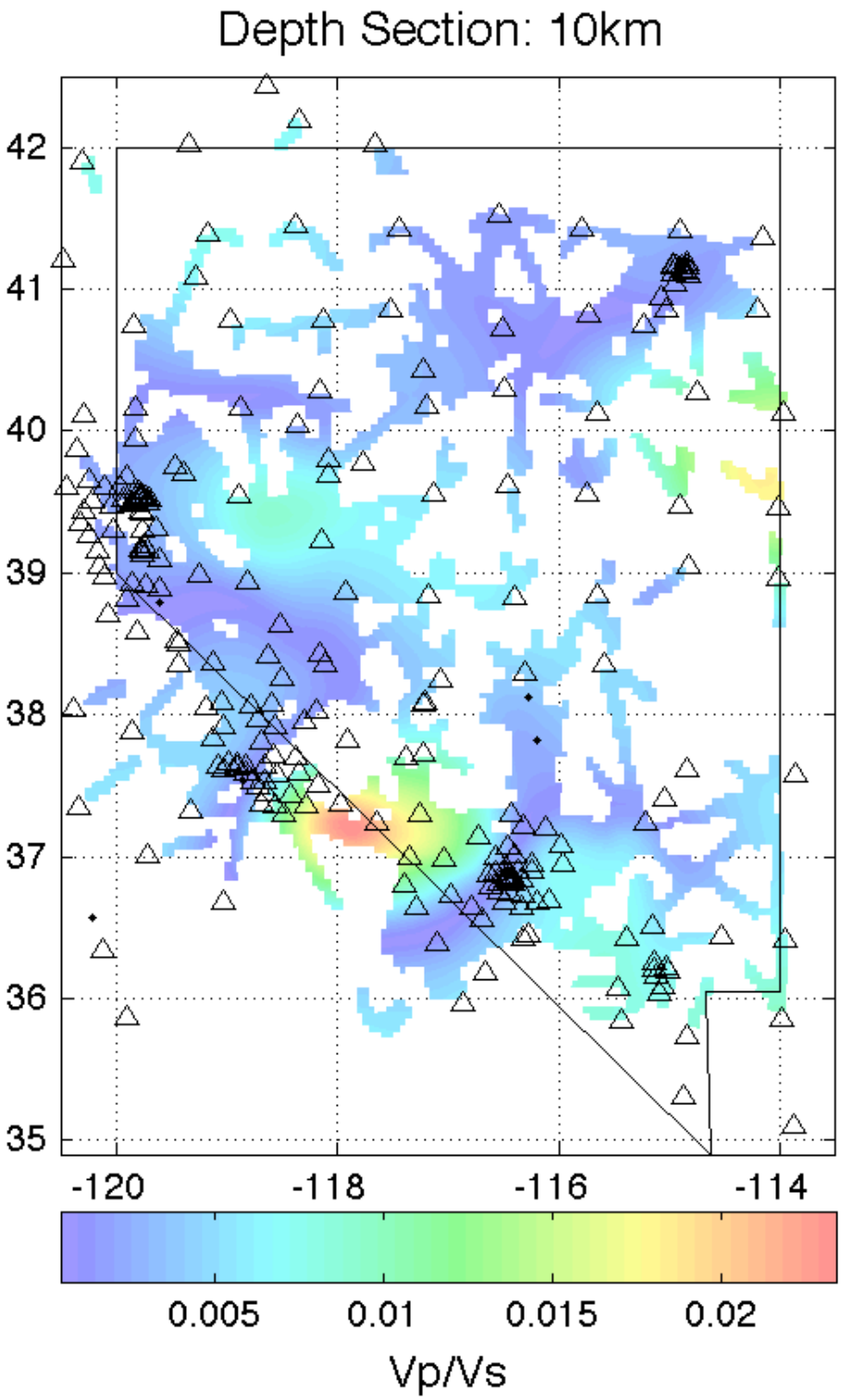

Figure 69

**Vp/Vs Jackknife**

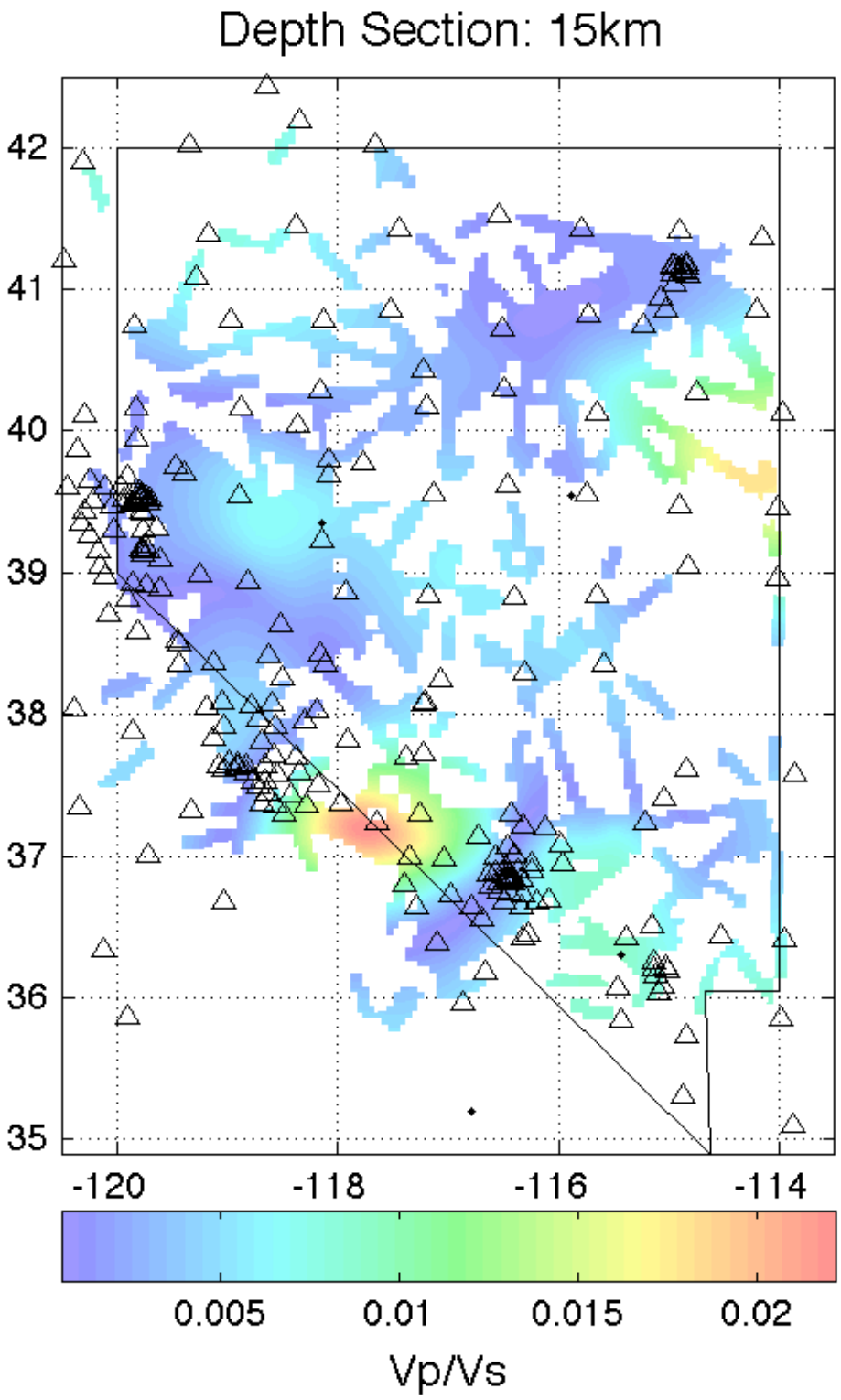

Figure 70

**Vp/Vs Jackknife**

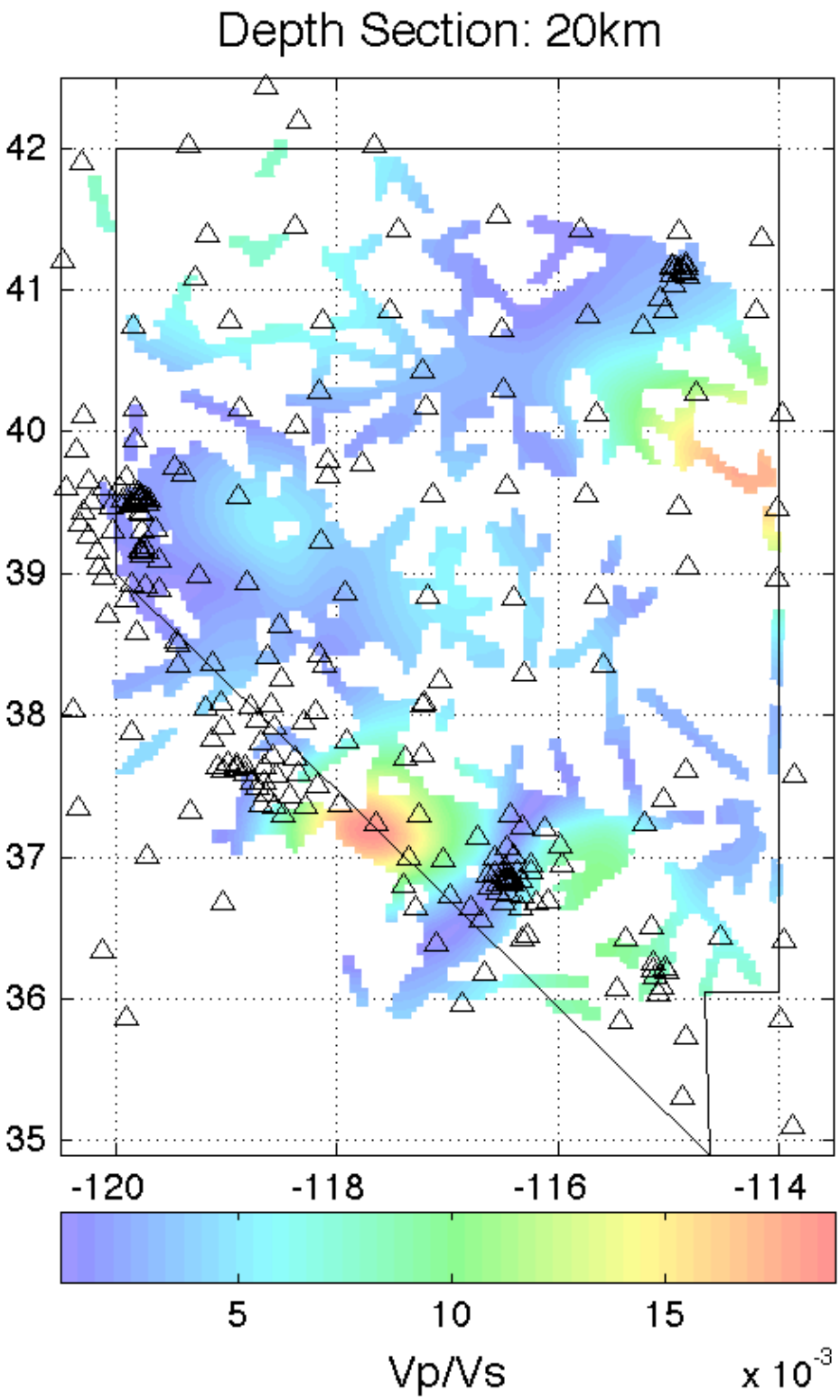

Figure 71

**Vp/Vs Jackknife**

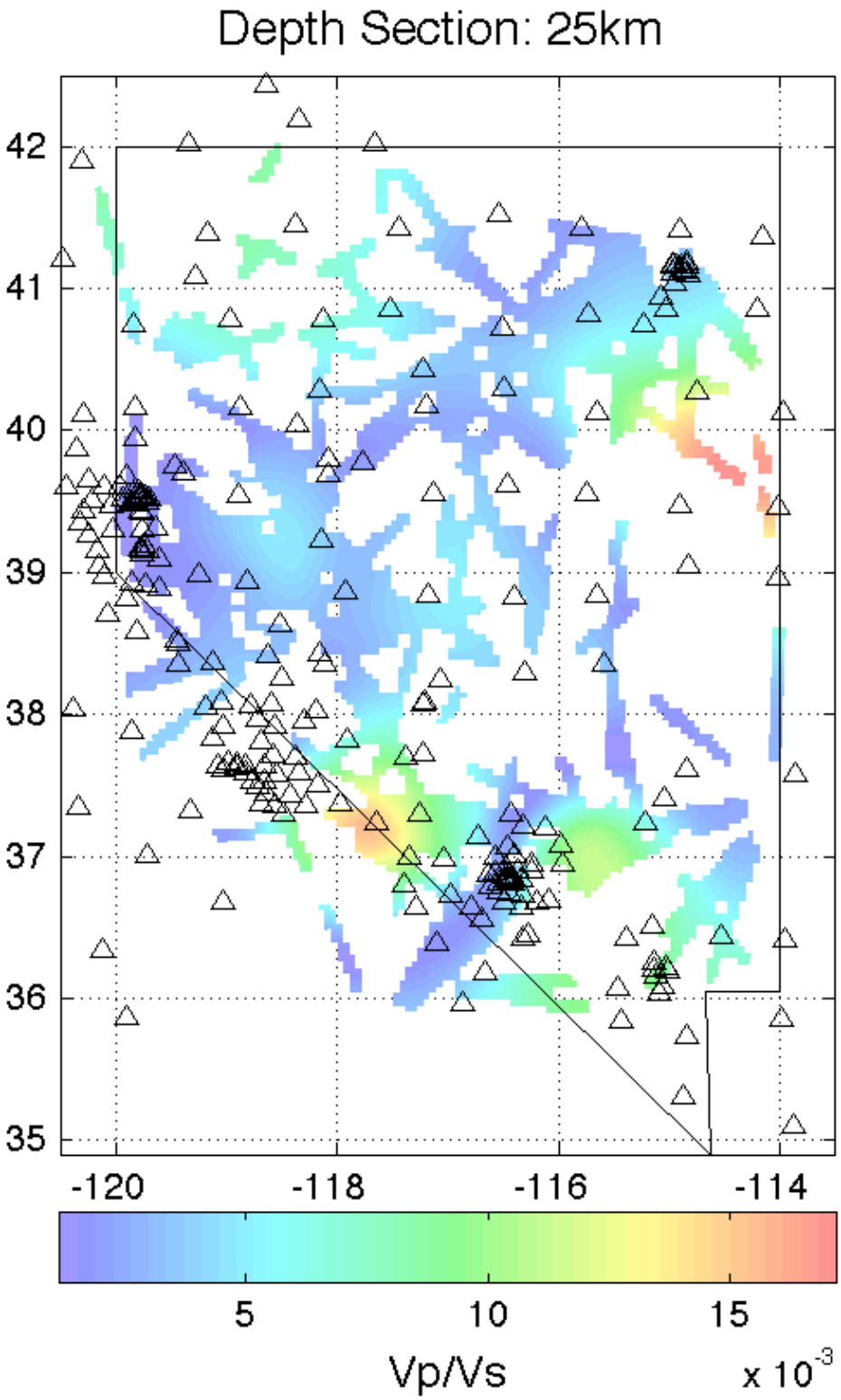

Figure 72

**Vp/Vs Jackknife**

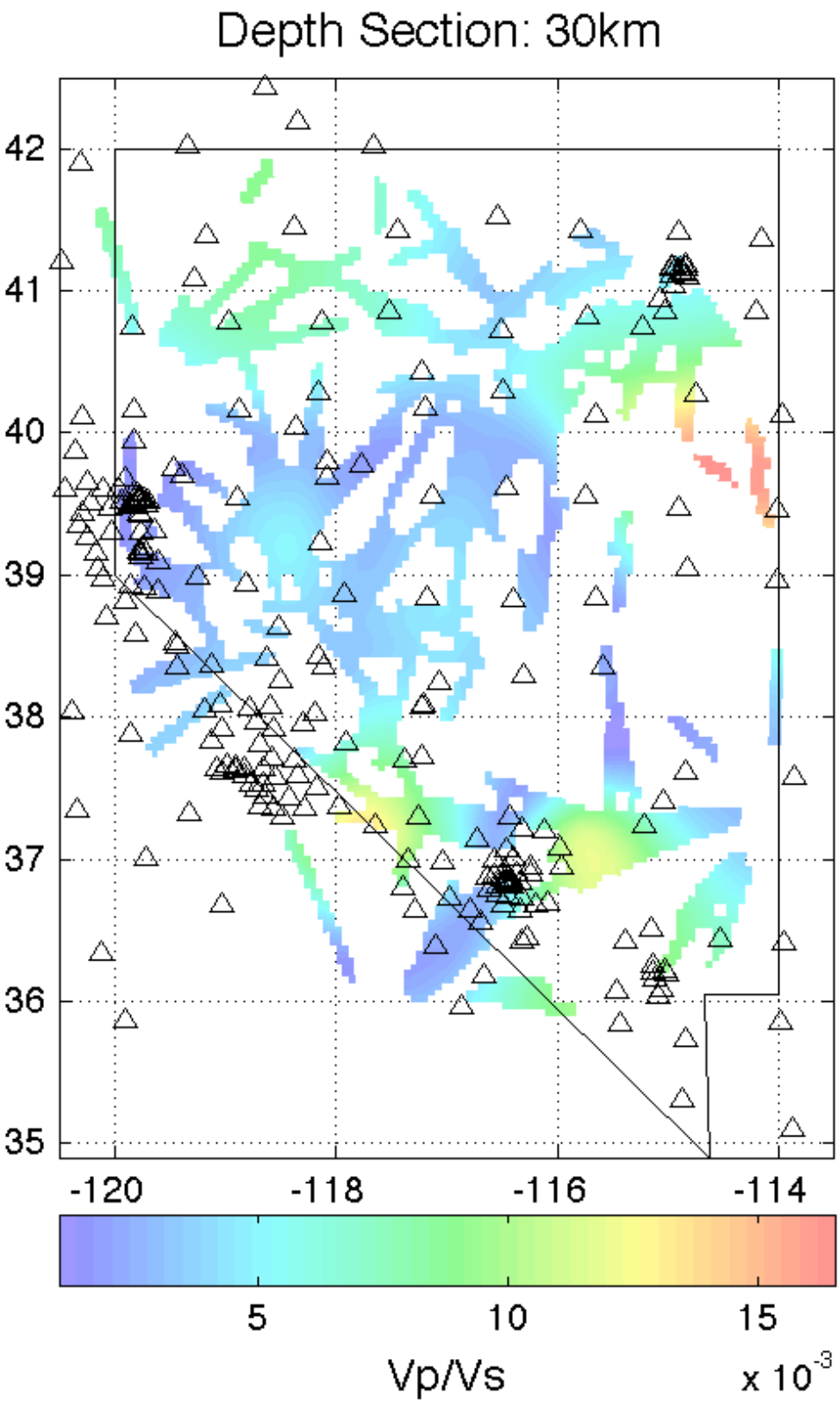

Figure 73

**Vp/Vs Jackknife**

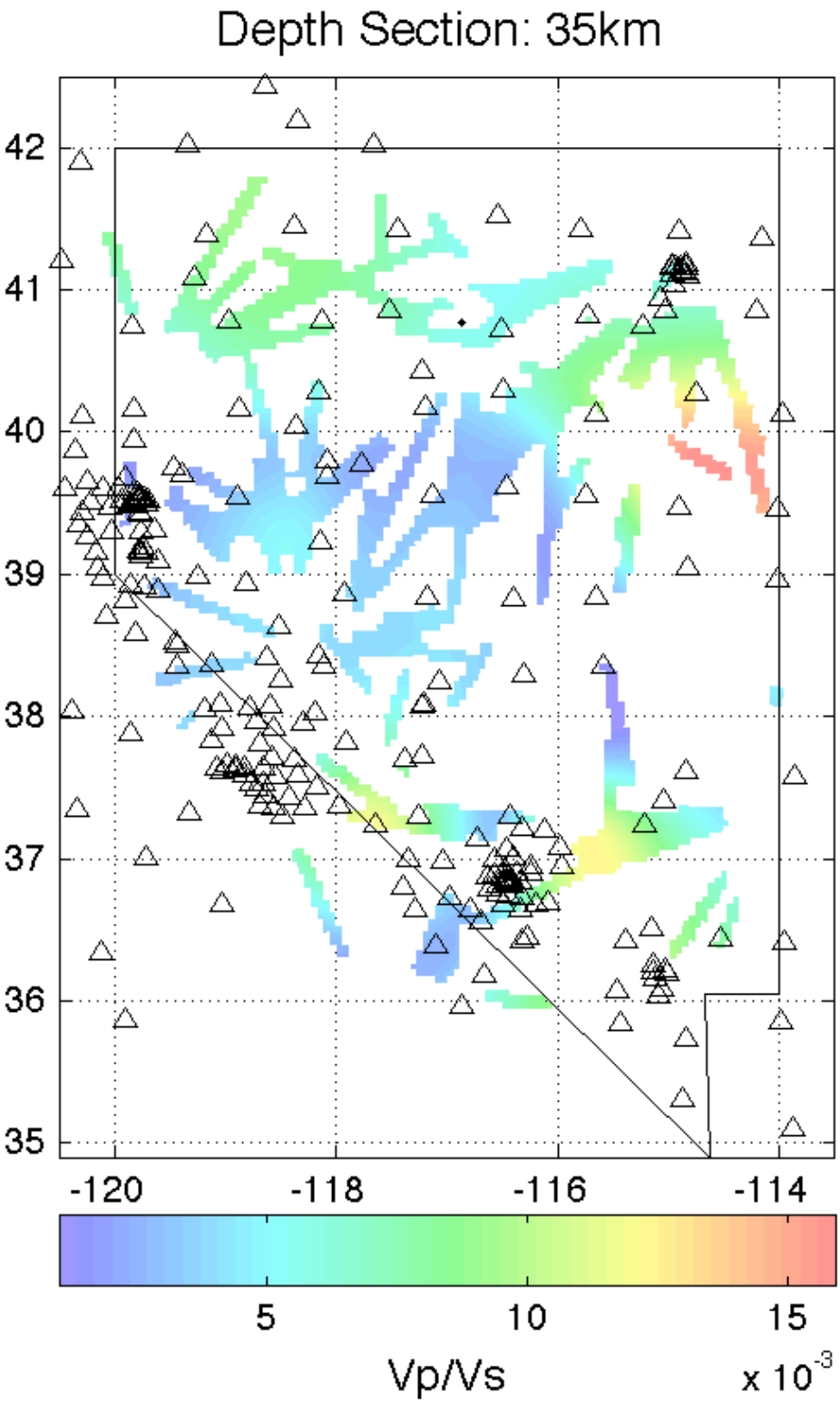

# Distribution

***External***:
Glenn Biasi
Nevada Seismological Laboratory MS174
University of Nevada Reno
Reno, NV 89557
glenn@seismo.unr.edu

Ileana Tibuleac
Nevada Seismological Laboratory MS174
University of Nevada Reno
Reno, NV 89557
ileana@seismo.unr.edu

***Internal***:

| Mail Stop | Name | Org |
|---|---|---|
| MS 0750 | Leiph Preston<br>lpresto@sandia.gov | 6734 |
| MS 0750 | Greg Elbring<br>gjelbri@sandia.gov | 6734 |
| MS 0899 | Technical Library | 9536 |
| MS 9018 | Central Technical Files | 8944 |


Sandia National Laboratories